ANALYSIS AND DETECTION OF HUMAN MOTION IN TIME-FREQUENCY DOMAIN

NYAN MYO NAING
B.E (ELECTRONICS)
YANGON TECHNOLOGICAL UNIVERSITY
YANGON, MYANMAR

A THESIS SUBMITTED
FOR THE DEGREE OF DOCTOR OF PHILOSOPHY
DEPARTMENT OF MECHANICAL ENGINEERING
NATIONAL UNIVERSITY OF SINGAPORE

2006

Acknowledgements

I wish to express my sincere appreciation and gratitude to my supervisors, Dr. Tay Eng Hock, Francis and Dr. Seah Kar Heng for their encouragement, valuable suggestions, and guidance without which the research could have not been finished.

I owe my thanks to Dr Yih Yiow Sitoh and Dr Noor Hafizah B Ismail from Tan Tock Seng Hospital, for their help and assistance. Thanks are also given to staffs from the Department of Geriatric Medicine, Tan Tock Seng Hospital, for their help during the experiment.

I would like to thank my friends, Mr. Nay Lin Tun and Mr. Pyi Soe, and other friends who helped me throughout the research.

Special thanks must go to my mother for her support, and encouragement during my PhD candidature.

Table of Contents

Summary

Falls and activities of daily living (ADL) detection in humans require an objective and reliable technique to be used under free-living conditions. The emphasis of this study is to develop a wearable fall and ADL detection system that can detect a broad range of ADL using relatively fewer sensors, in comparison to other researchers' systems, for the comfort of the user in long term application. The system can also raise fall notifications without user intervention to get a shortened interval before the arrival of assistance.

To provide long term comfort for the wearer, we use a garment as a wearable platform. A triaxial accelerometer measuring in lateral, antero-posterior and vertical directions is attached at the shoulder position of the garment. ADL detected in our studies are vital daily activities such as sitting, standing, lying down, lying to sitting, level walking, ascending stairs and descending stairs. However, in sitting, standing, and lying down detection, instead of detecting static postures, we detect stand-sit/sit-stand, and lie-sit/sit-lie posture transition activities.

In fall detection, we have developed a fall notification system that can summon medical assistances via SMS (Short Messaging Service). This is the detection system as perfect in its kinds as that which can detect fall with no detection range limitation and can raise fall alarm (fall SMS) on its own to individuals and health care unit to shorten the interval of the arrival of assistance. A new method of time-frequency based ADL detection using two acceleration signals, vertical acceleration signal and antero-posterior acceleration signal, from the accelerometer attached onto the shoulder part of a garment is proposed. Real-time wearable falls and ADL detection system is implemented and

normal healthy three male and three female subjects involved in approximately five-hour-long experiment. Overall sensitivity (defined as the ability of the system that can correctly detect the activities) 94.98 per cent and specificity (defined as the ability of the system that generates no false detection) 98.83 per cent were achieved.

We have also explored the possibility of pre-impact fall detection that is distinguishing sideways and backward falls, which can cause hip fractures among the elderly, from ADL using angular rate sensors (gyroscopes). The purpose of this study is to investigate a method for the automatic detection of fall, which can cause hip fractures, during its descending phase before the subject hits the floor so that this favorable method can be used to develop a fall injury minimization system for the elderly.

In conclusion, our experimental results show that a new wearable detection system by securing a miniature triaxial accelerometer on a garment allows detection of falls and a broad range of ADL, in comparison to other researchers' systems, in high accuracy. Moreover, the method of fall pre-impact detection can also be used to complement an injury minimization system such as an inflatable hip protection device to be activated upon imminent fall.

List of Symbols

$\psi(t)$	Continuous-time wavelet function
$\phi(t)$	Continuous-time scaling function
$\Psi(\omega)$	Fourier transform of $\psi(t)$
$\Phi(\omega)$	Fourier transform of $\phi(t)$
a	Dilation parameter in wavelet transformation
b	Location or translation parameter in wavelet transformation
$\boldsymbol{R}$	The set of real values
$\boldsymbol{Z}$	The set of integer values
$L_2(\boldsymbol{R})$	Space of square-integrable functions
$l_2(\boldsymbol{Z})$	Space of square-summable sequences
$f(t)$	Square integrable function
$\overline{\psi_{a,b}}(t)$	Complex conjugation of $\psi_{a,b}(t)$.
$\boldsymbol{W}_f(a,b)$	Continuous wavelet transform(CWT)
N	Number of coefficients
J	Maximum scale of DWT decomposition
j	Decomposition level
$\boldsymbol{V}$	Vector of wavelet coefficients at scale maximum scale M
$\boldsymbol{W}$	Vector of coefficients at each scale of decomposition
$\boldsymbol{S}$	Reconstructed approximation signal
$\boldsymbol{D}$	Reconstructed detail signal

$\mathcal{V}$	Approximation vector space
$\mathcal{W}$	Orthogonal complement of $\mathcal{V}$
g	Impulse response of scaling filter
h	Impulse response of wavelet filter
$H(\omega)$	The absolute value of transfer function of $\{h_n\}$
$G(\omega)$	The absolute value of transfer function of $\{g_n\}$

List of Figures

List of Tables

Chapter 1

Introduction

1.1 Background

Singapore has one of the fastest aging populations in the world, with an anticipated increase in the proportion of older persons above 65 years of age from 7.3 per cent in 1999 to 18.9 per cent in the year 2030 [1]. Alongside the rapid graying of the population, the economic burden of managing multiple chronic conditions commonly encountered in the elderly is likely to put a strain on the healthcare system, as has been demonstrated in other developed countries [2]. Falls constitute a major healthcare concern in older persons and can affect 30% of community dwelling older persons each year [3]. Apart from causing physical injury, falls can result in psychological trauma and lead to an increased risk of admission to nursing homes [4]. Studies examining injuries in community-dwelling elderly indicate that falls are the leading cause of traumatic brain injury (TBI) followed by motor vehicle crashes [5, 6]. Another serious major fall-related injury is hip fracture. Twenty six percent of the elderly with hip fractures died within a year [7]. Moreover, the consequences of falls may lead to institutionalization, restricted activity, other minor injuries, fear of falling, or death. Therefore, prevention and detection of falls have been an important research area since two decades ago [8-18]. In this context, the ability to monitor different movements and postures involved in the daily routine of older persons who are living alone may help to pave the way for identifying persons who have fallen or are at risk of falling. Such an ability may also allow a better

assessment of activities of daily living (ADL) and the effects of numerous medical conditions and treatments [19], thus paving the way for planning interventions aimed at maintaining independence and enhancing safety of the elderly people. This surveillance can also be the detection of long periods of inactivity in older persons who will be spending significant portions of their daily routines alone. Moreover, the assessment or detection of ADL is an essential issue in ambulatory monitoring because physiological responses, such as changes in heart rate or blood pressure, may result from changes in body position and physical activity. Besides, it is a key determinant in evaluation of the quality of life of subjects with limited mobility, such as elderly persons [19].

Even though extensive research has been done in fall and activities of daily living (ADL) detections, some limitations are still observed and are listed below.

(1) There is no consideration for the comfort of the wearer in fall and ADL detection for long term application.

(2) All fall detection systems developed over the past two decades are with detection range limitation.

(3) There is no implementation of wearable real-time ADL detection system that can be used to detect abnormal activities in real time, for example, extended walking of an elderly, which could mean that the subject is in a state of trance, or wandering of subjects suffering from dementia.

(4) Fall detection and fall risk assessment, assessment of physical and mental conditions of the elderly or environmental condition that can lead to fall incident, have been mostly focused in elderly fall safety research and no investigation of pre-impact fall detection is conducted using wearable sensors in distinguishing

fall activities from normal ADL in the earlier stage of fall before the person touches the ground. The advantage of the investigation is that a fall injury minimization system can be developed, for example, by incorporating the pre-impact fall detection system with an inflatable hip protection device.

1.2 Objectives

In this thesis, a novel approach of falls and activities of daily living (ADL) detection based on a normal garment (vest) is described. The objectives of this study are listed below:

(1) Develop a wearable system that can detect a broad range of ADL using relatively fewer sensors, in comparison to other researchers' systems, for the comfort of the user in long term application.

(2) Design a novel fall detection system (post impact detection) with no detection range limitation and the system can raise fall notifications, without user intervention, to individuals and health care unit at the same time to get a shortened interval before the arrival of assistance.

(3) Implement a real-time fall and ADL detection system using the methods developed by objectives number 1 and number 2.

(4) Investigate a method of pre-impact fall detection that can distinguish fall activities from normal activities at the earlier stage of fall process before the subject touches the ground.

1.3 Outline of the thesis

This dissertation is organized into seven chapters. In Chapter 1, the background information and objectives of the research are explained, and then previous applications falls and ADL detection systems are reviewed in Chapter 2. Chapter 3 illustrates the three basic blocks of wavelet time-frequency analysis: continuous wavelet transform, discrete wavelet transform and multiresolution analysis. A brief description of discrete dyadic wavelet transform is also discussed. Chapter 4 describes the detection procedure of ADL in time frequency domain. Fall detection (post impact detection) including implementation of fall notification system and pre-impact fall detection using angular rate sensors are discussed in Chapter 5. Chapter 6 then presents the implementation of real-time fall (post impact detection) and ADL detection system using the methods developed in Chapter 4 and Chapter 5. Finally, the summary of achievements and the recommendations are presented in Chapter 7.

Chapter 2

Literature review

2.1 Studies on previous activities of daily living (ADL) detection methods

ADL detection research works can be separated into two groups, home-based detection and body-worn devices. Yamaguchi et al. [20] and Noury et al. [21] have developed indoor monitoring systems using infrared position sensors and magnetic sensors. The sensors are located at designated locations such as furniture, doors and corridors to monitor behaviors during daily life. Daily life behaviors and activities such as how many hours the subject stays in bathroom, living room, and kitchen and on bed in his/her daily life are studied. In addition to sensors mentioned above, Ogawa et al. [22] added carbon dioxide sensor to improve the measurement accuracy of the presence of the subject in the room. In these home-based detection methods, the sensors are fixed at designated locations. If the subject were to venture beyond the designed sensor range, as in the case of wandering of subjects suffering from dementia, the effectiveness of the sensors would be compromised. It is thus more viable for the sensors to be directly located on the subject for applications in free-living condition.

ADL detection requires an objective and reliable technique to be used under free-living conditions. From a physiological point of view, daily activity, regarded as any movement or posture that is produced by skeletal muscles, results in energy expenditure [23]. The energy expenditure due to physical activity is widely accepted as the standard reference for physical activity assessment [24], but measurement of this variable under

conditions of daily living is impractical and not feasible for population studies. Therefore, interests for estimates of energy expenditure based on observations, questionnaires, heart rate recordings, or movement registration are growing. At present, movement registration with body-worn motion sensors offers the best alternative for ADL detection. Various motion sensors have been designed for this purpose, ranging from mechanical pedometers [25] and actometers [26] to accelerometers [27-29]. Accelerometers respond to both frequency and intensity of movement, and in this way accelerometers are superior to pedometers and actometers, which are attenuated by impact or tilt and only count body movement if a certain threshold is passed. Due to the current state of art in integrated circuit technology there is also good opportunity to build very small and lightweight accelerometer systems that can be worn for days or even weeks. Moreover, accelerometers have been used for several decades to study human motions and other movements [30-33] and also for the measurement of tremor and motor activity in neurological patients [34-36]. However, precise detection of ADL using accelerometer requires classification of activities such as walking, ascending stairs, descending stairs and lying down, etc.

In human motion activities (level walking, ascending stairs, and descending stairs) detection, Najafi et al. [19], Bouten et al. [32], Veltink et al. [33], Foerster et al. [34], Aminian et al. [37], Mantyjarvi et al. [38], Sekine et al. [39, 40], and Coley et al. [41] used uniaxial or triaxial accelerometers in their detections. Najafi et al. [19] detected ADL using a kinematic sensor, which is composed of one miniature gyroscope measuring in sagittal plane and two miniature accelerometers measuring vertical and frontal accelerations of the subject. The sensor was located on the subject's chest, but no detail

expression is provided on how the sensor was placed on it. Level walking activity was simply detected using a fixed threshold, no threshold value was reported, and successive peaks with intervals of 0.25-2.25 seconds were chosen as walking steps. The detection method is very simple and it cannot distinguish among level walking, ascending stairs and descending stairs. Bouten et al. [32] described the development of a triaxial accelerometer (TA) for the assessment of ADL. The TA is composed of three orthogonally mounted uniaxial piezoresistive accelerometers and is attached to the low back of the subjects at the level of the second lumbar vertebra by using an elastic belt around the waist. The main objective of the research is to evaluate the relationship between energy expenditure due to physical activity and body acceleration, the sum of the integrals of the absolute value of accelerometer output from all three measurement directions (IAAtot), during different types of ADL. Energy expenditure was measured from indirect calorimetry, and sleeping metabolic rate (SMR) [32]. In this method, IAAtot can be effectively used to evaluate the relationship between energy expenditure and physical activities, but it cannot classify types of activities. Veltink et al. [33] attempted to classify static activities such as sitting, standing, and lying and dynamic activities such as cycling, level walking, ascending stairs and descending stairs, using three uniaxial accelerometers mounted tangentially (forward) and radially (vertical) on the mid-sternum and tangentially (perpendicular to the front thigh surface) on the upper half of the thigh using double-sided tape. It is recommended that the tangential thigh accelerometer can be used to distinguish among the three subgroups of dynamic activities, (1) level walking, (2) ascending stairs and descending stairs, and (3) cycling. The mean values of individual cycles of motion activities (walking on level ground and

stairs) of the thigh tangential accelerometer signals were used to distinguish level walking from ascending stairs and descending stairs and the finding was statistically significant among five able-bodied subjects between 23 and 42 years of age (248 times walking through a building (distance was not shown in the paper), 40 ascending stairs and 35 descending stairs activities, sign test, $\alpha < 0.05$). However, this method cannot be used to differentiate between ascending stairs and descending stairs. Maximum correlation coefficients between individual cycles of walking on stairs activities and reference templates were used to distinguish between ascending stairs and descending stairs, but the technique still resulted in poor classification rate, 17% error for ascending stairs and 20% error for descending stairs for 40 ascending stairs and 35 descending stairs activities. Foerster et al. [34] detected ADL using four uniaxial accelerometers located at sternum, wrist, thigh, and lower leg. The sensors were fastened with Velcro bands and the sensitivity axis of the sensors was roughly perpendicular to the surface, i.e., to the frontal aspect of the sternum, dorsum of the lower arm segment, frontal aspect of thigh, and lower leg segment [34]. Twenty four male subjects, 21 to 34 years of age, were recruited to perform standard protocols consisting of seven types of activities, sitting, standing, lying supine, level walking, ascending stairs, descending stairs, and cycling. The recorded acceleration signals were manually separated in length of 20 seconds time-interval for each activity and similarity was determined by the so called L1 distances by referring to the standard protocol variable profiles [34]. In motion activities (walking on level ground and stairs) classification, 107 out of 121 level walking activities, 80 out of 108 descending stairs activities and only 20 out of 49 ascending stairs activities were correctly detected. Aminian et al. [37] presented the estimation of the incline and speed

of walking using neural networks. Then, Mantyjarvi et al. [38] classified level walking, ascending stairs, and descending stairs using two triaxial accelerometers. Sensors were located at the left and right sides of the hip with belt. Six channels of acceleration signals were processed with PCA (principal component analysis) or ICA (independent component analysis) and then DWT (discrete wavelet transform) was applied. Powers of wavelet coefficients of levels 5 to 8 were used as features in classification using three multilayer perception neural networks. It is proved that applications of ICA or PCA with wavelet transformation to six channels of acceleration signals can give better classification rate than the original data by using three multilayer perception neural networks. The best classification results were 83 % (ascending stairs), 84 % (descending stairs), and 90 % (level walking) and their method gives poor classification rate for three channels of acceleration signals. Moreover, application of neural networks needs a large number of training patterns to reduce the error. Sekine et al. [39] studied distinguishing walking on level ground from walking on a stairway using a triaxial accelerometer located at waist level. Walking patterns (level walking, and walking of stairs) were classified in two stages. In the first stage, walking patterns were separated using low-frequency components of antero-posterior acceleration signal and vertical acceleration signal. Low-frequency components were taken out from the original signals using MRA (multiresolution analysis). In detection of pattern changes in separation of ascending stairs activity from level walking activity, they manually set an individual threshold level for each subject at the low frequency component of antero-posterior acceleration signal. Times of pattern changes between ascending stairs and level walking were obtained from crossing points of the threshold level and the low frequency component of the signal.

Then, descending stairs activity was separated from level walking activity by detecting peak points, synchronous with changes between level walking activity and descending stairs activity, at the low frequency component of vertical acceleration signal. In the second stage, the three types of walking patterns were classified by comparing powers of wavelet coefficients computed from the separated activities. Twenty male subjects were involved in the experiments. Even though, high classification rates, p-values<0.01 for discriminating descending stairs from other activities and p-values<0.01 for classification between level walking and ascending stairs, were achieved, manual thresholding for each subject in activity separation is not practical for a large number of subjects. Again, Sekine et al. [40] used wavelet-based fractal analysis method in human motion activities classification. The fractal dimensions were computed from triaxial accelerometers located to the subject's back in the lumbosacral region of the vertebral column by attaching with an elastic waist belt. Even though the fractal dimensions from three dimensional acceleration signals were different (p-values <0.01) among the three walking types (level walking, ascending stairs and descending stairs), this significant result was achieved by setting individual threshold value for each individual subject. Finally, Coley et al. [41] presented the detection of ascending stairs using miniature gyroscope attached to the shank of the subject. Ascending stairs was classified from level walking and descending stairs by measuring the time intervals between toe-off and heel-strike and between heel-strike and foot-flat. High sensitivity, >94 %, in identifying 50 ascending stairs activities from level walking and descending stairs activities was obtained using only one sensor at the shank, but this method could not identify stairs descent from level walking.

In static activities (sitting, standing and lying) detection, Najafi et al. [19], Veltink et al. [33], Foerster et al. [34], Mathie et al. [42], and Lyons et al. [43] used gyroscope and accelerometer or accelerometers in their detection methods. Najafi et al. [19] detected sit-stand/stand-sit transitions activities instead of detecting sitting/standing static postures. The gyroscope measuring in sagittal plane was used to detect the locations of the transition activities and then sit-stand/stand-sit transitions were classified using the vertical displacement by double integrating the vertical acceleration signal. The method resulted in about 90% accuracy in classification for both sit-stand and stand-sit transition activities, but the most important limitation, in practice, of the above method is the integration error due to dc (steady state) component present in the vertical acceleration signal. Even though a simple kinematic sensor was used in detection, the sensor is protruding out of the body because of the gyroscope measuring the sagittal plane information and may cause injury when the subject faces severe incident such as fall. In lying static posture detection, the vertical acceleration signal was low-passed filtered (0~0.16Hz) to remove other activities, and the mean value of filtered signal, < 0.4 g (threshold), was used in detection. Veltink et al. [33] used dc (steady state) responses of accelerometers from the radial (vertical) accelerometer on the sternum and tangential (perpendicular to the front thigh surface) accelerometer on the thigh in detecting sitting, standing, and lying static activities. The dc response of the radial sternum accelerometer was used to distinguish sitting/standing posture from lying posture and that of the tangential thigh accelerometer was used to differentiate between sitting and standing postures. Mathie et al. [42] also detected sit-stand/stand-sit transition activities instead of detecting sitting/standing static postures. The transitions were detected in two steps using

a triaxial accelerometer located on the waist belt. First, the presence or absence of transition activity was determined by comparing the signal magnitude areas calculated from low-passed and high-passed filtered three acceleration signals with a preset threshold value. The signal magnitude area is equal to the sum of the areas under the modulus of the integral from three acceleration signals [42]. The comparison was done for each non-overlapping one second moving window. Secondly, the classification between sit-stand and stand-sit transitions was done by pattern matching with a reference pattern. Ninty-three- point-five percent (93.5%) sensitivity was achieved in classification of total 183 sit-stand/stand-sit transition activities from 26 subjects using this detection method. Finally, Lyons et al. [43] detected lying, sitting and standing static postures using two uniaxial accelerometers located at sternum (vertical) and on thigh (parallel to the front thigh surface). Static postures were classified by detecting the orientation in degree of the sensors through mathematical relation between accelerometer dc (steady state) response and sensor orientation [43]. The study is more specific to distinguishing between static and dynamic activities [43].

2.2 Falls among the elderly and previous elderly fall detection methods

A fall can be described as “an event which results in a person coming to rest inadvertently on the ground or other lower level as a consequence of the following: sustaining a violent blow; loss of consciousness; sudden onset of paralysis as in a stroke; or an epileptic seizure” [44]. Falls is one of the many other conditions such as dementia, incontinence, osteoporosism and immobility that are common and serious problems for the aged. It can cause pain, fractures, disability, immobility, hospitalization, and is the

fifth leading cause of death in persons over ages of 65 [45]; resulting huge costs for the medical care system [46].

Statistics on falls

Each year, between 25% and 50% of adults over the age 65 years experience a fall depending upon age and number of risk factors [3,47-50]. A study by Cummings et al. [51] showed that during a 12-month period, the aged who live at home are said to fall approximately once, those in hospitals 1.5 times, and nursing home residents at a rate that exceeds 2.0 falls per person [12]. At least half of those who fall seem to do so repeatedly [3] and some may experience innumerable episodes. Among the elderly, most injuries (87% of fractures) result from falls [52,53]. Fall-related injuries and their sequelae tend to become more serious with advancing age, i.e., among older adults falls are seven times more likely to be fatal than for those younger than 65 years [54] and 60% of fatal falls occur in older adults [52]. The frequency of falling seems to be higher among women than men, at least until age 75 [55], after which the rates become approximately equal.

Economic impacts of falls

The total direct and indirect costs of fall-related injuries have been projected to reach $85 billion by the year 2020 (in 1994 dollars) [56,57]. Slips, trips and falls accounted for 24% of the total costs of worker's compensation insurance claims between 1989 and 1990 [58]. Not only direct medical costs were high for fall-related injuries in those over the age of 65 years ($7.7 billion), total costs were also high in those between the ages of 25 and 44 years because of higher morbidity costs ($8.3 billion) associated with restricted activity levels and lost productivity [59]. These costs indicate that fall-related injuries are a problem that is not limited to the elderly population.

Complications of falling

The expensive complication from falling is the loss of independence due to injuries that may necessitate institutionalization or at least a need for family or paid caregivers. Other complications include osteoporosis, joint contractures, and even psychological impairment, such as fear of falling and not being able to stand up leading to the "walk avoiding syndrome" [52,60,61].

The most obvious and serious consequences of falling are injuries. Common injuries due to receiving the main impact include fractures involving the hand, hip and spine, head and brain injuries with/without intra-cranial hemorrhage, and soft tissue trauma [62]. Among the injuries, hip fracture is a serious condition as it usually requires surgical fixation and leads to reduced mobility in the elderly. About one-third of fall-related hip-fractured patients become wheelchair or bed bound, another one third need aids for walking and only 28 % are able to walk without aids [7]. A better understanding of why hip fractures occur in fall incidents and how treatment of these injuries can maximally restore function and prevent further injuries, in face of the rising hip fracture incidences [63-65], is the major challenge in elderly healthcare applications [66].

Fall directions and fractures

Moreover, fall direction and impact site are important factors affecting injury risk and type. Smeesters et al. [67] examined the fall direction and impact location resulting from four disturbances (fainting, slip, step down, trip) at three gait speeds (fast, normal, slow) using a four-camera, 3D motion measurement system. From the experiment, it is found that slip in normal gait speed and fainting resulted in backward or sideways falls with impact on the hip. Trips and steps down usually resulted in forward falls with frontal

impacts regardless of gait speed. At fast gait speed, slips and faints also usually resulted in forward falls with frontal impacts. As gait speed decreased, slips usually resulted in sideways and backwards falls with impacts on the hip or buttocks, and faints resulted in a greater number of sideways falls. Sideways falls, backwards falls and impact at the hip are associated with hip injury; forward falls, trips and impact with the hands are associated with upper-extremity injury [14,68-71]. Studies have shown that falling to the sides, compared to other fall directions, increases hip fracture risk between three-fold to five-fold [70-74]. Moreover, impacting on or near the hip, compared to other impact locations, increases hip fracture risk by 21 to 49 fold [70,71,74].

Falls in the elderly: Prevention and Detection

As presented earlier, falls and its associated complications lead to decrease in the quality of life. It is therefore in the interest of the community to recognize individuals at risk of falling and provide necessary interventions to minimize the chances of falling. Components of these intervention programs can be separated into prevention and detection. Preventive intervention includes two or more fall-risk factors into the multifactorial risk-based prevention programme and the efficacy is examined through long-term observation [72-85]. Myers et al. [12] have summarized potential factors, considered in several studies [72-85], which are effective in reducing the incidence of falls in community-dwelling geriatric patients. These risk-factors can be divided into nine categories: general physical functioning; gait, balance and physical performance; musculoskeletal and neuromuscular measures; demographic factors; sensory impairments; medical conditions; indicators for general health; medication use; and psychological , behavioral, social, and environmental factors.

Besides prevention, detection is also an important factor among the elderly, particularly for those living alone. An undetected fall in an older person can result in a person lying conscious and uncomfortable for hours before being saved. This scenario commonly known as a “long lie” (prolonged recumbency) can lead to rhabdomyolysis with renal failure, dehydration, pressure injury and psychological trauma consequent to the event. It is therefore crucial to detect the event of a fall as early as possible, so that the elderly can receive timely medical aid. There are two basic approaches for the detection of a fall, activity detector [20,86,87] and fall sensors [21,42,88,89]. Activity detector is the detection of abnormal activity such as long time spending in the bathroom [20]. In such case, an alarm can be sent to a person living closely to check the status of the subject. Nait-Charif and McKenna [86] detected unusual inactivity such as a long lie using a vision system operating in a home environment. The person’s position in the image along with a coarse representation of his/her shape and orientation in the image were tracked using an ellipse. The ellipse centre and the other parameters such as orientation, scale and eccentricity are used to support recognition of relevant actions and events such as falling, lying down, sitting and standing. The method has gone some way to providing useful cues for fall detection. Sixsmith et al. [87] developed a considerably more intelligent fall and abnormal activity detector (SIMBAD- Smart Inactivity Monitor using Array-Based Detectors) using wall mounted IRISYS (infrared integrated systems) thermal imaging sensors. The IRISYS sensor’s low-element-count infrared array technology can locate and track the subject in the sensor’s field of view by providing size, location, and velocity information [87]. The system considers two distinct characteristics of observed behavior. Firstly, it analyzes target’s (subject’s) motion, i.e.,

vertical velocity estimation, to detect falls' dynamic characteristics. Secondly, it detects target's inactivity and compares it with a map of acceptable periods of inactivity in different locations. In fall detection, the system employs a neural network to classify falls from other normal movement using real-time data from IRISYS. The system communicates with a host computer, installed with a GSM (Global System for Mobile Communications) modem, to report fall alarms. Noury et al. [21] developed a fall sensing system, "actimeter", composed of a "fusion" of vertical axis acceleration using a piezoelectric accelerometer, body orientation using a position tilt switch and mechanical vibration of the body surface using a vibration sensor. A Boolean data is generated for the position, orientation and vibration and sent to a PC (computer). The communication with the PC is performed with a half-duplex radio transceiver. The RF link enables non-line-of-sight communication and suits an indoor mobile task. Then, these Boolean information are sent to the health care center through the network using TCP-IP packets. Mathie et al. [42] detected falls using a triaxial accelerometer located at the waist. Pattern matching between the recorded accelerations signal and the reference patterns were used in fall detection and resulted in 80.5 % sensitivity in detecting eight fall activities from two subjects. Pattern matching is not a suitable method in fall detection as fall patterns are not repeatable in different fall incidents. The study emphasized only on classification among falls and ADL and fall notification was not discussed in that paper. Then, Hwang et al [88] developed a real-time fall detection system for elderly people. The system is comprised of accelerometer, tilt sensor and gyroscope. Accelerometer measures kinetic force and, tilt sensor and gyroscope estimate body posture. A threshold value for tilt signal in posture detection and another threshold value for acceleration signal level

difference in fall impact detection are used to detect fall. Gyroscope signal is used to distinguish fall activities from normal activities. Ninety-six point seven percent of 123 fall trials could be detected successfully. Even though fall could be detected with high accuracy, fall notification was not considered in their development. Again, Williams et al. [89] used a piezoelectric shock sensor to detect the impact in fall detection. Communications to the community alarm system or a telecare system are via a license-exempt radio telemetry module using half-duplex transmitting at 418 MHz (UK) or 433 MHz (Europe). The detector is intended to be used in an under-developed integrated telecare system for the elderly. Generally, it can be observed that all fall detection systems discussed above were designed for limited detection range applications. Therefore, the effectiveness of the sensors would be compromised if the subject were to venture beyond the designed sensor range.

Another key concern in preventing or reducing the severity of fractures in the elderly is to detect falls before the person hits the ground, i.e., fall pre-impact detection. If fall incidence is detected in its early stage, an alarm system or fall injury minimization system can be activated to break the fall before he/she hits the ground or to minimize the injuries such as hip injuries. Wu has studied fall pre-impact detection through camera-based motion measurement system [90]. Velocity profiles during normal and abnormal (i.e., fall) activities are used to make the automatic detection of fall in its descending phase. Falls are detected 300-400 msec before end of the fall. As a complement of the fall pre-impact detection, Kroonenberg et al [91] studied kinematics and dynamics data of falls in developing new intervention strategies of hip fractures such as airbag to be activated upon detection of the initial stage of fall. Each fall was videotaped at 60 frames

per second in the experiment. Hip impact velocities, ranges of body configuration at impact and protective reflexes such as muscle activation or the use of an outstretched hand influence fall kinematics were studied.

2.3 Review of previous falls and ADL detection research works

According to the literature review, accelerometers are located at different body segments such as foot, thigh, waist, and sternum using belt, elastic belt, double-sided tape or Velcro™ in ADL detection (Table 2.1). Falls and ADL detection using considerable number of sensors located at different parts of the body may not be suitable for long-term use. Moreover, tightness of fixing materials in long term use is also a necessary consideration in applying elastic belt, belt, double-sided tape or Velcro™ in securing the sensors on the body.

Even though fall and activities of daily living (ADL) detection are studied extensively, some weaknesses are still observed. Investigation of pre-impact fall detection using wearable sensors is not conducted in distinguishing fall activities from normal ADL in the earlier stage of fall before the person touches the ground. The advantage of the investigation is that a fall injury minimization system can be developed, for example, by incorporating the pre-impact fall detection system with an inflatable hip protection device. In addition, no previous research works have considered for the comfort of the wearer in falls and ADL detection for long term application. Fall detection systems have been developed, but all of them are designed for limited-range applications. Moreover, all ADL detection methods developed are used in off-line analysis and it is useful that if we can detect the human activities real-time as the system can help detect

Table 2.1 Literature review of previous researchers' work in falls and ADL detection

Researchers' name	Year	Types of activities	Types of sensors	Locations of sensors	Sensor attachment
Najafi B [19]	2003	ST,SI,LY,GU,L	Two 1-axis aces, one gyroscope	Sternum	With belt
Yamaguchi A [20]	1998	Monitoring daily behaviors at home, F	Infrared position sensors, magnetic switches	At furniture, doors, in the bath room	
Noury N [21]	2000	Fall, human behaviors	Infrared position sensors, magnetic switches, smart sensor (accelerometer, tilt sensor, vibration sensor)	Home security equipments, On the body	With belt
Ogawa M [22]	2000	Monitoring daily behaviors at home	Infrared position sensors, magnetic switches, carbon dioxide sensor	In the kitchen, dining room, doors	
Bouten CVC[32]	1997	ST,SI,LY,L,U,D,CL	Three 1-axis aces	Lower part of the back	With elastic belt
Veltink PH [33]	1996	ST,SI,LY,L,U,D,C	Three 1-axis aces, membrane switches	Sternum, thigh, under the heels	With double-sided tape
Foerster F [34]	1999	ST,SI,LY,L,U,D,C	Four 1-axis aces	Sternum, wrist, thigh, lower leg	With Velcro Bands
Aminian K [37]	1995	Incline and speed of walking	One 3-axis and one 1-axis aces	Back of the waist, the top of the right heel	With belt
Mantyjarvi J [38]	2001	L,U,D	Two 3-axis aces	Left and right sides of waist	With belt
Sekine M [39]	2000	L,U,D	One 3-axis ace	Back of the waist	With belt
Sekine M [40]	2002	L,U,D	One 3-axis ace	Back of the waist	With belt
Coley B [41]	2004	U	One gyroscope	Shank	With elastic belt
Mathie MJ [42]	2003	ST,SI,LY,GU,L,F	One 3-axis ace	Waist	With belt
Lyons GM [43]	2004	Static (ST,SI,LY) and dynamic activities	Two 1-axis aces	Trunk, thigh	With elastic belt
Nait-Charif and McKenna [86]	2004	Unusual inactivity detection (Long lie after Fall)	Camera-based detection system	In a designated space	
Sixsmith A [87]	2004	F	Array of infrared detectors	In a designated space	
Hwang [88]	2004	F	Accelerometer, tilt sensor, and gyroscope	At sternum	With elastic belt
Williams G [89]	1998	F	Piezoelectric shock sensor		
Nyan (My work)	2006	ST,SI,LY,GU,L,U,D,F	One 3-axis ace	Shoulder	Attached onto the normal daily clothing

L= Level walking, U= Ascending stairs, D= Descending stairs, ST= Standing, SI= Sitting, LY= lying, GU= Lying to sitting, C= Cycling, F= Fall, CL=Cleaning, ace= accelerometer

and send alarm for the patient's abnormal behavior such as patient is attempting to get out of the bed at night time, another fall prevention scenario as this attempt can lead to fall incident, or wandering of a patient suffering from dementia. Considering all these factors, we have developed a system that can detect falls and ADL real-time using a garment (vest) as a platform for the comfort of the wearer in long term application. Relatively fewer sensors, in comparison to other researchers' systems (Table 2.1), are used in detection for the comfort of the wearer. Moreover, the system can send SMS (Short Messaging Service) to alarm fall incidents through the mobile phone together with the wearer. The advantage is that there is no limitation on the effective detection range in fall detection. All discussions of previous falls and ADL detection systems closely related to my study are summarized in Table 2.1.

2.4 Activities of daily living detection and time-frequency analysis

In activity detection using accelerometers, these sensors respond to both frequency and intensity of movements and the sensor outputs are nonstationary signals [19]. In signal analysis methods, traditional spectral analysis such as the Fourier transform tell us about frequency components contained in a signal. However, it does not provide the time at which those frequency components occurred [92,93]. This information is important in analyzing nonstationary signals, where frequency content changes over time. In contrast to the Fourier analysis, wavelet transform (time-frequency domain transformation) provides good frequency resolution at both low and high frequencies with time information. Moreover, it is an optimal technique for describing the local regularity of signals [94,95]. A clear example of nonstationary signals in daily

activity movements are the acceleration patterns during level walking, ascending stairs, descending stairs, sit-stand/stand-sit transitions and lie-sit/sit-lie transitions (Figure 2.1). In these activities, the information of interest is a combination of features that are well localized in time and frequency domains. Since wavelet transform is capable of providing the time and frequency information simultaneously, it is a suitable technique in investigation of the acceleration signals related to ADL. In Chapter 3, time-frequency analysis methods such as wavelet decomposition, wavelet reconstruction, multiresolution analysis (MRA), and discrete dyadic wavelet decomposition will be discussed.

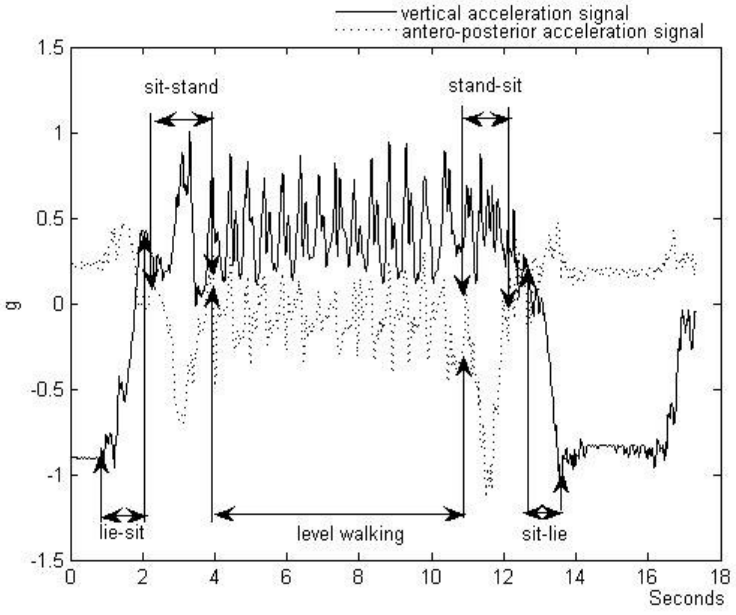

Figure 2.1. Acceleration signals during level walking, sit-stand/stand-sit transitions and lie-sit/sit-lie transitions.

Chapter 3

Multiresolution analysis and wavelets

In wavelet (time-frequency) analysis, *multiresolution analysis* (MRA) was formulated based on the study of orthonormal, compactly supported wavelet bases [96]. It was initiated by Mallat [93] and Meyer [96]. MRA is based on the existence of the sequence of successive approximation spaces $\mathcal{V}$. The concept is analyzing a signal at different levels of resolution, i.e., if it is not necessary to observe the signal in great detail; a coarse approximation (***S***) is sufficient or if we are looking for a particular section of the signal; we can zoom into that particular portion in great detail (***D***). It is therefore useful to analyze the signal in coarse-to-fine strategy, widely used in pattern recognition algorithms. Before MRA is discussed, some fundamentals regarding the wavelet transformation (continuous and discrete) will be presented.

3.1 Wavelet transform: Continuous and discrete

3.1.1 Continuous wavelet transform (CWT)

A real or complex-value continuous-time function $\psi(t)$ which satisfies the two properties:(1) the function integrates to zero $\int_{-\infty}^{\infty}\psi(t)dt = 0$ and (2) the function is square integrable or, equivalently, has finite energy: $\int_{-\infty}^{\infty}|\psi(t)|^2 dt < \infty$ and the admissibility condition

$$0 < C = \int_{-\infty}^{\infty} \frac{|\Psi(\omega)|^2}{|\omega|} d\omega < \infty, \qquad 3.1$$

can be called a mother wavelet or wavelet. In equation (3.1), $\Psi(\omega)$ is the Fourier transform of $\psi(t)$. The mother wavelet is orthogonal to all functions which are obtained by dilating (stretching) the mother by a factor of 2^j (2 to the j^{th} power) and shifting or translating the mother right or left by an integer amount by multiples of 2^j units, where $j \in \boldsymbol{Z}$ ($\boldsymbol{Z}$ is the set of integer values). The collection of shifted and dilated wavelet functions is called a wavelet basis and the doubly-indexed family of wavelets is written as

$$\psi_{a,b}(t) = \frac{1}{\sqrt{|a|}} \psi\left(\frac{t-b}{a}\right), \qquad 3.2$$

where a and b are dilation and scaling parameters or location and translation parameters, $a, b \in \boldsymbol{R}$ ($\boldsymbol{R}$ is the set of real values) and $a > 0$. These functions are scaled so that their $L_2(\boldsymbol{R})$ (space of square-integrable functions) norms are independent of a, i.e., for all a *and* b, $\left\|\psi_{a,b}\right\| = \|\psi\|$ with assuming $\|\psi\| = 1$. The continuous wavelet transformation of any square integrable function $f(t) \in L_2(\boldsymbol{R})$ is defined as

$$W_f(a,b) = \int_{-\infty}^{\infty} f(t)\overline{\psi_{a,b}(t)}dt, \qquad 3.3$$

or

$$W_f(a,b) = \left\langle f(t), \psi_{a,b}(t) \right\rangle, \qquad 3.4$$

where $\overline{\psi_{a,b}}(t)$ denotes complex conjugation of $\psi_{a,b}(t)$. Since the inner product of the two finite energy signals, denoted by $\langle x(t), y(t) \rangle$, is defined as

$$\langle x(t), y(t) \rangle = \int_{-\infty}^{\infty} x(t)\overline{y(t)}dt, \qquad 3.5$$

the CWT is essentially a collection of inner products of a signal $f(t)$ and the translated and dilated wavelet $\psi_{a,b}(t)$ for all *a* and *b* (Equation (3.4)).

3.1.2 Discrete wavelet transform (DWT)

We saw in the previous section that the CWT maps a one-dimensional function $f(t)$ to a function $W_f(a,b)$ of two continuous real variables *a* and *b*, which are the wavelet dilation and translation respectively. The region of support of $W_f(a,b)$ is defined as the set of ordered pairs (*a, b*) for which $W_f(a,b) \neq 0$. In principle, the region of support of a CWT is unbounded; i.e., it can be the entire plane defined by $\boldsymbol{R}^2$, the set of all ordered real pairs. In empirical application, the CWT suffers from two drawbacks: redundancy and impracticality. The first is obvious from the nature of the wavelet transform and the second from the fact that both transform parameters are continuous. The discrete wavelets or wavelet series are merely the discrete representation of CWT. This discretization allows the wavelet transform to be numerically computed as a series of discrete convolutions in time at discrete intervals of scales.

In discretization, the integer (positive or negative) powers of one fixed dilation parameter $a_0 > 1$, i.e., $a = a_0^j$, is chosen for a. As discussed in the previous section that

different values of j correspond to wavelets of different widths. It follows that the discretization of the translation parameter b should depend on j: narrow (high frequency) wavelets are translated by small steps in order to cover the entire time range, while wider (lower frequency) wavelets are translated by larger steps. Therefore, to discretize b, we choose $b = nb_0 a_0^j$, where $j, n \in \mathbf{Z}$, for some fixed $b_0 > 0$. In this way, the time-frequency plane is discretized as

$$a = a_0^j, \text{ and } b = na_0 b_0^j, \tag{3.6}$$

where $j, n \in \mathbf{Z}$, $a_0 > 1$ and $b_0 > 0$. The corresponding discretely labeled wavelets are therefore

$$\psi_{j,n}(t) = a_0^{-j/2} \psi(a_0^{-j} t - nb_0), \tag{3.7}$$

where fixed $a_0 > 1$ and $b_0 > 0$. Although equation (3.7) is called a discrete wavelet, it is a piecewise continuous function normally. Consequently, the effect of discretizing the wavelet is sampling of the time-frequency plane at discrete intervals. Commonly, choices for discrete wavelet parameters a_0 and b_0 are 2 and 1 respectively. This type of scaling in the dilation and translation steps is known as the dyadic grid arrangement. The dyadic grid is perhaps the simplest and most efficient discretization for practical purposes and lends itself to the construction of an orthonormal wavelet basis. Substituting $a_0 = 2$ and $b_0 = 1$ into equation (3.7), we see that the dyadic grid wavelet can be written as

$$\psi_{j,n}(t) = 2^{-j/2} \psi(2^{-j} t - n). \tag{3.8}$$

Now the wavelet transformation using discrete wavelets is given by

$$W_f(j,n) = a_0^{-j/2} \int f(t)\psi(a_0^{-j}t - nb_0)dt, \text{ where } (j,n) \in \mathbf{Z}. \qquad 3.9$$

Equation (3.9) implies that the transformation of a continuous signal using the discrete wavelets results in a *series* of wavelet coefficients. Generally, the transform that uses the dyadic values of *a* and *b* as in equation (3.9) was called the *discrete wavelet transform*.

3.2 Multiresolution approximations of closed subspaces

The multiresolution analysis (MRA) is an approximation of functions in a sequence of nested linear vector spaces. In addition to the nesting property, the vector spaces need to satisfy certain other properties [97-99]. The properties of the MRA are as follows:

(1) an MRA consists of the nested linear vector spaces

$$..... \subset \mathcal{V}_1 \subset \mathcal{V}_0 \subset \mathcal{V}_{-1} \subset .....;$$

(2) the union of these subspaces is dense in the space of square integrable functions $L_2(\boldsymbol{R})$;

(3) the intersection of these subspaces is a singleton set containing the all-zero function or zero vector;

(4) $f(t) \in \mathcal{V}_j \leftrightarrow f(2^j t) \in \mathcal{V}_0$;

(5) $f(t) \in \mathcal{V}_0 \rightarrow f(t-n) \in \mathcal{V}_0$ for all $n \in \boldsymbol{Z}$, and

(6) there exists a function (called a scaling function) $\phi(t)$ such that $\phi_{0,n}(t) = \phi(t-n)$ constitutes an orthonormal basis for $\mathcal{V}_0$.

The beauty of the multiresolution approach is that whenever a ladder of spaces $\mathcal{V}_m$ satisfies the six properties above, then there exists $\psi(t)$ so that $V_{j-1}f = V_j f + \sum_{n \in Z} \langle f, \psi_{j,n} \rangle \psi_{j,n}$ holds, where V_j is the orthogonal projection to $\mathcal{V}_j$. Therefore, $\psi(t)$ and $\phi(t)$ are complements in the MRA.

The multiresolution analysis (MRA) of $L_2(\boldsymbol{R})$ is defined as a sequence of closed subspaces $\mathcal{V}_j$ of $L_2(\boldsymbol{R})$ with the properties presented above. The space $\mathcal{V}_j$ can be viewed as the set of all possible approximations of functions at the resolution 2^{-j}. MRA is then obtained by computing the approximation of signals at various resolutions with orthogonal projections onto different spaces $\{\mathcal{V}_j\}_{j \in \boldsymbol{Z}}$. In order to calculate the approximation, the orthogonal basis of each space $\mathcal{V}_j$ is generated by dilating and translating a single function ϕ called *scaling function*, $\phi_{j,n}(t) = 2^{-j/2}\phi(2^{-j}t - n)$, $n \in \boldsymbol{Z}$. If we denote V_j is the orthogonal projection operator onto $\mathcal{V}_j$, then $\overline{\bigcup_{j \in \boldsymbol{Z}} \mathcal{V}_j} = L_2(\boldsymbol{R})$ (property 2) ensures that $\lim_{j \to -\infty} V_j f = f$ for all $f \in L_2(\boldsymbol{R})$. Moreover, $\bigcap_{j \in \boldsymbol{Z}} \mathcal{V}_j = \{\boldsymbol{0}\}$ (property 3) implies that if the resolution 2^{-j} goes to zero, all details of f will be lost, i.e., $\lim_{j \to +\infty} \| V_j f \| = 0$.

Additional requirement needed in MRA is that all the spaces are scaled versions of the central space $\mathcal{V}_0$, stated as

$$f \in \mathcal{V}_j \Leftrightarrow f(2^j *) \in \mathcal{V}_0, \tag{3.10}$$

and in which $\{\phi_{0,n}; n \in \mathbf{Z}\}$ is orthonormal basis in $\mathcal{V}_0$. Moreover, another feature that we require from MRA analysis is invariance of $\mathcal{V}_0$ under integer translation, i.e.,

$$f \in \mathcal{V}_0 \Rightarrow f(* - n) \in \mathcal{V}_0 \text{ for all } n \in \mathbf{Z}. \tag{3.11}$$

The conditions $\phi \in \mathcal{V}_0 \subset \mathcal{V}_{-1}$, and $\phi_{-1,n}$ is an orthonormal basis in $\mathcal{V}_{-1}$ imply $\phi = \sum_n g_n \phi_{-1,n}$ and it can be written as

$$\phi(t) = \sqrt{2} \sum_n g_n \phi(2t - n) \tag{3.12}$$

or

$$\Phi(2\omega) = G(\omega)\Phi(\omega), \tag{3.13}$$

where G is a 2π periodic function defined by

$$G(\omega) = \frac{1}{\sqrt{2}} \sum_{n=-\infty}^{\infty} g(n) e^{-jn\omega} \tag{3.14}$$

and $\Phi(\omega)$ is the Fourier transformation of $\phi(t)$. With the Poison's summation formula [100], we can express the orthogonality of the family $((\phi(t-n))_{n \in \mathbf{Z}}$ as

$$\sum_{n=-\infty}^{\infty} \left|\Phi(\omega + 2n\pi)\right|^2 = 1. \tag{3.15}$$

Since $\Phi(2\omega) = G(\omega)\Phi(\omega)$, the summation can be rewritten as

$$\sum_{n=-\infty}^{\infty} \left|G(\omega+n\pi)\right|^2 \left|\Phi(\omega+n\pi)\right|^2 = 1. \qquad 3.16$$

The function $G(\omega)$ is 2π-periodic. We regroup the terms for $n \in 2\mathbf{Z}$ and $n \in 2\mathbf{Z}+1$ and inserting into equation (3.14) yields

$$\left|G(\omega)\right|^2 + \left|G(\omega+\pi)\right|^2 = 1. \qquad 3.17$$

Moreover, it can be proved that $\left|G(0)\right| = 1$, yielding $\left|\Phi(0)\right| = 1$ [63]. Now, we can see that $G(\omega)$ is a low pass filter with the conditions $\left|G(0)\right| = 1$, $\left|G(\omega)\right|^2 + \left|G(\omega+\pi)\right|^2 = 1$ and $G(\omega) \neq 0$ on $\left[-\pi/2, \pi/2\right]$.

3.3 Orthogonal wavelet functions and detail spaces

By considering a space $\boldsymbol{W}_j$ to be the orthogonal complement of $\boldsymbol{V}_j$ in $\boldsymbol{V}_{j-1}$, we can construct wavelets from MRA. The space $\boldsymbol{W}_j$ satisfies

$$\boldsymbol{V}_{j-1} = \boldsymbol{V}_j \oplus \boldsymbol{W}_j, \qquad 3.18$$

where the symbol $\oplus$ stands for direct sum. Because $\boldsymbol{V}_j \subset \boldsymbol{V}_{j-1}$, the orthogonal projection of f on $\boldsymbol{V}_{j-1}$ can be decomposed as

$$\boldsymbol{V}_{j-1} f = \boldsymbol{V}_j f + \boldsymbol{W}_j f, \qquad 3.19$$

where $\boldsymbol{W}_j$ denotes the orthogonal projection operator onto $\boldsymbol{W}_j$. The space $\boldsymbol{W}_j$ contains the "detail" information of f that is needed to go from a coarser approximation at resolution 2^{-j} to a finer approximation at resolution 2^{-j-1}.

Since $\boldsymbol{W}_j \subset (\boldsymbol{V}_{j-1} \perp \boldsymbol{W}_{j-1})$, it follows that $\boldsymbol{W}_j$ is also orthogonal to $\boldsymbol{W}_{j-1}$. It is therefore immediate that all the subspaces $\boldsymbol{W}_j$ are mutually orthogonal unlike the subspaces $\boldsymbol{V}_j$. Consequently, it implies that we can decompose

$$L_2(\boldsymbol{R}) = \oplus_j \boldsymbol{W}_j . \tag{3.20}$$

Similar to the definition of scaling function ϕ, if a collection of closed subspaces satisfies the properties presented in section 3.2, there exist a wavelet function ψ such that $\{\psi(t-n)\}_n \in \boldsymbol{Z}$ is an orthonormal basis of $\boldsymbol{W}_0$. For all scales, the entire collection $\{\psi_{j,n}\}_{(j,n)\in \boldsymbol{Z}}, \psi_{j,n}(t) = 2^{-j/2}\psi(2^{-j}t - n)$ is then an orthonormal basis of $L_2(\boldsymbol{R})$. Since $\psi_{0,n} \in \boldsymbol{W}_0 \subset \boldsymbol{V}_{-1}$, a sequence $h[n] \in l_2(\boldsymbol{Z})$ ($l_2(\boldsymbol{Z})$ is the space of square-summable sequences) exists such that

$$\psi(t) = \sqrt{2}\sum_n h[n]\phi(2t-n). \tag{3.21}$$

The Fourier transform of equation (3.21) is given by

$$\Psi(2\omega) = H(\omega)\Phi(\omega), \tag{3.22}$$

where $H(\omega)$ is a periodic function, i.e.,

$$H(\omega) = \frac{1}{\sqrt{2}} \sum_{n=-\infty}^{\infty} h[n]e^{-jn\omega} . \tag{3.23}$$

If the sequence $h[n]$ and $g[n]$ are conjugate mirror filters, the sequence $h[n]$ can be directly obtained from $g[n]$ using the relation

$$h_l = (-1)^l g_{L-1-l} \tag{3.24}$$

where $\{g_l, h_l : l = 0, ..., L-1\}$ is the nonzero impulse responses of the scaling filters G and H, and L is the length of the filter. The sufficient conditions for an orthogonal MRA and for an orthogonal wavelet, i.e., $\langle \psi(t), \phi(t-n) \rangle = 0$ and $\langle \psi(t), \psi(t-n) \rangle = \delta_n$, are equivalent to

$$\sum_{n \in Z} \Psi(\omega + 2n\pi)\overline{\Phi(\omega + 2n\pi)} = 0, \tag{3.25}$$

and

$$\sum_{n \in Z} \left|\Psi(\omega + 2n\pi)\right|^2 = 1, \tag{3.26}$$

respectively. From these conditions, the necessary and sufficient condition on $H(\omega)$ for designing an orthogonal wavelet is given as

$$\left|H(\omega)\right|^2 + \left|H(\omega + \pi)\right|^2 = 1. \tag{3.27}$$

Then, according to equation (3.18), the Fourier transform of any function f can be decomposed as

$$F(\omega) = A(\omega)\Phi(\omega) = B(\omega)\Phi(2\omega) + C(\omega)\Psi(2\omega), \tag{3.28}$$

where $A(\omega)$ is a 2π-periodic and a member of $L_2([0, \pi])$ and $B(\omega)$, and $C(\omega)$ are both $\pi-$periodic and members of $L_2([0, \pi])$. By inserting equation (3.13) and equation (3.22) into equation (3.28), it follows that

$$F(\omega) = B(\omega)G(\omega) + C(\omega)H(\omega). \tag{3.29}$$

The orthogonality of the decomposition is equivalent to

$$\int_0^{2\pi} \left|A(\omega)\right|^2 d\omega = \int_0^{\pi} \left|B(\omega)\right|^2 d\omega + \int_0^{\pi} \left|C(\omega)\right|^2 d\omega. \tag{3.30}$$

It is satisfied for any $A(\omega)$ if and only if

$$\begin{cases} |H(\omega)|^2 + |G(\omega)|^2 = 1 \\ H(\omega)\overline{G(\omega)} + H(\omega+\pi)\overline{G(\omega+\pi)} = 0. \end{cases} \quad 3.31$$

Equation (3.31) is also another necessary and sufficient conditions on $H(\omega)$ to build $\psi(t)$ and imply that, if the scaling filter resembles a low-pass filter, the wavelet filter should resemble a high-pass filter.

3.4 Practical implementations of discrete wavelet transform and multiresolution analysis

In discrete wavelet transformation (DWT), a signal $f(n)$, discrete time sampled signal where $n = 0,..,N,$ passes through two complementary filters, low-pass filter g and high-pass filter *h*, and is split into an approximation signal $\boldsymbol{V}_1$ and a detail signal $\boldsymbol{W}_1$ (Figure 3.1) [93]. The approximation is the high-scale, low-frequency component and the detail is the low-scale, high-frequency component of the signal. The approximation signal is then split into a second level approximation signal $\boldsymbol{V}_2$ and a detail signal $\boldsymbol{W}_2$. This decomposition is continued up to the desired maximum decomposition level *J*.

In wavelet multiresolution analysis, the signal can be reconstructed from the approximation and the detail signals. This is the extraction of a signal component in a certain frequency range [93]. The J^{th} detail $\boldsymbol{D}_J$ is obtained by taking the inverse transformation of $\mathbf{0}_1,.....,\mathbf{0}_{J-1},\boldsymbol{W}_J$ and $\mathbf{0}_J$. It is computed by successively applying the

inverse transformation for $J, J-1, \ldots\ldots, 1$ starting with $\boldsymbol{W}_J$ and $\mathbf{0}_J$ in the inversion process. At the end of the *J* iterations, the desired $\boldsymbol{D}_J$ signal is obtained (Figure 3.2(a)).

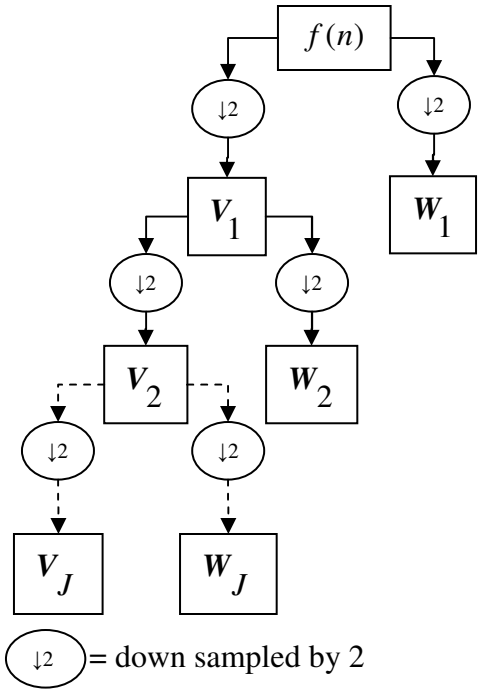

Figure 3.1. Discrete wavelet transform.

Similarly, the approximation signal $\boldsymbol{S}_J$ can be obtained by applying the inverse transformation to $\mathbf{0}_1, \mathbf{0}_2, \ldots\ldots, \mathbf{0}_J$, and $\boldsymbol{V}_J$ (Figure 3.2(b)). In this way, only the desired frequency band of the original signal is reconstructed and the other frequency components are rejected.

After exploring the DWT decomposition and reconstruction process, we still need to understand the nature of the frequency bandwidth of decomposed and reconstructed signals. Table 3.1 shows the frequency bandwidths of decomposed and reconstructed

signals at different levels of decomposition. The relation between scales and decomposed levels are also presented in Table 3.1.

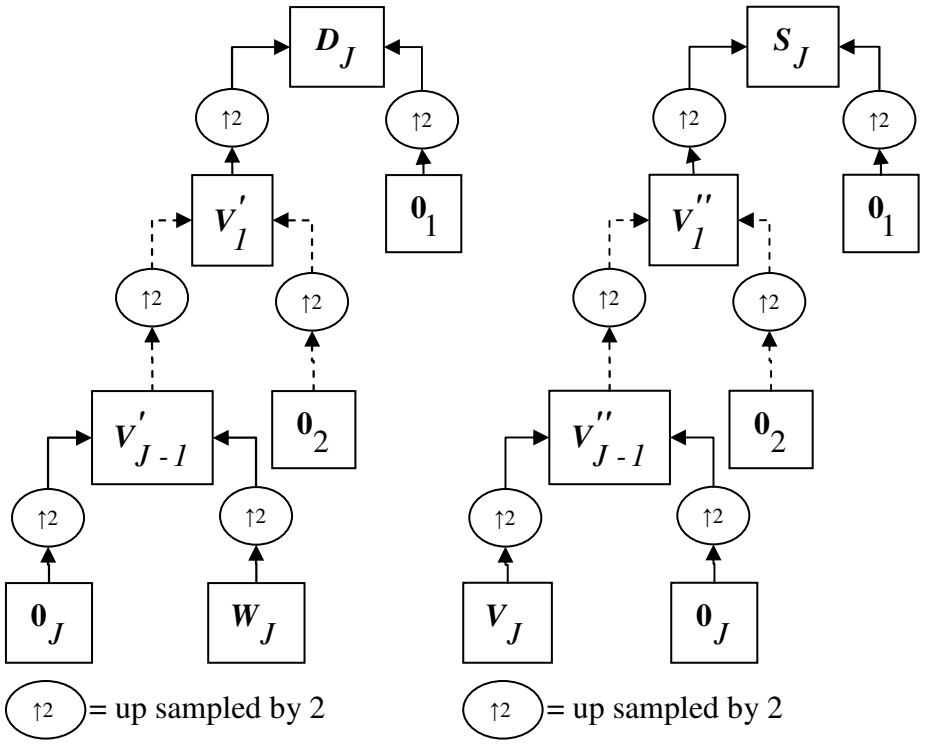

Figure 3.2. Wavelet reconstruction (a) detail signal (b) approximation signal.

3.5 Discrete dyadic wavelet decomposition

There are two types of decomposition in wavelet transformation, decimated and undecimated. In the first type of decomposition, the decomposed coefficients are down sampled for each level of decomposition. Therefore, the number of coefficients becomes fewer and fewer as the decomposed level is increased. The approximation signal and detail signals for required frequency bands are reconstructed from these coefficients.

Table 3.1 The frequency bandwidths of decomposed and reconstructed signals at different scales of decomposition (an example of decomposition of a signal with 256 Hz sampling rate for J=7 (scale 8) is shown, where only Nyquist-frequency, 0~128Hz, is necessary to include in decomposition [97])

Decomposed level (j)	Scale	High frequency components			Low frequency components		
		Decomp-osed signal	Reconst-ructed signal	Frequency bandwith	Decomp-osed signal	Reconst-ructed signal	Frequency bandwith
1	1	$\boldsymbol{W}_1$	$\boldsymbol{D}_1$	$1/4 \le \lvert f \rvert \le 1/2$ *(64~128Hz)*			
2	2	$\boldsymbol{W}_2$	$\boldsymbol{D}_2$	$1/8 \le \lvert f \rvert \le 1/4$ *(32~64Hz)*	$\boldsymbol{V}_1$	$\boldsymbol{S}_1$	$0 \le \lvert f \rvert \le 1/4$ *(0~64Hz)*
3	3	$\boldsymbol{W}_3$	$\boldsymbol{D}_3$	$1/16 \le \lvert f \rvert \le 1/8$ *(16~32Hz)*	$\boldsymbol{V}_2$	$\boldsymbol{S}_2$	$0 \le \lvert f \rvert \le 1/8$ *(0~32Hz)*
. . .		. . .	. . .	. . .	$\boldsymbol{V}_3$	$\boldsymbol{S}_3$	$0 \le \lvert f \rvert \le 1/16$ *(0~16Hz)*
J	J	$\boldsymbol{W}_J$	$\boldsymbol{D}_J$	$1/2^{J+1} \le \lvert f \rvert \le 1/2^J$ *(1~2Hz) for J=7*	. . .	. . .	. . .
	$J+1$				$\boldsymbol{V}_J$	$\boldsymbol{S}_J$	$0 \le \lvert f \rvert \le 1/2^{J+1}$ *(0~1Hz)*

In undecimated decomposition (discrete dyadic wavelet decomposition), the coefficients are not down sampled at each level of decomposition. However, the filter is up sampled as the decomposed level is increased (Figure 3.3). The number of coefficients in each decomposed level is the same as that of the original discrete signal for all levels of decomposition. Undecimated wavelet decomposition is mostly used in computer vision in order to detect the contours of small structures as well as the boundaries of larger objects [94].

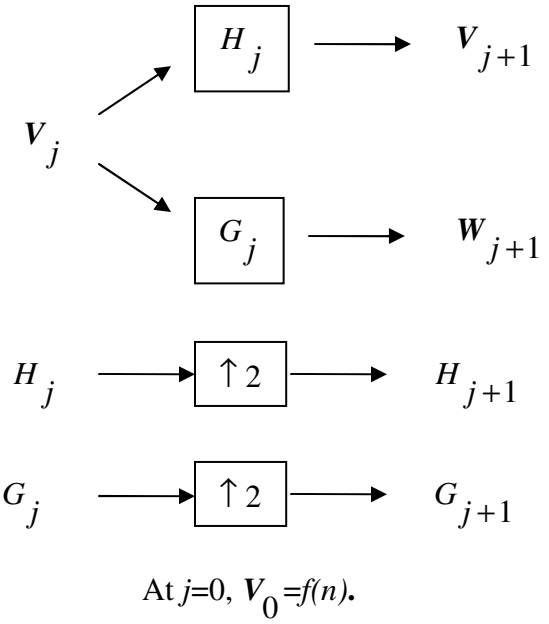

Figure 3.3. Discrete dyadic wavelet decomposition.

3.6 Discussion on application of wavelet analysis

This section will highlight on the advantages of different analysis methods—DWT, MRA and discrete dyadic wavelet decomposition—in different applications, choice of maximum decomposed level (*J)* and choice of filter types in wavelet decomposition.

Detail and approximation coefficients after applying DWT with *J*=4 maximum decomposition level to an acceleration signal sampled at 256 Hz sampling rate are shown in Figure 3.4, where only Nyquist-frequency, 0~128Hz, is necessary to include in decomposition [97]. ***W*** and ***V*** are decomposed coefficients of different frequency bandwidth and numbers of coefficients (samples) are down sampled by 2 in each decomposed level as discussed in section 3.4. Even though the numbers of samples of the approximation signal V_4 are much lower than those of the original signal, it still carries the pattern of the original signal. Actually, the transformation of a signal to a

shorter length of signal carrying important information of the original signal is called feature extraction in pattern classification. Therefore, DWT is very useful in some pattern classification applications and used in sit-stand/stand-sit transition pattern classification.

As discussed in section 3.4, multiresolution analysis (MRA) uses the DWT to decompose a signal in a cascade from the low-scale components (high-frequency components) to the high-scale components (low-frequency components). The main advantage of MRA is that the original signal can be decomposed to get a signal component of the required frequency bandwidth with no significant phase shift [97,101], so that the locations of the events are not shifted significantly after decomposition (Figure 3.5). Using FIR (finite impulse response) digital filter can result in liner phase shift, but it reduces the data processing speed in real-time processing as this type of filtration requires

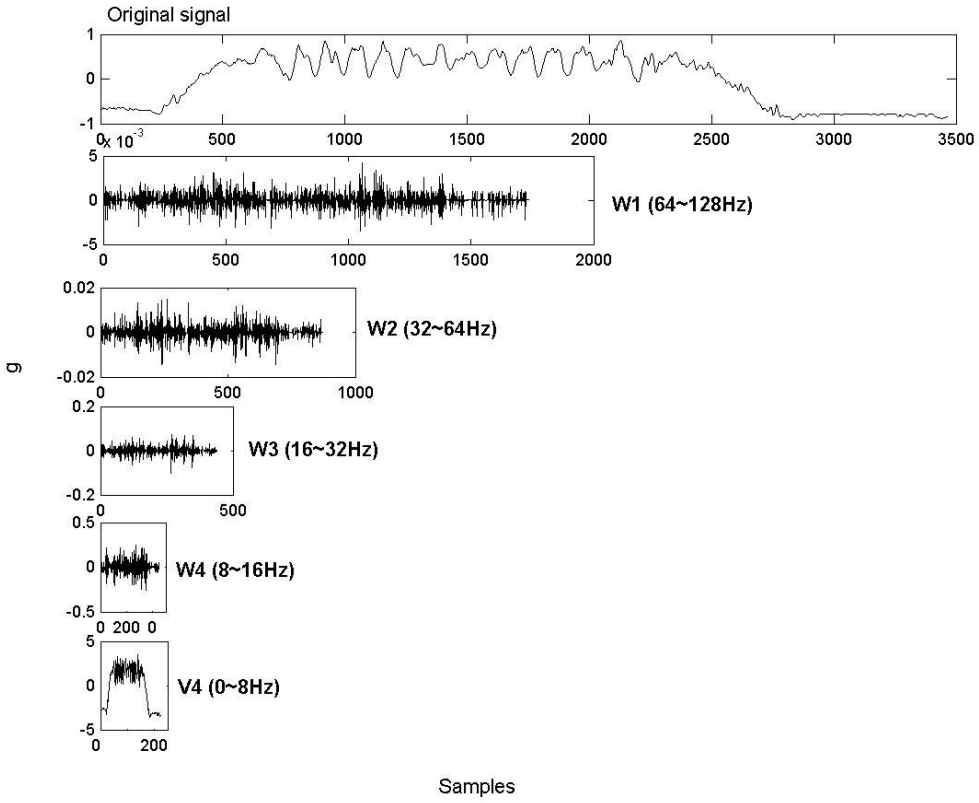

Figure 3.4. Detail and approximation signals of DWT decomposition.

large number of coefficients to closely imitate the frequency response of MRA. Moreover, filtering the input signal forward and reverse directions in achieving zero-phase distorted filtered response causes processing speed to be worse. Therefore, MRA is very useful in extraction of a signal component of the required frequency bandwidth from one signal with minimum phase shift (Figure 3.5) and is used in lie-sit/sit-lie and sit-stand/stand-sit transition segments extraction.

It is presented in our earlier section (section 3.5) that there are two types of wavelet decomposition, decimated (DWT) and undecimated (discrete dyadic wavelet decomposition). In decimated decomposition, the numbers of coefficients are down

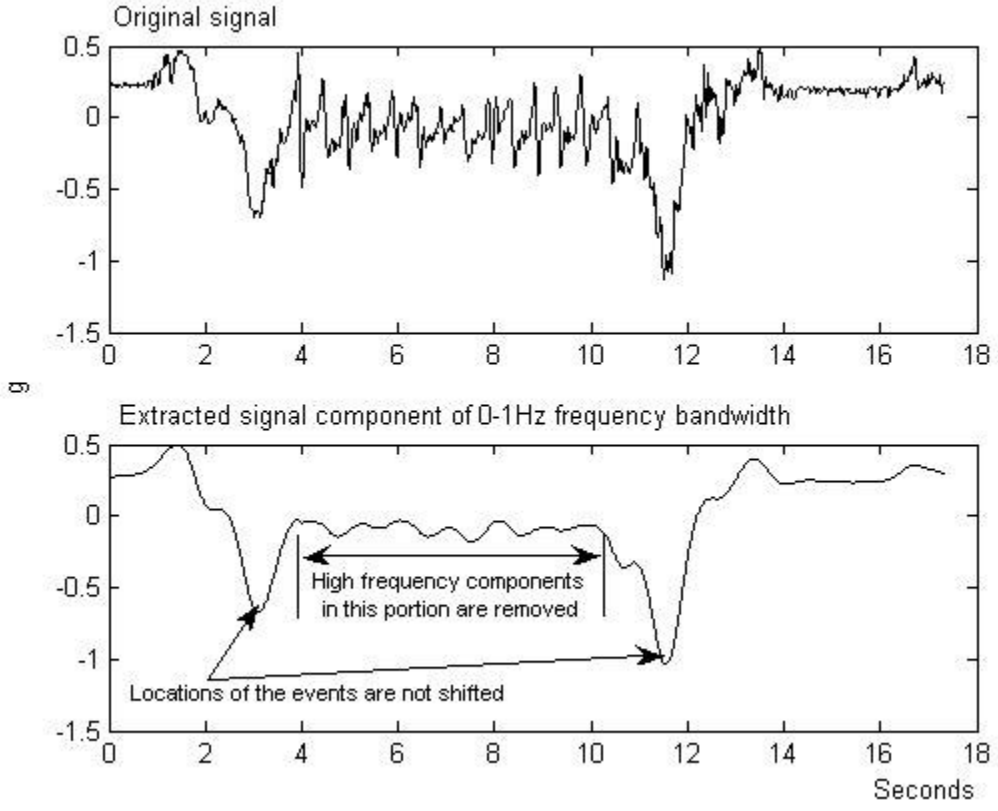

Figure 3.5. Original signal and its extracted signal component using MRA.

sampled, but it is not performed in undecimated decomposition. Therefore, the numbers of coefficients in each decomposed level are equal in undecimated decomposition. The main applications of undecimated wavelet decomposition are denoising and edge detection in image processing [95,102,103]. Rationale is that if wavelet coefficients across decomposed levels are generated from the signal, the coefficients are highly correlated across the decomposed levels (j). Otherwise, the amplitudes of coefficients will die out swiftly across the levels if they are produced from noise. The direct spatial correlation or direct multiplication of wavelet coefficients over adjacent levels sharpens and enhances major signal while suppressing noise. Therefore, direct correlation or direct multiplication of adjacent low frequency (high scale) levels similar to the first step in Table 4.3 of Chapter 4 is required to suppress noise [103]. Decimated wavelet decomposition is not appropriate in multiplication as the numbers of coefficients are not equal across decomposed levels. The equal length of coefficients across decomposed levels is one of the advantages of undecimated wavelet decomposition in denoising application. Since level walking, ascending stairs and descending stairs segments separation is based on the denoising method, discrete dyadic wavelet decomposition is useful in segments separation algorithm.

Relations between the frequency bandwidth and wavelet analysis (DWT or MRA) is shown in Table 3.1 and an example of decomposition of a signal at 256 Hz sampling rate for J=7 (scale 8) is included in the table. In MRA, choice of maximum decomposition level (J) can only be conducted empirically by observing that which level can carry important information more of a given signal for a designated application. For example, in figure 3.5, maximum decomposition level, $J=7$, is appropriate to get a signal

in which amplitude of unwanted signal in 4 seconds to 10 seconds interval of the original signal are reduced while still preserving the patterns of required events in 2 seconds to 4 seconds interval and 10 seconds to 12 seconds interval. In choosing filter for MRA, filter length and phase shift at the filtered signal are considered for our application. If longer filter length is used, processing time will be long in real-time application. If shorter filter length is used, filtered signal is not smooth enough. The choice of filter types, Daubechies, Coiflet, Symlet, etc. is not critical in our application and hence, the filter with minimum phase shift at the filtered signal can be used (Figure 3.5). Therefore, "Daubechies order 5" mother wavelet with 10 filter coefficients was chosen considering these two factors for our application. However, in discrete dyadic wavelet decomposition, nonorthogonal wavelets, first introduced by Mallet et al., were used. Nonorthogonal wavelets, linearly dependent and redundant frames opposed to orthogonal wavelets, e.g., Daubechies wavelets, are well suited for applications where correlations between decomposed levels, one of the steps applied in motion activities separation in Chapter 4, are used [94]. The points presented above are important concepts of wavelet analysis methods and applied in subsequent chapters.

Chapter 4

Wavelet analysis for Activities of Daily Living (ADL) detection

This chapter will focus on the wavelet analysis of activity classification. The activities included in our detection process are ADL such as level walking, ascending and descending stairs, and posture transition activities such as stand-sit, sit-stand, sit-lie and lie-sit transition activities as these are the common ADL among the elderly [19,42]. This chapter is organized as starting with the experimental setup used in ADL detection, followed by the validation of accelerometer data used in the experiment. Finally, detection of ADL in time-frequency domain (wavelet analysis) is presented.

4.1 Development of wearable Micro-Electro-Mechanical system (MEMSWear)

MEMSWear, as we call it, involves the attachment of MEMS sensors to a garment that is worn by a person to monitor his/her movements, and to detect fall incidents. MEMSWear was developed in view of the need for comfort in long term use (Figure 4.1). In our experiment, MEMSWear was fitted with MMA1220D (Motorola, ±8g, 250 mV/g) low g micromachined out-of-plane accelerometer and two ADXL105 (Analog Devices, ±5g, 250 mV/g) accelerometers at the shoulder position. For accelerometers, sensitivity (mV/g) and measurement range (±g) are inversely proportional. Therefore, we compromised between these two factors as measurement range can cover all types of activities including falls and sensitivity is also high enough to measure ADL, so that the system can measure falls and ADL without loss of any

information. In previous applications, Najafi et al. [19] used the accelerometer with specifications ±2g and 300 mV/g for ADL detection and Mathie et al. [42] used the sensor with ±10g measurement range for fall detection. Therefore, the specifications of our sensors chosen are between those of these two previous applications. Shoulder position is chosen under three considerations. Firstly, the sensor on the body will be least interfered by the subject's activities. Secondly, the sensor will cause minimal discomfort to the subject and finally, the sensor will not injure the wearer during the severe incidents such as falls.

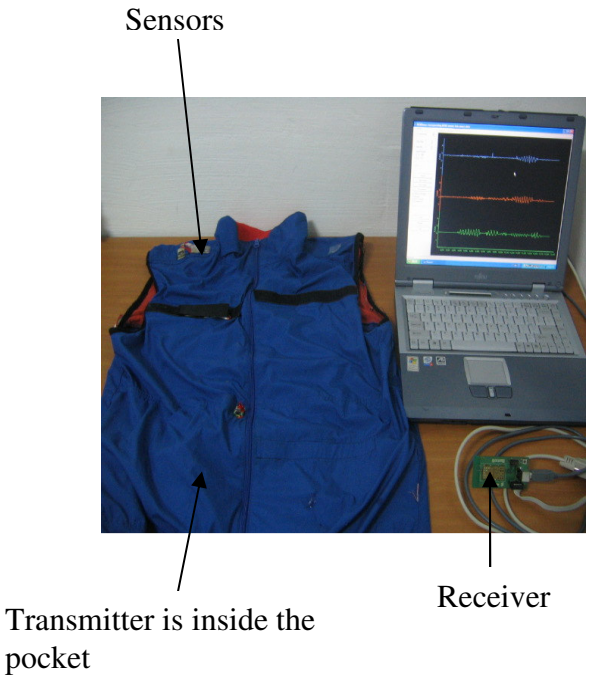

Figure 4.1. Experimental setup.

Accelerometers are arranged to measure three directional movements, lateral, vertical and antero-posterior, of the body. Bluetooth™ facilitated wireless communications from the vest to a Notebook™ was used for signal transmission. The

transmitter (90mm x 50mm x 20mm) and the DC power supply were placed inside the pocket of the vest (MEMSWear). The receiver was connected to the serial port of a Notebook™ and accelerometer data were captured with 256Hz sampling rate. In our prototype, ten-meter data transmission range Bluetooth™ chips were used for less power consumption. The experimental setup is shown in Figure 4.1.

4.2 Validation of acceleration signals using motion analysis system (Vicon™)

In motion analysis, the Vicon™ system is being used as the 'gold standard' to validate systems/models developed using the other movement detection methods [19]. Vicon™ system captures the positions of markers on the subject's body with image capture rate of 50 Hz (Figure 4.2).

(a) (b)

Figure 4.2. Front and rear views of markers on the subjects

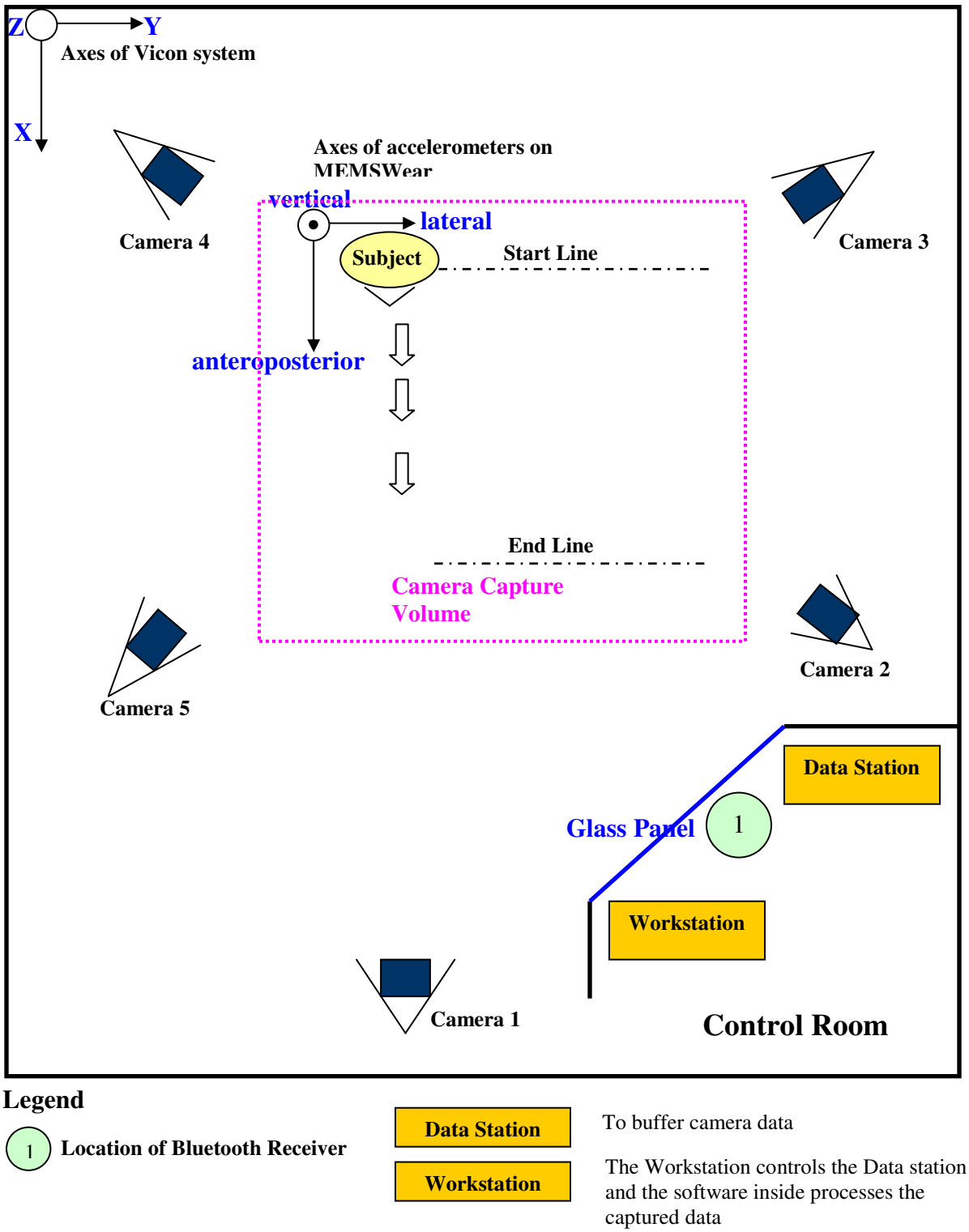

Figure 4.3. Schematic Layout of the Laboratory (Top View)

Then it gives the 3-D co-ordinates (X,Y,Z) of the marker throughout the motion (Figure 4.3). After which, the absolute velocity and acceleration are being computed as follows.

$$\text{Velocity} = \text{change in displacement (S)/change in time (T)}$$

$$= (S_2 - S_1) / (T_2 - T_1), \qquad 4.1$$

and

$$\text{acceleration} = \text{change in velocity (V)/change in time(T)}$$

$$= (V_2 - V_1) / (T_2 - T_1), \qquad 4.2$$

where 1 refers to position 1 and 2 refers to position 2. The rate of change of displacement/velocity is calculated as displacement/velocity difference between position 1 and position 2 divided by change in time. Change in time is simply the length of time it took to move from position 1 to position 2. The motivation of this work is to validate the accelerometer signals with a reference system (Vicon™ system).

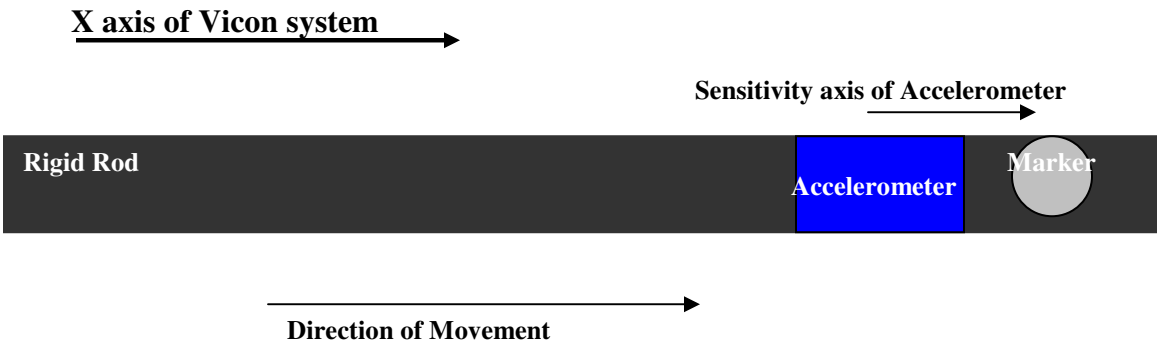

Figure 4.4. Movement direction of the Rigid Rod and the axis of the Vicon™ system (Top View)

4.2.1 Experimental procedure for validation of accelerometers

Two different experiments were conducted to validate the accelerometer readings with Vicon™ system readings. One experiment was done on a rigid rod and the other was

done on a human subject. The experimental setup using the Vicon™ system is shown (Figure 4.3). The following sections describe the procedures for the two experiments.

4.2.1.1 Experiment done on a rigid rod

With reference to Figure 4.3 and Figure 4.4, the procedure was:

(1) The Bluetooth™ receiver was placed at location 1 in the laboratory (Figure 4.3).

(2) Then, one of the accelerometers on the vest together with a marker was attached to a rigid rod.

(3) The rod was moved back and forth for a few times along the X axis of the Vicon™ system (Figure 4.4). The acceleration of the marker along that axis was calculated using equation (4.1) and equation (4.2). Then, the sensor acceleration was validated with the acceleration of the marker as shown in Figure 4.5.

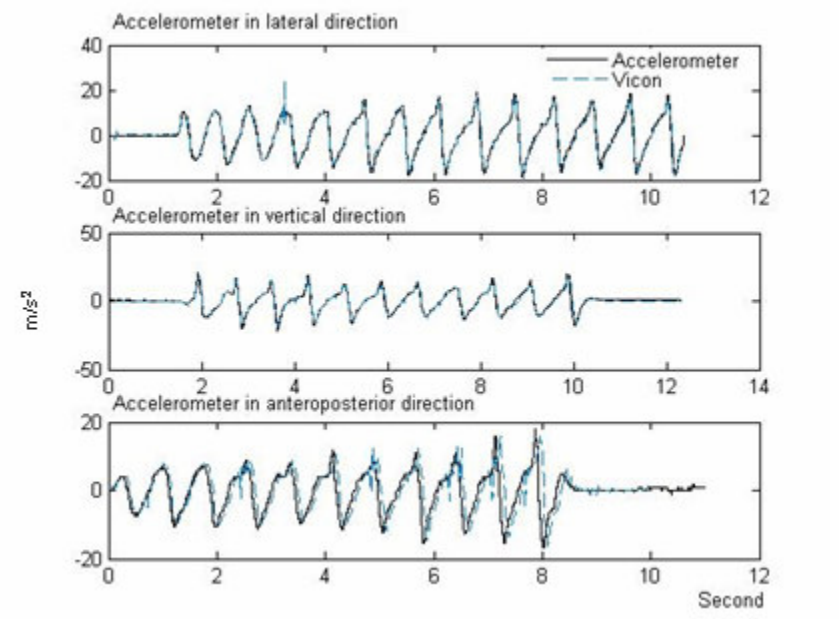

Figure 4.5. Graph of Acceleration (m/s^2) Vs Time (s) for the comparison done on a rigid rod.

Then procedure was repeated for all the remaining accelerometers on the vest. The experimental results are shown in Figure 4.5. The observation showed that all accelerometer readings from the sensors on MEMSWear coincided with the Vicon™ system readings. After the accelerometers have been validated by Vicon™ without the involvement of subjects, the experiment has moved on to another phase whereby the human subject is used to perform the activities to check if the accelerations from the two systems agree.

4.2.1.2 Experiment done on the human subject

A series of selected ADL were performed by one healthy male subject (aged 25, weight 60kg) in the Vicon™ laboratory. A retro-reflective marker was placed near the accelerometers located on the shoulder of the subject (Figure 4.2). Movements in ADL are more significant in vertical and antero-posterior directions than in lateral direction, i.e., vertical and antero-posterior acceleration signals carry more important information of ADL movements than lateral acceleration does and hence, only these two acceleration signals are used in ADL detection. Therefore, the comparison was done only for the accelerometer signals in these two directions. The figures comparing accelerometer readings and Vicon™ system readings for accelerometers and the marker at right shoulder position (RSHO) are shown in Figure 4.6. There are three major issues regarding the signal pattern inconsistency of readings from two systems (MEMSWear and Vicon™ system). These are noises caused by differentiation in Vicon™ system readings, the variation of DC component, i.e., acceleration-related gravity, in

accelerometer readings (Appendix A) and the artifacts due to the movements of clothes during the activities (Figure 4.6(a)).

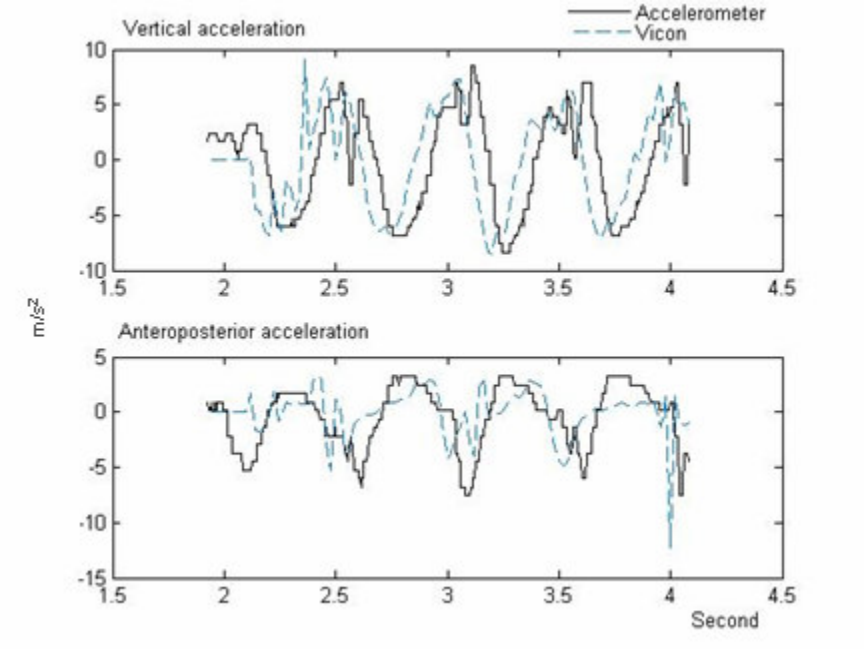

(a)

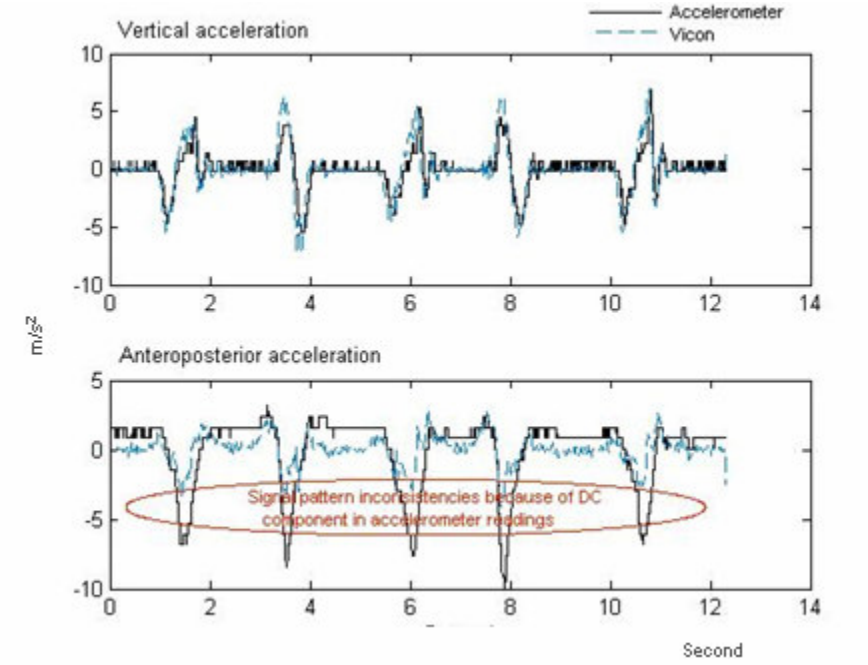

(b)

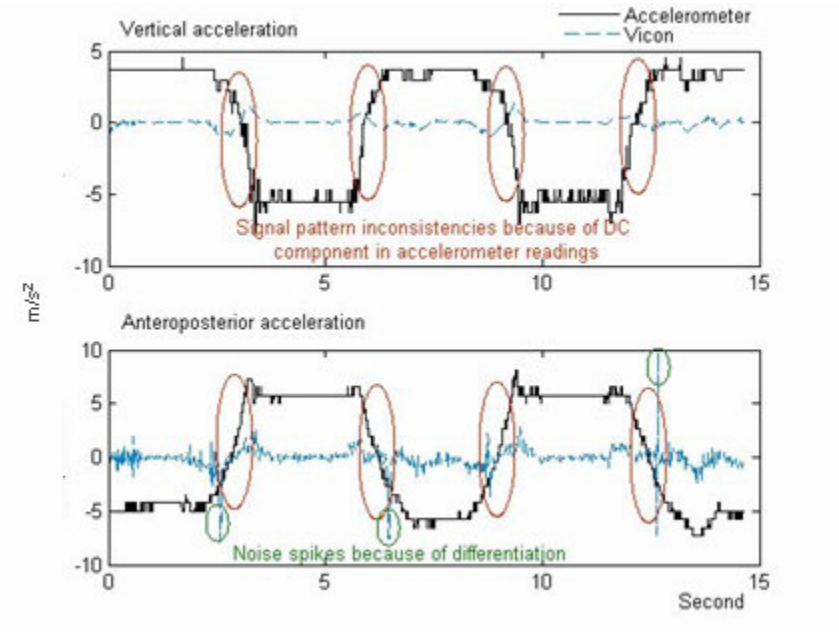

(c)

Figure 4.6. Comparison of accelerometer readings and Vicon™ system readings for accelerometers and a marker at right shoulder position (a) level walking, (b) sit-stand/stand-sit transition activities, and (c) sit-lie/lie-sit transition activities

The distinct noise spikes because of differentiation can be seen in Figure 4.6(c). The signal pattern inconsistency caused by DC component is because of the variation of sensor's DC component level due to the changes in orientation of the sensor. During posture transition, there is a tilt in the trunk. The tilt of the trunk will cause the DC component of the accelerometer reading to change from one value to another (Figure A.1). Therefore, the combination of DC and AC (acceleration along the sensitivity axis of the accelerometer- Appendix A) components make the accelerometer's readings much larger than Vicon™ 's acceleration patterns (Figure 4.6(b) and Figure 4.6(c)).

With reference to Figure 4.6(a), there is a phase difference between the accelerometer and Vicon™ system readings. The Vicon™ system readings are faster than

the accelerometer readings. The cause of the time lagging in accelerometer readings might be the location of the Bluetooth™ receiver. Since our validation was only for signal patterns between the two systems, we did not perform thorough investigation for time lagging.

4.3 ADL detection in time-frequency domain

In this section, activity detection is separated into three different parts, namely, lie-sit/sit-lie transition detection, stand-sit/sit-stand transition detection, and human motion activities (level walking, ascending stairs and descending stairs) detection.

4.3.1 Lie-sit/sit-lie transition detection

The lie-sit/sit-lie posture transition is detected by considering the orientation of the accelerometer with respect to the gravitational axis (Appendix A). In the lying posture, the vertical accelerometer measures almost 0 g, while in sitting and standing posture the accelerometer measures approximately 1 g. Therefore, detection of transition between 0 g and 1 g can be used to detect lie-sit/sit-lie transition. In detection, the DWT was applied to vertical acceleration signal with decomposition into level J=7 by "Daubechies order 5 (db5)" mother wavelet [97]. The reconstructed vertical acceleration signal (<1Hz, $\boldsymbol{S}_7$) was applied to cancel additional peaks with different frequency components (Figure 4.7). A Daubechies mother wavelet (db5) was used in decomposition and reconstruction [97]. The corresponding low pass and high pass filters are finite impulse response (FIR) filters with lengths of ten. After reconstruction, sit-lie/lie-sit transitions were detected using a predefined threshold value (0.8g) (Figure 4.7). In Figure 4.8, the reconstructed vertical

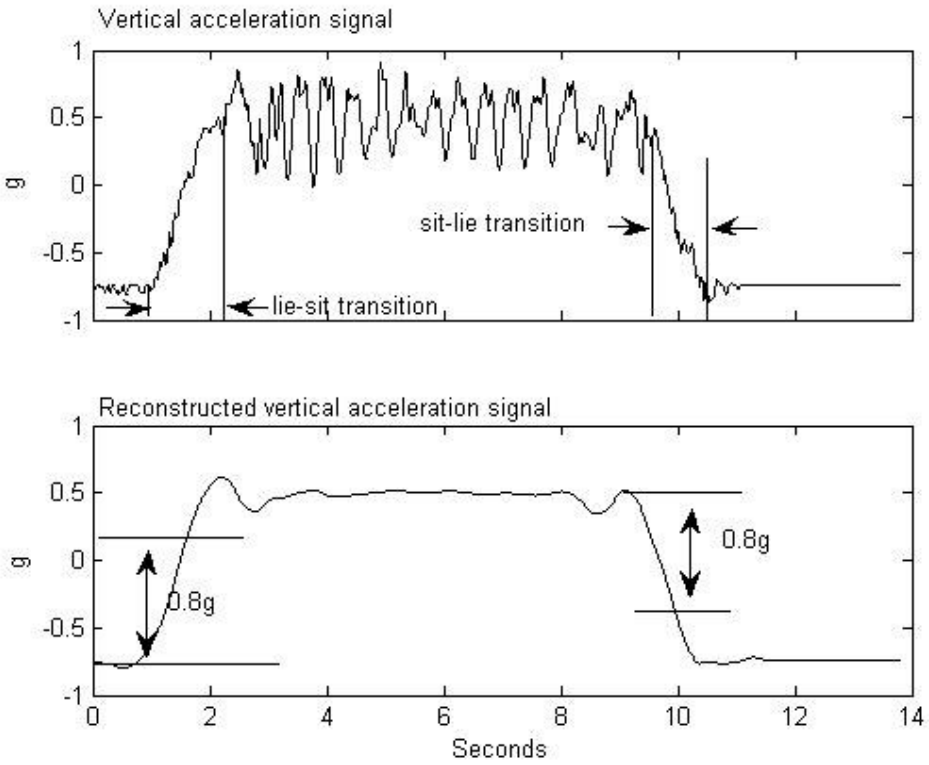

Figure 4.7. Vertical acceleration signal and its reconstructed signal used in lie-sit/sit-lie transition detection.

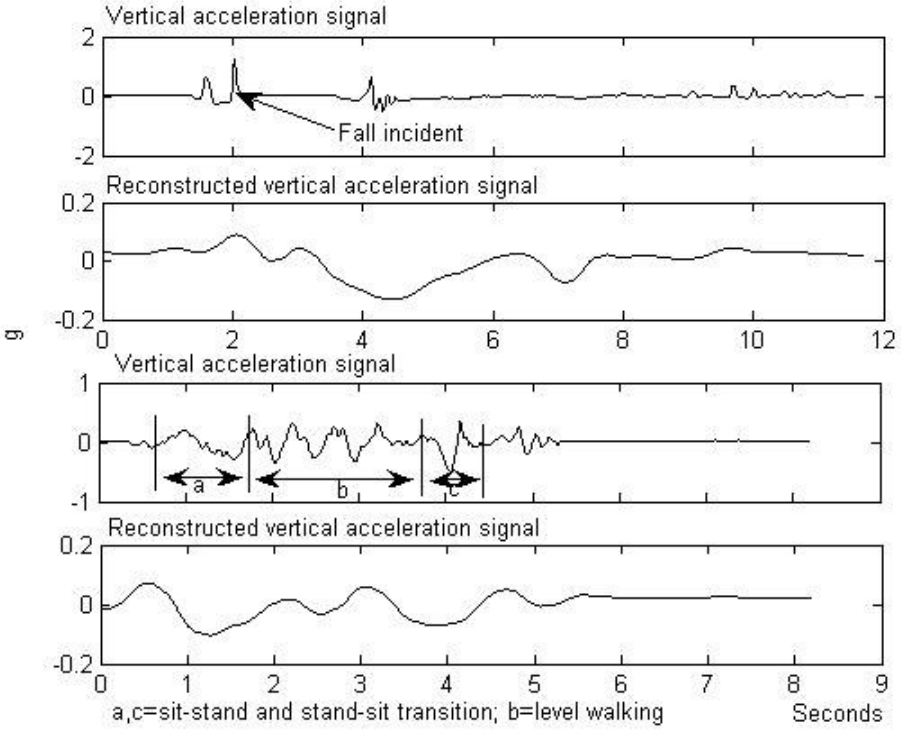

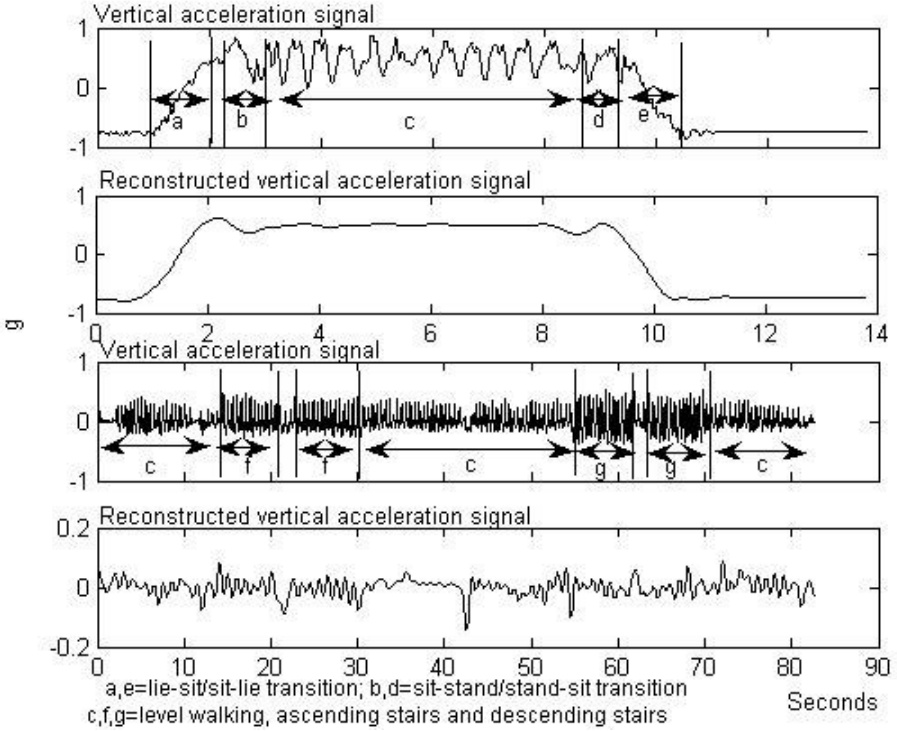

Figure 4.8. Vertical acceleration signals and their reconstructed signals (<1Hz) for falls and ADL.

acceleration signals of level walking, walking on stairs, fall, and sit/stand-stand-sit activities are within ±0.2 g range except the reconstructed signal with lie-sit/sit-lie transition. Therefore, threshold value 0.8g can be used in lie-sit/sit-lie transition detection.

4.3.2 Sit-stand/stand-sit transitions detection

In this study, we conducted an investigation of the detection of stand-sit, and sit-stand posture transition activities using two dimensional acceleration signals located in antero-posterior and vertical directions on the shoulder part of a garment. There are two steps in the detection process, extraction of the transition segment from the continuous acceleration signal and classification. In segment extraction using wavelet

decomposition/reconstruction algorithm, wavelet-reconstructed antero-posterior acceleration signal (the frequency band corresponds to less than 1Hz, S_7) was used to detect the locations and start/end points of transition segments. Using these start/end points, the stand-sit/sit-stand transition segments from the vertical acceleration signal were extracted and used in classification. Stand-sit and sit-stand transition segments were classified using the features from time-frequency domain.

Table 4.1 Type of activities performed by each subject

Test number	**Type of activity**	**Equipment used in the experiment**
1	sit-stand+ stand-sit+ sit-stand+ stand-sit+ sit-stand+ stand-sit	Chair without armrest (height: 46cm)
2	sit-stand+ level walk (about 2) + stand-sit	Chair without armrest (height: 46cm)
3	lying+ lie-sit + sit-stand+ level walk+ stand-sit+ sit-lie	Bed(height:38cm)
4	level walk + stairs up+ level walk + stairs down+ level walk	The stairway is half-turn stair, which changes its direction at a landing by 180 degree and consisted of 30 steps. The landing is at 15th step and there are fourteen steps between two landings. The slope of the flight is 30°.

4.3.2.1 Subjects and experimental procedure

The experiments were performed on five male and four female subjects (age ranged between 25 and 46 years, height between 1.5m and 1.74m, and weight between 48kg and 60kg). The experiment was carried out as shown in Table 4.1. The activities done in the experiment were assumed as the basic required ADL for the elderly [19,104,105]. Activities were executed without any proper instructions from the investigator. All subjects repeated their activities for test number 2 and test number 3. For each trial, the camera and the sensor data capture system in the Notebook^{TM} were activated simultaneously by the investigator. All subjects signed a consent form that was

approved by the Tan Tock Seng Hospital Medical Research Ethics Committee. MEMSWear (Figure 4.1) was used in our experiment. During the experiment, the Notebook™ was always in the transmission range (10-meter) of the transmitter on the subject. Signals were digitized at 256-Hz sampling rate and recorded into a Notebook™.

4.3.2.2 Detection methodology

Transition segments extraction from the continuous acceleration signals

Figure 4.9 shows the normalized antero-posterior and vertical acceleration signals for test number 3 (Table 4.1). There are two steps in segment extraction, detection of the location of transition segments (point P) and detection of start/end points of transition

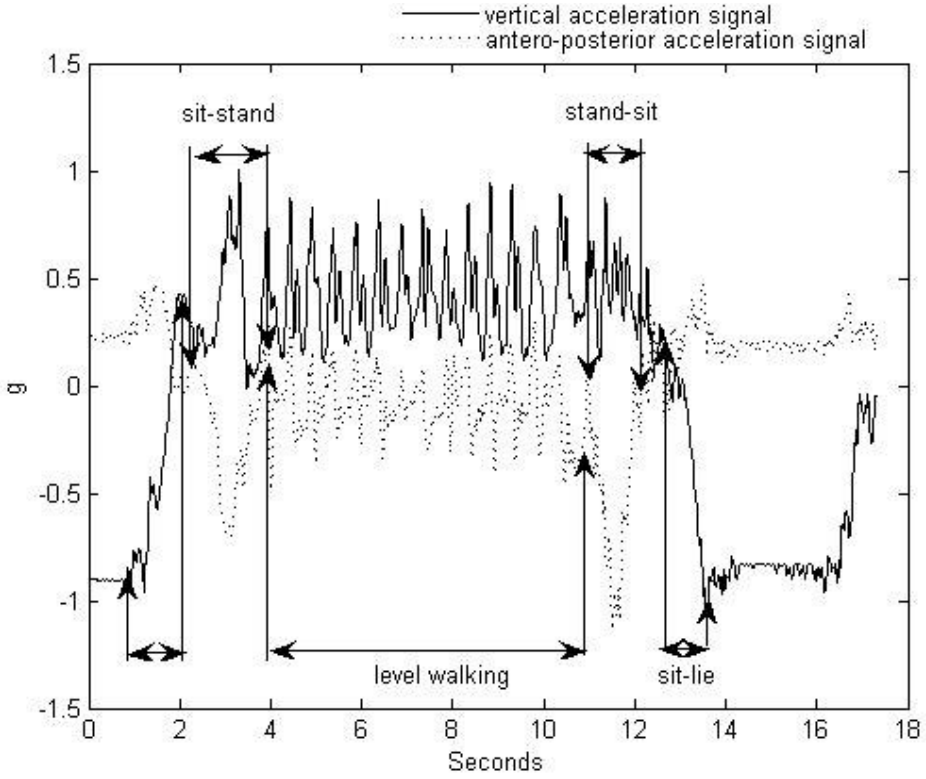

Figure 4.9. Activities related to test number 3 shown in Table 4.1.

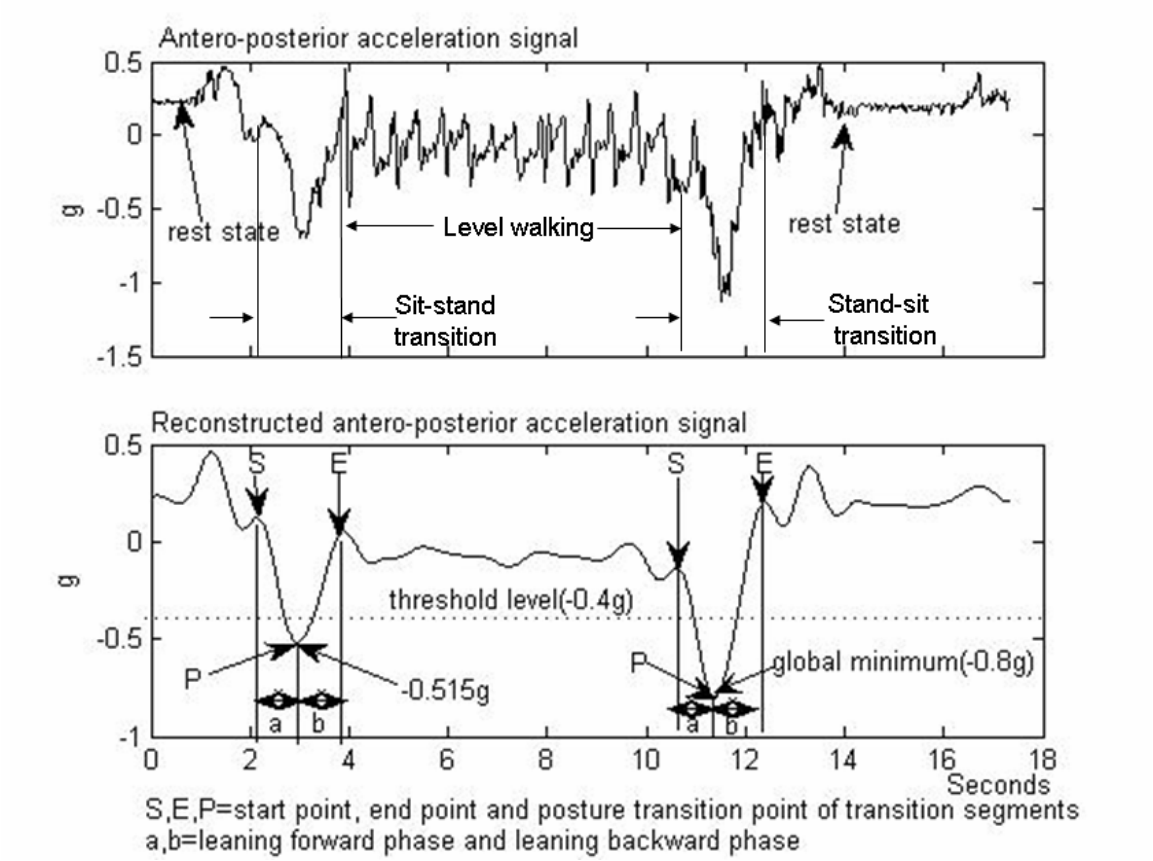

Figure 4.10. Antero-posterior and its reconstructed acceleration signal.

segments (points S and E) (Figure 4.10). In order to detect the locations of transition segments, the DWT was applied to antero-posterior acceleration signal with decomposition into level *J*=7 by "Daubechies order 5 (db5)" mother wavelet [97]. The approximation signal corresponding to level *J*=7 was reconstructed in which the amplitudes of other signals (level walking in Figure 4.10) having higher frequency than the transition segments were reduced. The reconstructed approximation signal ($\boldsymbol{S}_7$) corresponds to a frequency band less than 1 Hz. In location detection, threshold value was defined as half of the global minimum (threshold value g_{th}=global minimum/2).

The global minimum value (g_m) should be less than or equal to -0.3g. All minimum points lower than the threshold level were considered as the locations of sit-stand and stand-sit transitions (Figure 4.10).

After tracing the locations of sit-stand/stand-sit transition segments, start and end points of transition segments were detected. There are two phases in sit-stand/stand-sit transitions, a leaning forward phase followed by a leaning backward phase (Figure 4.10) [105]. The transition segment was determined by an interval from the beginning of the leaning forward phase (point S) of the transition to the end of the leaning backward phase (point E) (Figure 4.10). These two points were detected using gradient thresholding approach. The intervals (between S and E) greater than 0.7sec were chosen as transition segments. The intervals of transition segments were found to be between 0.7 seconds and 2 seconds, which is also consistent with previous researcher's statement [104]. Moreover, the transition segments were confirmed by rest states with 1-second time duration in 4-second time interval before or after the posture transition point (P) or both (Figure 4.10 and Figure 4.11). The rest state is the rest period during which the variance of the acceleration signal was less than a predefined value (<0.002g). Therefore, the segment of time duration between 0.7-2 seconds with 1-second long rest state before or after the segment was taken as a true transition segment. Using these start point (S) and end point (E), the segments related to transition activities from the vertical acceleration signal were extracted and used in classification. The reason why the signals from the vertical acceleration were used in the classification is that they have more significant feature compared to antero-posterior acceleration signal, i.e., a positive peak followed by a

negative peak in sit-stand transition activity and a negative peak followed by a positive peak in stand-sit transition activity.

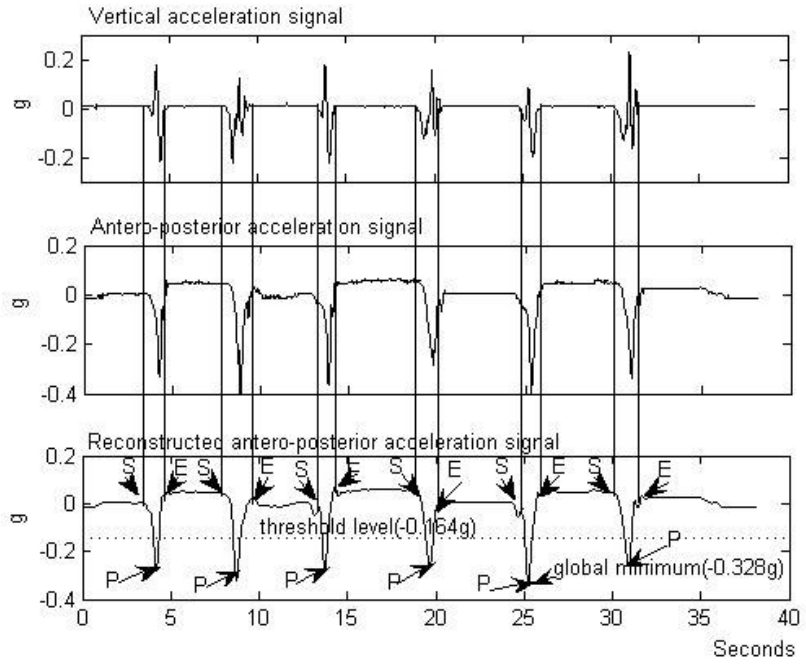

(a)

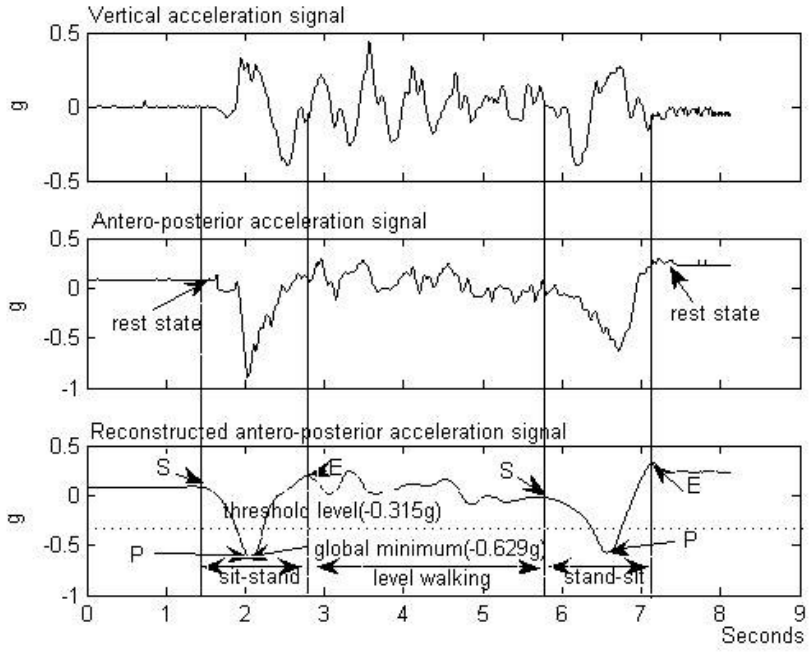

(b)

Figure 4.11. Vertical acceleration signals, antero-posterior acceleration signals and reconstructed antero-posterior acceleration signals for (a) test number 1 and (b) test number 2, test number are shown in Table 4.1.

Sit-stand and stand-sit classification using features from time-frequency domain

After extracting the transition segments from vertical acceleration signals, classification was implemented using DWT coefficients (the coefficients of ***V*** and ***W***). In practice, the data sampling gives a finite number of samples: $f(n)$, which is the starting point of decomposition. $f(n)$ was decomposed as $\boldsymbol{W}_1, \boldsymbol{W}_2, \boldsymbol{W}_3, ..., \boldsymbol{W}_J$ and a coarse approximation of $\boldsymbol{V}_J$. In feature extraction, the extracted segment was decomposed to level *J*=3 by "Daubechies order 5 (db5)" mother wavelet [97] and coefficients were arranged as $\boldsymbol{V}_3, \boldsymbol{W}_3, \boldsymbol{W}_2, \boldsymbol{W}_1$. Level *J*=3 corresponds to the frequency band less than 16 Hz and that is the satisfactory frequency band in revealing the important feature, a positive peak followed by a negative peak for a sit-stand transition while the reverse occurs during a stand-sit transition, to be used in classification. The first fifty wavelet coefficients were used as features. In order to reduce the number of wavelet coefficients to be used as features representing each segment, every ten successive components were averaged. Therefore, the feature vector size was reduced to 50/10=5 components for every sit-stand or stand-sit transition signal.

4.3.2.3 Results

The vertical acceleration signals, antero-posterior acceleration signals and reconstructed antero-posterior acceleration signals of test number 1 and test number 2 are presented in Figure 4.11. Figure 4.12 shows a set of extracted sit-stand/stand-sit transition segments from vertical acceleration signal. For the assurance of our threshold level, we checked the global minimum values of the reconstructed antero-posterior approximation signals for test number 4 (Figure 4.13). The global minimum values of nine subjects for

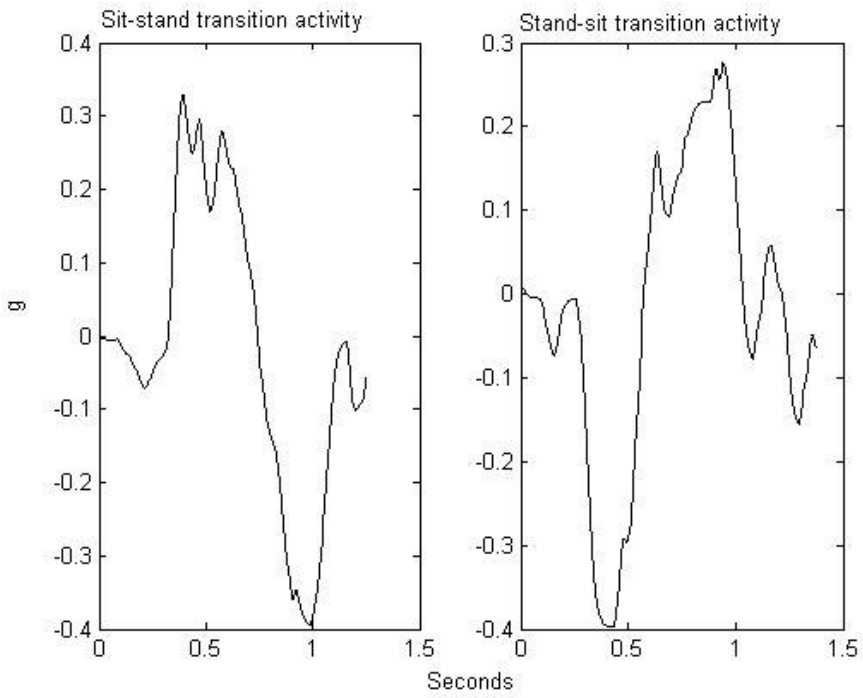

Figure 4.12. Extracted vertical acceleration signals for sit-stand and stand-sit transition activities.

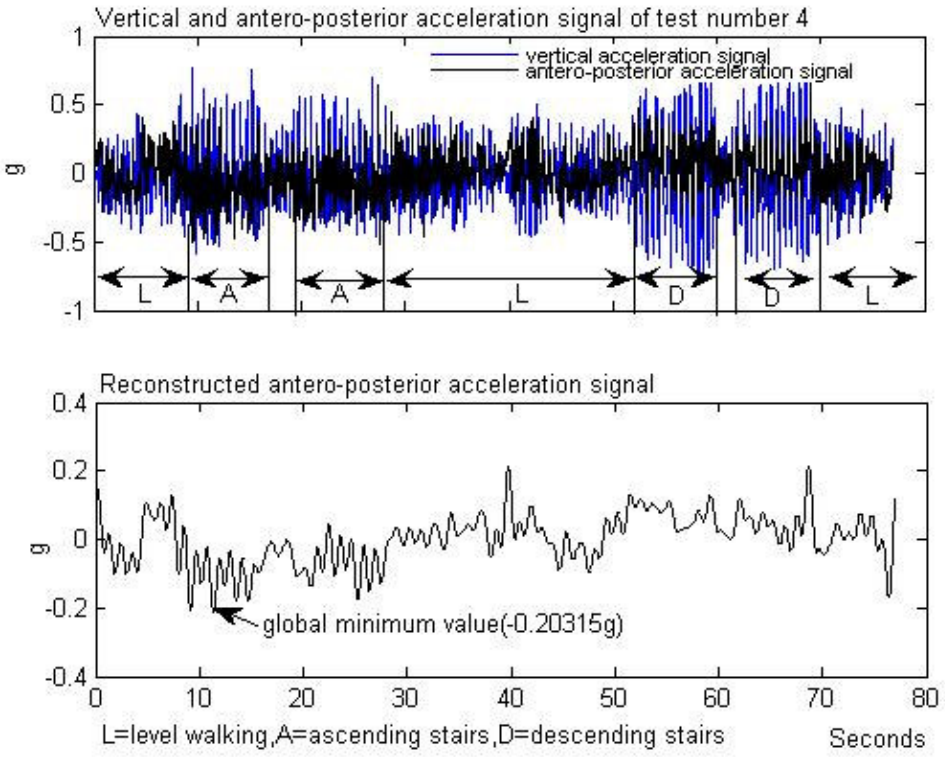

Figure 4.13. Vertical, antero-posterior and reconstructed antero-posterior acceleration signals for test number 4.

test number 4 were -0.257, -0.20315, -0.2244, -0.1801, -0.2043, -0.2529, -0.186, -0.172, -0.164. They are still above the value g_m (-0.3g).

To estimate the performance of the segment extraction methods, absolute error, percentage error, sensitivity, and specificity were estimated as follows:

•Absolute error = |time interval of an extracted segment –actual time interval of that segment |.

•Percentage error = (absolute error/actual time interval of that segment)*100%.

•Sensitivity = (true positives/(true positives + false negatives))*100%.

•Specificity= (true negatives/(true negatives + false positives))* 100%.

The recorded video clips were observed using "VirtualDub 1.5.10" media player to get the actual time intervals of transition segments. The digit in the second decimal place is 3 in this player. The investigator noted the duration of each transition activity and actual time intervals of the activities were taken from the time when the subject's trunk was vertically straight during the initial phase of transition to the time when his/her trunk became vertically straight again after the transition. In sensitivity/specificity estimation, true positives were equal to the time intervals of transition activities that were correctly extracted and false negatives were equal to the intervals of remained unextracted portions of the activities. True negatives were equal to time intervals that were not transition activities and not extracted using the extraction method and false positive was equal to time intervals that were not transition activities and wrongly extracted by the extraction method. Start/end time of segments observed in the video clips and that of segments extracted by the method were compared in Table 4.2. Overall absolute error, percentage error, sensitivity and specificity for 9 subjects were also presented (Table 4.2). Fifty-nine

Table 4.2 Error, sensitivity, specificity of separated segments and comparison of start/end time of segments observed in the video clips and extracted by the algorithm.

	Sit-stand transition activity						Stand-sit transition activity						
Subject / test number	Video records		Extraction algorithm		Sensit-ivity	Specif-icity	Video records		Extraction algorithm		Sensit-ivity	Specif-icity	T^*
	Start	End	Start	End	(%)	(%)	Start	(%)	Start	End	(%)	(%)	Seconds
	Seconds						Seconds						
1/1	3.633	4.966	3.366	4.833	90.02	99.25	7.93	9.133	7.924	9.189	100	99.83	36.8
	13.066	13.866	12.981	13.879	100	99.73	18.366	19.2	18.302	19.3	100	99.54	36.8
	24.233	25.033	24.057	25.023	98.75	99.51	29.166	30.2	29.113	30.245	100	99.73	36.8
1/2	1.867	2.9	1.95	3.049	91.97	97.38	4.7	5.6	4.584	5.528	92	98.00	6.634
	1.433	2.3	1.413	2.796	100	91.12	4.033	5.033	4.111	5.404	92.2	93.55	6.675
1/3	2.4	3.533	2.222	3.513	98.23	98.75	9.2	10.267	9.272	10.498	93.25	98.39	15.313
	2.267	3.067	2.2	3.151	100	98.82	8.2	9	8.151	9.581	100	95.09	13.638
2/1	5.833	7.2	5.785	7.26	100	99.73	11.033	12.566	10.916	12.638	100	99.52	41.2
	17.233	18.3	17.113	18.457	100	99.31	23.966	25.266	23.943	25.543	100	99.25	41.2
	29.4	30.4	29.272	30.46	100	99.53	35.5	36.6	35.404	36.649	100	99.64	41.2
2/2	1.033	2.166	0.972	2.292	100	97.61	4.866	6.033	4.832	6.047	100	99.38	8.955
	1.7	2.8	1.717	2.845	98.45	99.31	5.066	6.4	5.087	6.336	93.63	100.00	7.577
2/3	2.2	3.333	2.132	3.317	98.59	99.49	8.5	9.633	8.433	9.766	100	98.49	14.411
	1.866	3.033	1.845	3.072	100	99.50	8.1	9.133	8.034	9.185	100	99.02	13.068
3/1	5.833	7.2	5.849	7.136	94.15	100.00	11.433	12.567	11.373	12.656	100	99.60	38.6
	19.033	20.033	18.943	20.102	100	99.58	23.333	24.267	23.253	24.37	100	99.51	38.6
	29.767	30.633	29.698	30.811	100	99.35	34.9	35.933	34.789	36.041	100	99.42	38.6
3/2	1.233	2.233	1.192	2.234	100	99.48	5.5	6.467	5.517	6.77	98.24	96.27	9.072
	1.633	2.7	1.543	2.668	97	98.94	6.2	7.167	6.075	7.389	100	95.94	9.521
3/3	2.8	4.1	2.743	3.992	91.69	99.66	11.2	12.433	11.01	12.668	100	97.43	17.8
	1.9	2.9	1.935	3.075	96.5	98.87	10.133	11.067	10.07	11.362	100	97.69	16.411
4/1	3.333	4.267	3.411	4.351	91.65	99.83	7.367	8.567	7.46	8.506	87.17	100.00	51.36
	13.867	15.1	14.177	15.275	74.86	99.65	19.467	20.6	19.608	20.751	87.56	99.70	51.36
	25.9	26.867	26.132	27.06	76	99.62	31.167	32.333	31.302	32.479	88.42	99.71	51.36
4/2	1.1	2.3	1.045	2.351	100	99.41	4.267	5.367	4.23	5.464	100	99.25	19.03
	1.6	2.933	1.694	3.015	92.95	98.96	5.3	6.7	5.419	6.789	91.5	98.87	9.147
4/3	2.3	3.367	2.283	3.487	100	99.21	8.367	9.3	8.2	9.436	100	98.27	18.464
	1.8	2.7	1.819	2.955	97.89	98.06	7.667	8.567	7.479	8.763	100	97.07	13.996
5/1	**0.2**	**1.333**	**0**	**0**	0	100.00	**1.366**	**2.966**	**0**	**0**	0	100.00	15.23
	3.1	**4.566**	**0**	**0**	0	100.00	**4.666**	**6.166**	**0**	**0**	0	100.00	15.23
	6.266	**7.733**	**0**	**0**	0	100.00	7.933	9.267	7.83	9.275	100	99.94	15.23
5/2	1.367	2.3	1.2	2.343	100	96.89	4.807	5.733	4.808	5.89	99.89	97.68	7.694
	1.215	2.115	1.115	2.19	100	97.25	4.482	5.415	4.386	5.56	100	96.19	7.26
5/3	1.567	2.4	1.491	2.558	100	98.34	9.233	10.267	9.313	10.433	92.26	98.81	14.936
	1.533	2.433	1.543	2.57	98.89	98.94	8.533	9.6	8.502	10.033	100	96.36	13.823
6/1	2.667	3.633	2.709	3.677	95.65	99.77	**3.667**	**5**	**0**	**0**	0	100.00	20.33
	5.067	6.267	5.026	6.517	100	98.48	8.733	9.9	8.826	10.208	92.03	98.40	20.33
	10.033	**11.133**	**0**	**0**	0	100	11.2	12.267	11.309	12.434	89.78	99.14	20.33
6/2	1.467	2.4	1.313	2.453	100	97.82	5.1	6.333	5.181	6.366	93.43	99.64	10.43
	1.167	2.467	1.11	2.546	100	99.18	5.4	6.733	5.483	6.71	92.05	100.00	17.89
6/3	1.8	2.933	1.709	3.083	100	98.35	9.6	10.933	9.713	11.313	91.52	97.38	15.709
	1.743	3.1	1.683	3.238	100	98.77	9.933	11.1	9.77	11.177	100	98.53	17.479
7/1	4.621	5.633	4.634	5.653	98.71	99.96	9.233	10.366	9.279	10.317	91.62	100.00	47.25
	15.133	16.133	15	16.287	100	99.38	19.766	21.1	19.785	21.174	98.58	99.84	47.25
	26.1	26.933	26.026	26.906	96.76	99.84	34.8	35.833	34.728	35.838	100	99.83	47.25
7/2	1.467	2.2	1.509	2.23	94.27	99.52	4.067	4.9	3.962	5.015	100	96.42	6.974
	1.866	3.066	1.945	3.172	93.42	98.44	5.266	6.366	5.247	6.409	100	99.09	7.902
7/3	2.1	3	2.124	3.102	97.33	99.14	8.033	8.9	7.966	9.11	100	97.67	12.77
	2.033	2.966	2.072	2.981	94.3	99.88	7.8	9.166	7.819	9.132	96.12	100.00	13.332
8/1	2.833	4.166	2.819	4.189	100	99.93	7.633	9.066	7.59	9.092	100	99.86	51.45
	14.966	16.033	14.977	16.019	97.66	100.00	20.366	21.4	20.328	21.46	100	99.81	51.45
	24.8	25.633	24.755	25.641	100	99.90	31.9	32.866	31.902	32.913	99.79	99.91	51.45
8/2	1.533	2.367	1.438	2.468	100	97.65	6.1	7	6.041	7.155	100	100.00	9.181
	1.567	2.767	1.581	2.732	95.92	100.00	5.567	6.7	5.34	6.875	100	95.21	9.525
8/3	2.3	3.6	2.253	3.721	100	98.91	10.367	11.4	10.468	11.838	90.22	97.23	16.717
	2.267	3.2	2.09	3.309	100	97.84	8.2	9.167	8.071	9.277	100	98.19	14.147
9/1	1.767	2.833	1.683	2.875	100	99.64	5.03	6.067	5.32	6.381	72.03	99.12	36.55

	Sit-stand transition activity						Stand-sit transition activity						
Subject / test number	Video records		Extraction algorithm		Sensit-ivity	Specif-icity	Video records		Extraction algorithm		Sensit-ivity	Specif-icity	T^*
	Start	End	Start	End	(%)	(%)	Start	(%)	Start	End	(%)	(%)	Seconds
	19.9	20.7	19.973	21.015	90.87	99.12	23.467	24.433	23.778	24.769	67.81	99.06	36.55
9/2	1.267	2.2	1.211	2.238	100	98.63	4.767	5.6	4.774	5.709	99.16	98.44	7.804
	1.5	2.7	1.491	2.887	100	98.62	5.5	6.833	5.577	6.973	94.22	99.01	15.39
9/3	1.967	2.8	1.875	2.928	100	98.44	9.467	10.5	9.392	10.852	100	96.92	14.902
	2.6	3.567	2.566	3.668	100	99.19	9.833	10.867	9.842	11.211	98.84	97.94	17.725
Aaverage					90.852	98.98					91.367	98.55	
Absolute error (Sec)			0.21				Absolute error (Sec)		0.26				
Percentage error (%)			19.16				Percentage error (%)		22.99				

T^* =total time interval of each test number

out of 63 sit-stand transition segments and 60 out of 63 stand-sit transition segments were extracted successfully.

Fifty-nine segments of sit-stand activities and 60 segments of stand-sit activities from 9 subjects were classified (Figure 4.14). These are the segments successfully extracted by the extraction procedure (Table 4.2). The classification rate (segments that are extracted and classified correctly/total number of segments) of sit-stand and stand-sit activities are 93.65% and 95.24% respectively. In classification, Euclidean distance between a vector to be identified and the standard data set was used. Euclidean distance is computed according to the following equation.

$$\text{Euclidean distance} = \left(\sqrt{\sum_{k=1}^{n} (u_k - x_{ik})^2}\right) \qquad 4.3$$

where u= sit-stand or stand-sit transition segment from one subject is taken as a standard data set,

n= total number of components in a vector (n=5) and

i= index of vectors to be identified (i=1,…,59 for sit-stand and 1,…,60 stand-sit transition activities).

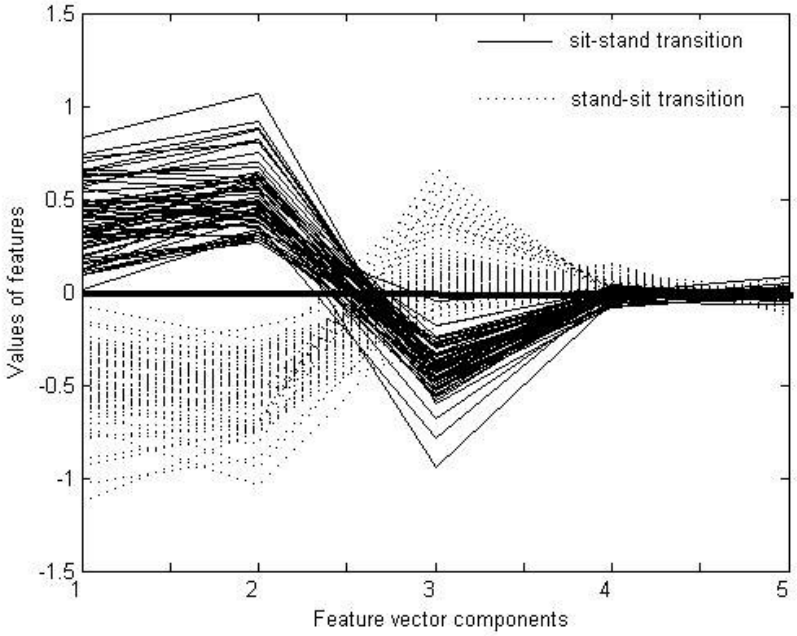

Figure 4.14. Feature vectors used in sit-stand and stand-sit transition activity classification.

4.3.2.4 Discussion

We detected sit-stand/stand-sit transition activities using features from time-frequency domain. In time domain, the significant features of these transition activities in vertical acceleration signal are a positive peak followed by a negative peak for sit-stand transition activity and a negative peak followed by a positive peak for stand-sit transition activity. The comparison of the peak values allows identification between the two activities. However, additional peaks, unrelated to the transition activities, can be present in the acceleration signal and can cause error in decision process.

Seven types of ADL, level walking, ascending stairs, descending stairs, sit-stand/stand-sit transitions, lie-sit/sit-lie transition were done in the experiment and these are common daily activities for the elderlys' daily living practices [19,104,105]. In

rejecting the activities those are not desired transition activities, four factors were used, namely global minimum value (g_m), threshold level, data length (0.7-2seconds) and rest state. We assume that if the extracted segment is true transition activities, there should be a rest state before or after, or both. When the data from all 9 subjects was analyzed, the data for test number 2 and test number 3 is in line with our assumption. However, for test number 1, subjects 5 and 6 did sit-stand and stand-sit transitions closely and rest states were not found (Figure 4.15). Nevertheless, we still keep our assumption since we assume that this situation in which 5 transitions are close to each other will be rarely seen in common daily activities, especially among the elderly. This assumption is also consistent with previous researchers' reports [19,104]. Bolded numbers in Table 4.2 indicates the segments that were not extracted by the extraction procedure.

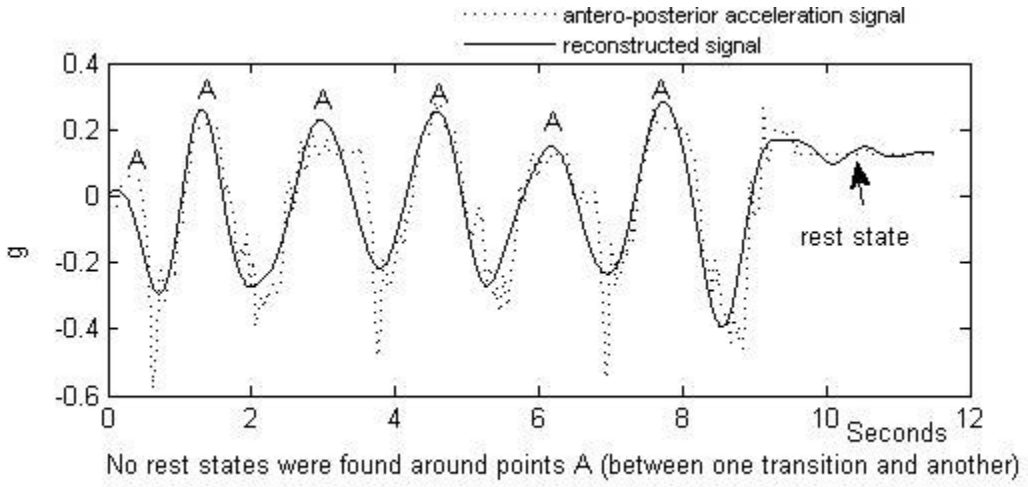

Figure 4.15. Antero-posterior acceleration signal and its reconstructed signal for test number 1.

We attempted to design digital filters that imitated the frequency response obtained by using wavelet reconstruction method in transition segment extraction. Using digital

filter reduces the data processing speed as these filters require large number of coefficients to closely imitate the frequency response (0-1Hz) of wavelet reconstruction method. Moreover, filtering the input data forward and reverse directions in achieving zero-phase distorted filtered response causes processing speed to be worse. Therefore, we chose wavelet reconstruction method in extracting low frequency component (0-1Hz) of the antero-posterior acceleration signal in segment extraction process.

Investigations using a similar detection approach, i.e., locating the sensors on the trunk, were published by Mathie et al., 2004 [104] and Najafi et al., 2002 [105]. Najafi et al. measured sit-stand/stand-sit transitions using a gyroscope, parallel to the sagittal plane and an accelerometer, vertical to trunk. The sensors are located on the sternum. The attachment is directly pasted onto the skin, seemed using a sticky material in the figure and no detail expression is provided on how it is attached. Even though this is a simple kinematic sensor, it is protruding out of the body and may cause injury when the subject faces severe incident such as fall. The way of attaching the sensor onto the body may not be appropriate for long term application. Furthermore, the gyroscope, measuring the sagittal plane information, is difficult to be located onto the garment as not to be interfered by arm movements and not to protrude out of the body significantly. If the sensor is embedded on the garment under arm position for the purpose of avoiding protruding out of the body, motion artifact because of the arm movement is a concern in sensor performance. Therefore, applying one of 3-axis accelerometer's outputs, instead of using additional sensor for the same performance, in transition segment extraction is a great advantage in activity detection as using only single 3-axis accelerometer can detect broad range of daily activities such as level walking, ascending stairs, descending stairs,

lying to sitting transition, sitting to lying transition, sitting to standing transition and standing to sitting transition and severe incidents such as falls [106-108]. In classification, their approach was using the vertical displacement calculated from double integrating the vertical acceleration signal and it resulted in about 90% accuracy in classification for both sit-stand and stand-sit transitions. The important limitation of the above method is the integration error due to dc component present in the acceleration signal and the requirement of initial conditions in integration. The initial conditions, initial trunk tilt angle and initial trunk velocity before the transition segment, are evaluated at the location where 1-sec period of antero-posterior acceleration signal is computed with variance around zero. Sometimes, the period is difficult to find in our experimental records, especially in activities such as performing walking and sitting continuously (Figure 4.10). Mathie et al. detected sit-stand/stand-sit transitions in two steps using a triaxial accelerometer located on the waist belt. First, the presence or absence of activities was determined by comparing the signal magnitude areas calculated from three low-pass and high-pass filtered acceleration signals with a preset threshold value. The comparison was done for each non-overlapping one second moving window. Secondly, the classification between sit-stand and stand-sit transitions was done by pattern matching. 93.5% sensitivity was achieved in sit-stand/stand-sit transition activity detection by using that approach. Even though the method can produce high classification rate, it may not be suitable for real-time detection because of its long processing steps. By way of comparison, our detection method, locating the sensor on the shoulder part of a garment, can make a comparable result in sit-stand/stand-sit transition detection. Therefore, our new wavelet-based approach is a remarkable innovation in wearable

activity detection system where garment is applied as a platform for the sake of comfort of the wearer.

In conclusion, we showed that a new wearable detection system by securing a miniature 3-axis accelerometer on a garment allows for non-intrusive monitoring of daily activities. We applied wavelet-based approach in detection and it gave the accuracy of 93.65% and 95.24%, respectively.

4.3.3 Human motion activities detection

Two dimensional, vertical and antero-posterior, acceleration signals were used in our detection process. Human motion patterns (level walking, ascending stairs and descending stairs) in continuous accelerometer records were classified in two steps. In the first step, direct spatial correlation of *discrete dyadic wavelet coefficients* was applied to separate the segments of human motion patterns in the continuous accelerometer records. In the second step, power of extracted coefficients of separated segments from the square of vertical acceleration signal (*PcoefsY*) and that of separated segments from antero-posterior acceleration signal (*PcoefsZ*) were used in classification. Our results proved a reliable technique of measuring human motion patterns in ADL detection.

4.3.3.1 Subjects and experimental procedure

MEMSWear was used in our experiment. During the experiment, the Notebook^{TM} was always in the transmission range (10-meter) of the transmitter on the subject. Signals were digitized at 256-Hz sampling rate and recorded into a Notebook^{TM}. The experiments were performed on 12 male and 10 female subjects (age ranged between

20 and 45 years, height between 1.67m and 1.94m, and weight between 45kg and 93kg). The subjects walked along a corridor, up a stair way and walked along another corridor, and then down the stairway, wearing their own shoes, with no instructions. The length of each corridor was 10m. The stairway is half-turn stair, which changes its direction at a landing by 180 degree and consisted of 30 steps. The landing is at 15^{th} step and there are fourteen steps between two landings. The slope of the flight is 30°. All experiments were captured by a video camera. For each trial, the camera and the sensor data capture system in Notebook^{TM} were activated simultaneously by the observer by switching the two systems on at the same time. All subjects signed a consent form that was approved by the Tan Tock Seng Hospital Medical Research Ethics Committee.

4.3.3.2 Detection methodology

Separation of human motion segments in continuous accelerometer record

The application of direct spatial correlation (direct multiplication) of the wavelet coefficients to separate the segments of human motion patterns is based on the spatially selective filtration technique for de-noising which uses the properties of the signal and noise modulus maxima of wavelet coefficients across scales [106,107]. The first step of the technique is decomposing the signal to be denoised into different frequency levels (from high frequency, smaller scale values, to low frequency, larger scale values) using discrete dyadic wavelet decomposition (Figure 4.16). As most noise power is confined to higher frequency levels (levels with smaller scales) and wavelet coefficients of noise are not well correlated across the decomposed levels, the direct spatial correlation or direct multiplication of wavelet coefficients over adjacent low frequency decomposed levels

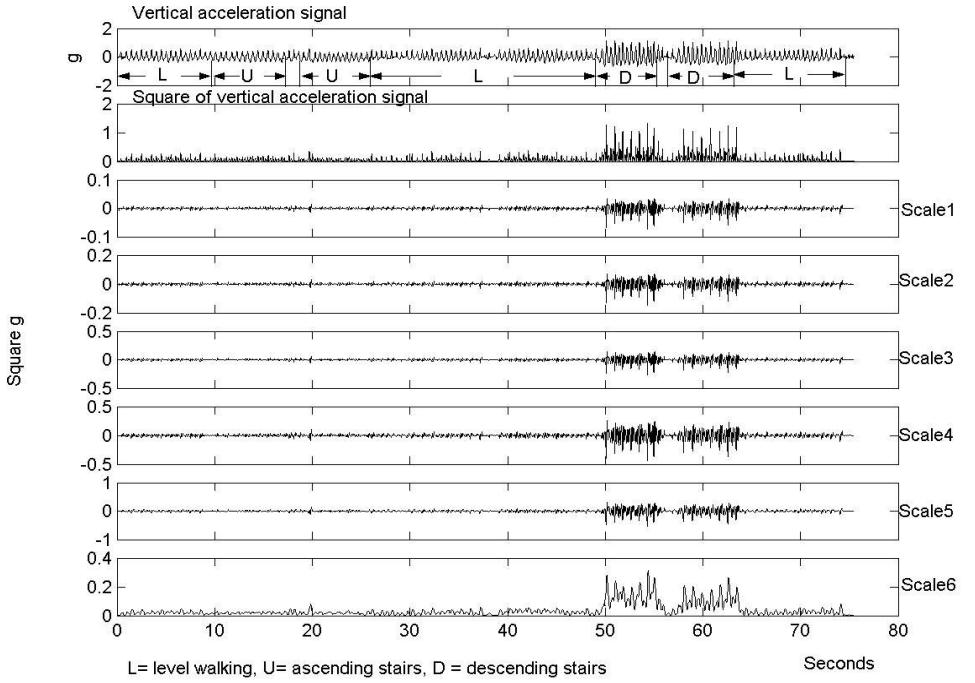

(a)

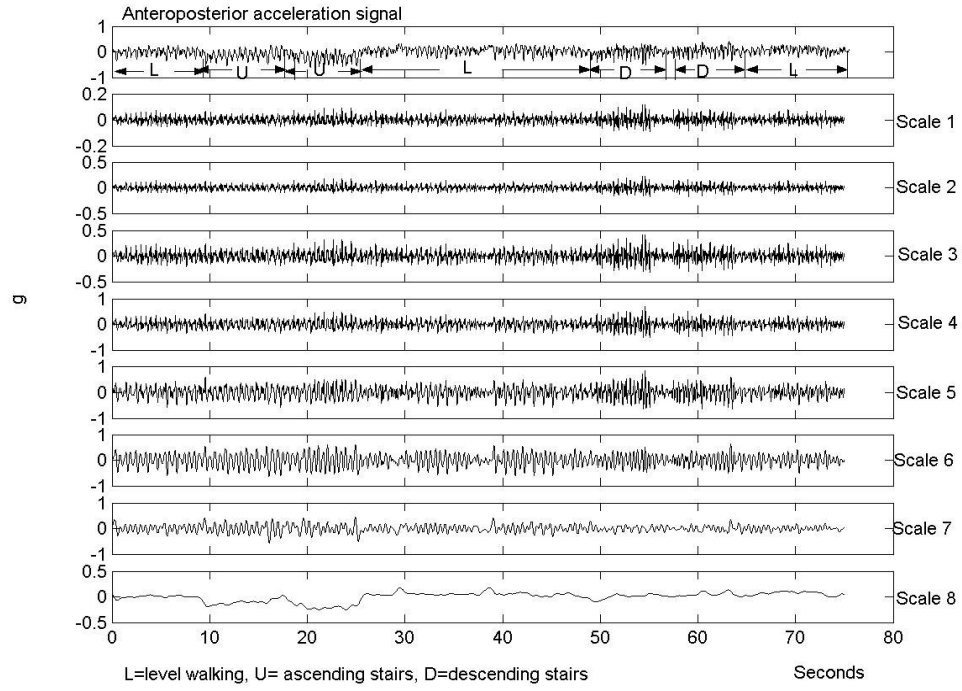

(b)

Figure 4.16(a). The square of vertical acceleration signal is decomposed into six scales through the dyadic wavelet transform. (b) The antero-posterior acceleration signal is decomposed into eight scales through the dyadic wavelet transform. (Relations between scales and frequency bandwidth can be seen in Table 3.1)

(levels with larger scales) sharpens and enhances major signal while suppressing noise. Therefore, in the spatial selective filtration technique, the signal is passed where the coefficients are highly correlated across scale and suppressed elsewhere [106] and this is the rationale that the technique can be used in the separation of the segments of human motion patterns in my application. In this decomposition, nonorthogonal wavelets, first introduced by Mallet et al.[94], were used because nonorthogonal wavelets are well suited for applications where correlations between decomposed levels are used [94,109].

In segment separation among level walking, ascending stairs and descending stairs in an accelerometer record, the filtration was applied to both vertical and antero-posterior acceleration signals. However, instead of using vertical acceleration signal directly, square of vertical acceleration signal was used to obtain larger amplitude difference between two successive segments. Vertical acceleration signal, square of vertical acceleration signal, antero-posterior acceleration signals and their discrete dyadic wavelet transform at multiple scales were presented in Figure 4.16.

The algorithm used in human motion patterns separation suppressed the low absolute amplitude portion such as level walking, around 0.1g in square of vertical acceleration signal, and enhanced the high absolute amplitude portion such as descending stairs portion, around 0.5g in square of vertical acceleration signal. This enhancement and suppression effect can be seen clearly after rescaling process (the power of the correlated data is rescaled to that of the decomposed signal with scale J+1) (Figure 4.17). That means that the descending stairs portion was treated as major signal because coefficients were well correlated across the decomposed levels, and level walking portion was treated as noise. This is the main rationale that the spatially selective filtration technique for

denoising can be applied in segment separation of human motion signals. In this algorithm, direct spatial correlation was done only between the two largest scales. For this, we define a scale correlation variable as

$$Corr(J,n) = \left(W(J,n) \times V(J,n)\right), \qquad 4.4$$

where J is the maximum level in decomposition and $n=1,2,3,..,N$. $V(J,n)$ and $W(J,n)$ represents the wavelet coefficients' n^{th} value at scale J and J+1.

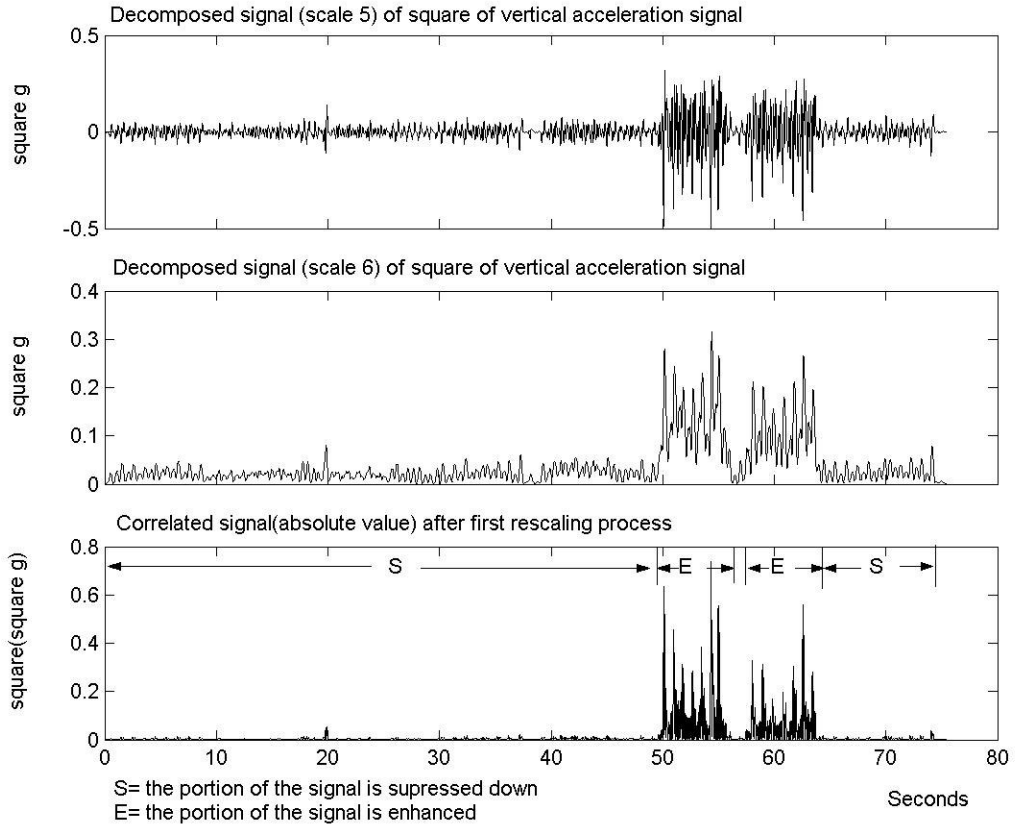

Figure 4.17. Decomposed signals of square of vertical acceleration signal and their correlated signal after rescaling process.

The power of the correlated data was rescaled to that of $\{V(J,n)\}$. Power rescaling method is as follows:

$$pcorr = \sum_{n=1}^{N} Corr(J,n)^2 \ , \qquad 4.5$$

$$ps = \sum_{n=1}^{N} V(J,n)^2 \ , \qquad 4.6$$

and rescaling as

$$Corr'(J,n) = Corr(J,n)\sqrt{\frac{ps}{pcorr}} \ . \qquad 4.7$$

Table 4.3
Segments of human motion activities separation algorithm

Direct spatial correlation over the two largest scales

$Corr(J,n) = \left(W(J,n) \times V(J,n)\right)$

Loop for the iteration m/**m is predefined iteration number*/*

{

$Corr'(J,n) = Corr(J,n)\sqrt{\frac{ps}{pcorr}}$

Loop for coefficient n

{

if $| Corr'(J,n) | > | V(J,n) |$

{

$V_{new}(J,n) = V(J,n);$

$Corr'(J,n) = 0;$

$V(J,n) = 0;$

} end if

} end loop n

} end loop m

After rescaling, we compared the rescaled version of $Corr'(J,n)$ with $V(J,n)$. If $\left|Corr'(J,n)\right| > \left|V(J,n)\right|$ at a certain point (*J, n*), the coefficient of $V(J,n)$ at that point was extracted and retained in a new vector $V_{new}(J,n)$. Zero was replaced in $Corr'(J,n)$ and $V(J,n)$ at that point. We then rescaled the power of the zero filled version of $Corr'(J,n)$ to the zero filled version of $V(J,n)$, compared their absolute values and

extracted the coefficient of $V(J,n)$ again. These procedures of power rescaling, absolute value comparison and coefficient extraction were iterated according to the predefined iteration number. The algorithm is summarized in Table 4.3. Descending stairs portion is separated from other activities by applying the algorithm to the square of vertical acceleration signal and ascending stairs portion is separated from other activities by applying the algorithm to the antero-posterior acceleration signal. In the discrete dyadic wavelet decomposition, maximum iteration number (m=3), the maximum decomposition scale of the antero-posterior acceleration signal and that of the square of vertical acceleration signal were determined empirically. In this segment separation process, the entire positive coefficients of extracted data from the antero-posterior acceleration signal were discarded. At last, energy transition from zero to a value in the energy profile of extracted coefficients was used to obtain the start point and end point of a segment. The segments which are less than two second time interval were eliminated. If the interval of the separated segments from vertical acceleration signal and antero-posterior acceleration signal were overlapping, the longer segment was selected.

Human motion patterns classification

In the classification of human motion patterns, coefficients of discrete wavelet transform were applied [97]. In the transformation, coefficients are decimated for each scale of decomposition. Two second time duration of separated segments of vertical and antero-posterior acceleration signals was decomposed into five scales by "Daubechies mother wavelet with order five". Two second time duration corresponds to $[t_m - 1s, t_m + 1s]$, where t_m is the centre of a segment. The power of wavelet coefficients

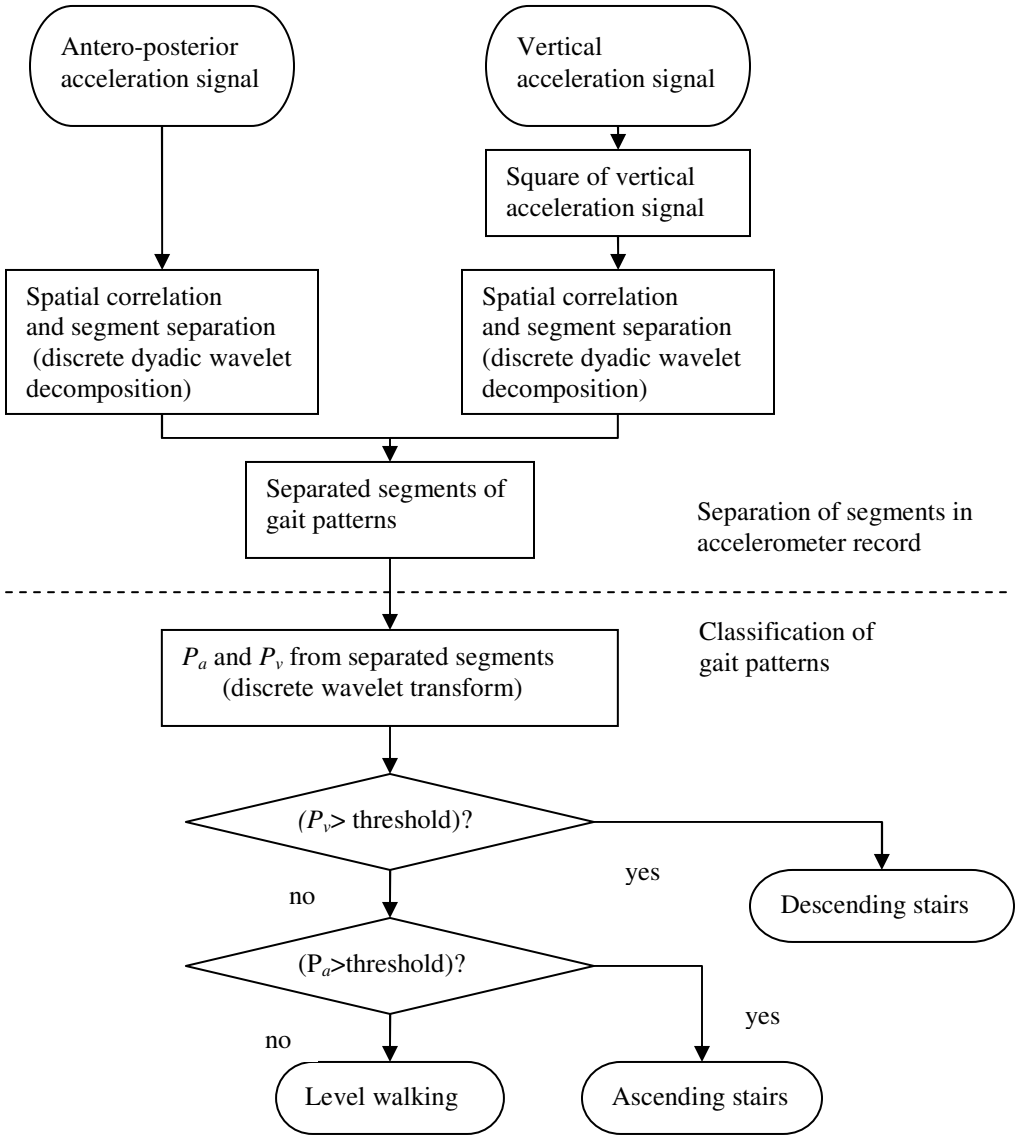

Figure 4.18. Human motion patterns classification flow chart (i).

at scales four and five was used as features in classification (Equation (4.8)). Scales 4 and 5 correspond to 0~16Hz cover the required information of human motion patterns [40].

$$P_{a \text{ or } v} = \sum_{j=4}^{5} \left\| x_j \right\|_2^2 \qquad 4.8$$

where x_j is the wavelet coefficients of scales 4 and 5. P_a represents the power of wavelet coefficients of the antero-posterior acceleration signal and P_v represents that of the

vertical acceleration signal. In classification, both P_a and P_v were calculated from a separated segment. If P_v was greater than the predetermined threshold value (P_{vt} = 43), the segment was classified as descending stairs segment. If P_v was smaller than the threshold value, P_a was used to classify between ascending stairs and level walking. If P_a was greater than the threshold value (P_{at} = 9.78), the segment was classified as ascending stairs and else it was classified as level walking. The predetermined threshold values are values determined from the experimental data used in the development stage of the algorithm before the experiment to validate the algorithm was done at the hospital. The motion activities classification procedure is illustrated in Figure 4.18.

4.3.3.3 Experimental results

The original acceleration signals, extracted coefficients of vertical acceleration signal square and antero-posterior acceleration signal and separated segments are shown in Figure 4.19. The algorithm (Table 4.3) separates the descending stairs segments from vertical acceleration signals and the ascending stairs segments from antero-posterior acceleration signals. These segments are normally more than two seconds in the experimental data. Therefore, the time intervals of extracted coefficients which are shorter than two seconds intervals were eliminated (Figure 4.19(d)). If extracted segments from vertical acceleration signal and antero-posterior acceleration signals were overlapping, the shorter segment was eliminated (Figure 4.19(g)).

To estimate the performance of the segment separation algorithm, absolute error, percentage error, sensitivity, and specificity for ascending stairs and descending stairs were estimated as follow:

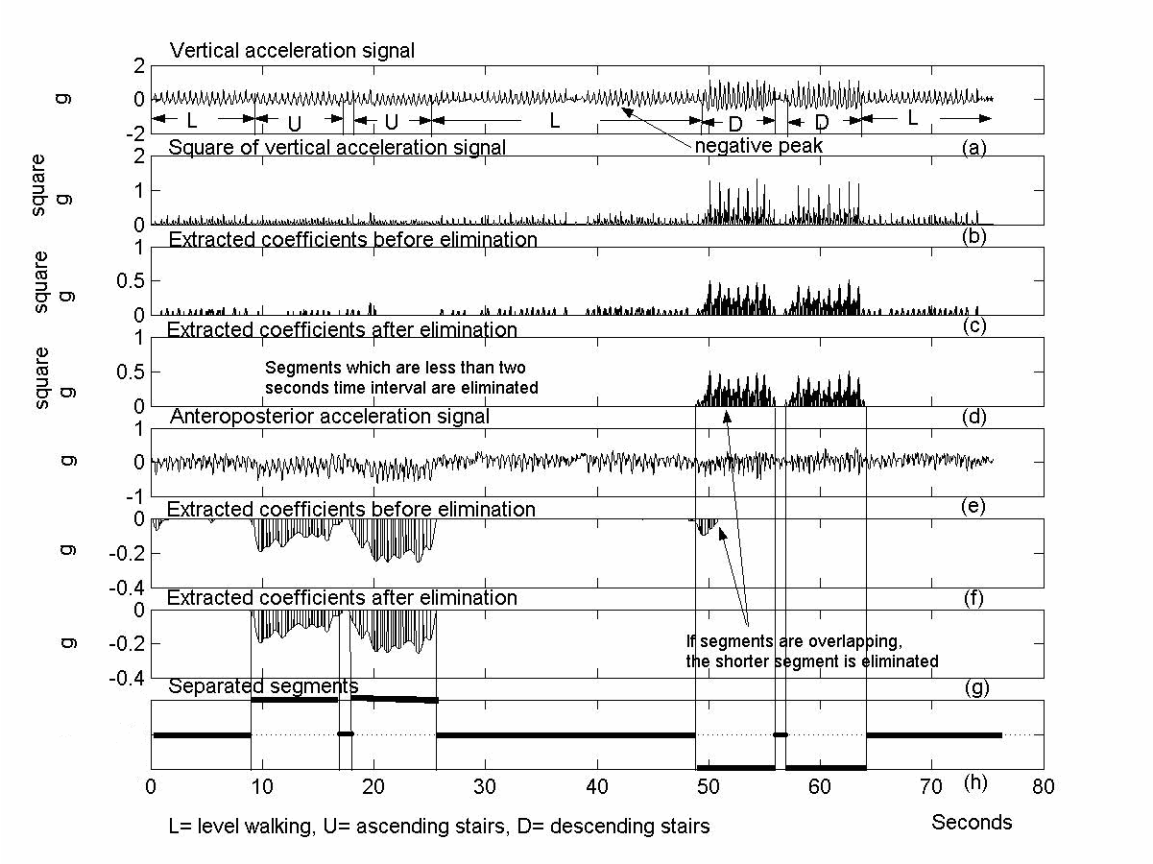

Figure 4.19. The acceleration signals, extracted coefficients and separated segments of human motion patterns in the acceleration signals.

•Absolute error = | time interval of a segment of extracted coefficients-actual time interval of a segment |.

•Percentage error = (absolute error/actual time interval of segment)*100%.

•Sensitivity = (true positives/(true positives + false negatives))*100%.

•Specificity= (true negatives/(true negatives + false positives))* 100%.

The recorded video clips were observed using "VirtualDub 1.5.10" media player to get the actual time intervals of descending and ascending stairs segments. The digit in the second decimal place is 3 in this player. The investigator noted the duration of each descending/ascending stairs activity and actual time intervals of ascending/descending

stairs segments were taken from the time when the subject's foot landed onto the first step of the stairs for descending or ascending to the time when he/she stepped onto the landing. In sensitivity/specificity estimation, true positives were equal to the number of cycles of ascending/descending stairs activities those were correctly extracted by the algorithm and false negatives were equal to the number of unextracted cycles of ascending/descending stairs activities. True negatives were equal to the number of cycles not included in the separated segment of ascending/descending activities and false positives were equal to the number of cycles wrongly extracted in the separated segment of ascending/descending activities. For sensitivity and specificity estimation, total numbers of steps encountered by each subject were counted by the investigator. From one negative peak to next negative peak of vertical acceleration signal was considered as one cycle human motion activity (Figure 4.19). Numbers of steps (cycles) for ascending/descending stairs were taken as fifteen. Start/end time of segments observed in the video clips and that of segments separated by the separation algorithm for stairs activities were compared in Table 4.4. Overall absolute error, percentage error, sensitivity and specificity for 22 subjects were also presented (Table 4.4).

Forty-four pairs of P_a and P_v for ascending stairs and descending stairs and 66 pairs of P_a and P_v for level walking from 22 subjects were classified (Figure 4.20). The classification rate (pairs that are classified correctly/total number of pairs) of descending stairs, ascending stairs and level walking are 97.72%, 93.18%, and 93.93% respectively.

Table 4.4 Error, sensitivity, specificity of separated stairs segments and comparison of start/end time of segments observed in the video clips and extracted by the algorithm

Ascending stairs							Descending stairs					
Subje-ct	Video records		Separation algorithm		Sensit-ivity	Specif-icity	Video records		Separation algorithm		Sensit-ivity	Specif-icity
	Start	End	Start	End	(%)	(%)	Start	End	Start	End	(%)	(%)
	Seconds						Seconds					
1	7.559	14.598	7.504	14.688	100	100	39.727	44.383	39.063	44.336	100	98
	16.090	23.543	15.094	23.105	93	98	46.027	50.789	46.039	50.730	100	100
2	6.895	14.176	6.531	14.363	100	99	47.676	53.836	47.332	53.848	100	99
	16.031	23.207	15.488	23.754	100	98	55.086	61.137	55.027	61.473	100	99
3	7.176	15.301	7.273	15.742	100	99	46.082	53.387	45.746	53.563	100	99
	17.020	24.828	16.789	25.410	100	99	54.613	61.496	54.809	61.875	97	99
4	6.465	12.137	6.523	12.805	100	99	43.531	49.590	43.410	48.863	87	100
	13.672	20.043	12.949	20.027	100	99	50.785	57.008	50.730	57.164	100	100
5	6.773	14.672	7.004	14.941	97	99	46.945	53.988	46.641	53.965	100	100
	16.988	25.094	17.148	25.469	100	99	55.430	62.578	55.250	62.719	100	100
6	6.078	12.859	6.410	12.934	93	100	45.688	51.688	45.355	52.777	100	98
	14.438	21.250	14.262	21.441	100	100	54.266	60.309	53.941	60.141	100	100
7	8.477	15.383	8.555	15.762	100	99	39.855	45.848	40.055	45.824	97	100
	16.523	24.148	16.590	24.543	100	100	46.879	51.566	47.063	51.551	97	100
8	7.074	15.043	7.363	15.148	93	100	50.813	57.277	51.027	57.551	100	100
	18.234	26.238	18.000	26.426	100	100	58.871	65.121	58.930	64.922	100	100
9	8.746	14.910	8.652	15.445	100	99	46.328	51.336	46.387	51.480	100	100
	16.473	22.543	16.395	22.449	100	100	53.313	58.449	53.258	58.469	100	100
10	7.645	15.129	7.770	14.844	93	100	43.113	49.563	42.797	49.922	100	100
	16.512	24.375	16.680	24.504	97	100	50.531	57.156	50.711	57.016	100	100
11	10.805	18.297	10.980	17.773	93	100	52.031	59.230	51.605	59.422	100	100
	19.641	27.504	19.789	27.551	100	100	60.473	67.695	60.070	67.547	100	99
12	7.785	14.805	7.633	15.297	100	100	47.340	53.652	47.027	53.641	100	99
	16.301	23.660	15.734	24.141	100	100	55.316	62.234	55.320	62.250	100	99
13	9.594	18.039	9.563	18.395	100	99	55.906	63.051	55.613	62.434	100	100
	19.172	27.625	18.840	27.891	100	99	64.871	71.723	64.711	71.613	100	100
14	7.176	12.184	6.875	12.230	93	99	36.180	40.414	36.141	40.691	100	99
	13.727	19.176	13.785	19.703	100	100	41.223	45.457	40.980	45.605	100	100
15	8.902	14.527	8.828	14.336	93	100	45.883	51.516	45.508	51.469	100	100
	15.906	22.426	15.816	22.352	100	100	52.242	57.699	55.737	57.742	37	100
16	7.789	14.813	8.207	15.324	100	100	44.063	48.781	43.980	49.121	100	100
	16.457	23.434	16.508	23.473	100	99	50.379	55.195	49.980	55.066	93	100
17	8.965	16.590	8.945	17.012	100	100	49.473	55.641	49.066	56.012	100	99
	18.102	25.309	17.816	25.621	100	100	57.324	64.023	56.895	64.012	100	100
18	7.574	12.621	7.367	12.770	100	100	33.539	38.016	33.426	37.996	100	100
	13.578	19.102	13.660	19.352	100	100	39.027	43.758	39.047	43.926	100	100
19	7.746	14.082	7.602	14.098	100	100	42.844	47.648	42.660	47.383	93	100
	15.203	21.883	14.766	22.191	100	100	48.750	53.902	49.203	53.930	100	100
20	9.352	17.844	9.078	17.711	100	100	52.816	59.852	52.715	59.762	100	99
	19.594	27.426	19.516	28.500	100	100	61.539	68.535	61.527	68.273	100	100
21	9.578	17.539	9.699	17.637	100	99	50.395	57.871	50.094	58.137	100	100
	18.828	26.813	18.738	27.000	100	99	59.293	66.414	59.000	66.578	97	100
22	8.941	14.742	8.523	14.715	100	99	43.855	49.250	43.711	49.594	100	99
	15.945	21.613	15.938	21.605	100	100	50.840	56.156	50.684	56.078	87	100
Aaverage					98.788	99.524					97.349	99.622
Absolute error (Sec)			0.387				Absolute error (Sec)		0.404			
Percentage error (%)			5.536				Percentage error (%)		6.929			

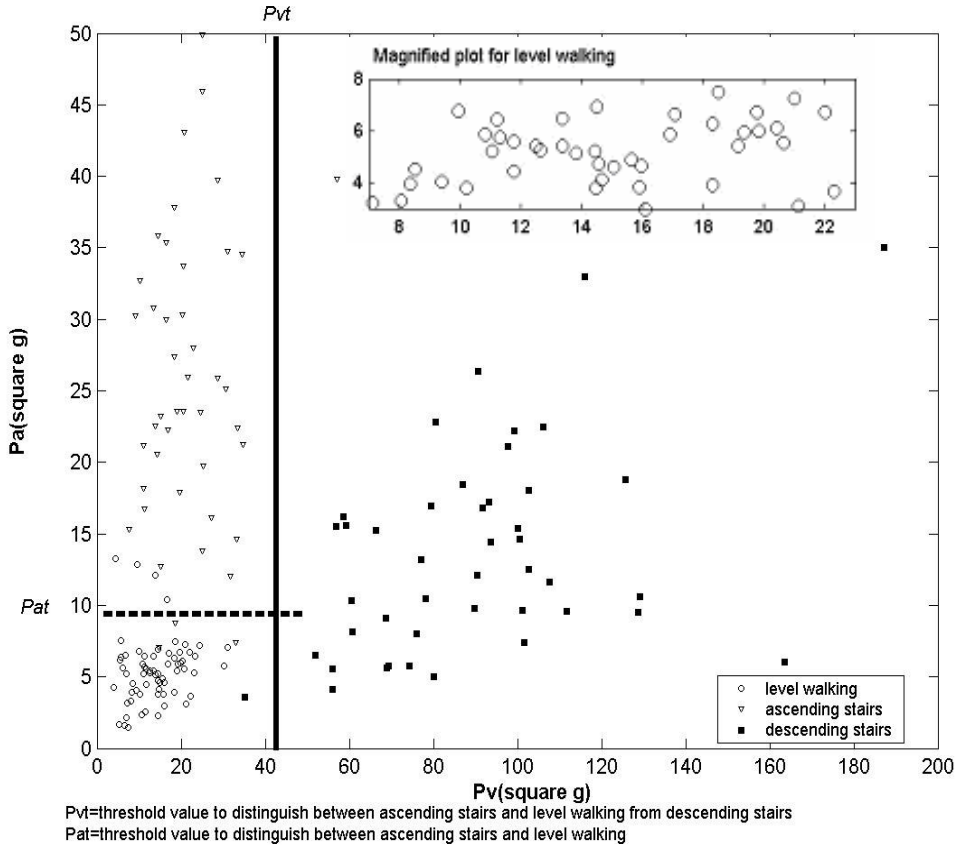

Figure 4.20. 44 pairs of P_a and P_v for ascending and descending stairs and 66 pairs of P_a and P_v for level walking from 22 subjects and their relationship in classification.

4.3.3.4 Discussion

Unlike the algorithm of spatially selective filtration technique for de-noising [106, 107], the spatial correlation was applied only between the two largest scales (scale J and scale $J+1$) in our segment separation algorithm. Moreover, rescaling of the power coefficients of correlated signal and comparison were executed to the decomposed signal of largest scale ($V(J,n)$). According to our empirical results, the coefficients were denser for the same extracted length if these processes were implemented to $V(J,n)$ and lower densities of the extracted coefficients caused inaccurate results in the start point and end point detection. Some of the parameters for optimization are now discussed.

Iteration times: In each iteration process, the coefficients of $V(J,n)$ at the position where the absolute amplitude of rescaled signal ($Corr'(J,n)$) is greater than that of $V(J,n)$ are retained. Therefore, if the iteration time is small, for example m=1, the extracted coefficients do not convey the actual length of the required segment. If the iteration time is large, processing time is a necessary factor to consider for long data length. For our experimental data, m=3 is the appropriate iteration time to extract the required segment.

Maximum decomposition scale: Our optimization of maximum decomposition scale is based on the ratio of desired signal (descending stairs or ascending stairs) to be extracted and undesired signal (level walking) to be rejected after rescaling process. Maximum decomposition scale was varied from 4 to 9 for both vertical and antero-posterior acceleration signals. For each maximum decomposition scale, ratios of the averaged value of one second time intervals of descending stairs portions and level walking portions (RDL_N, where $4 \leq N \leq 9$) and those of ascending stairs portions and level walking portions (RAL_N, where $4 \leq N \leq 9$) from the signals after rescaling process (Figure 4.17) were computed. One second time intervals were chosen randomly. Maximum ratios were obtained at scale 6 (RDL_6) for square of vertical acceleration signal and at scale 8 (RAL_8) for antero-posterior acceleration signal.

We compare our classification method with previous attempts. Mantyjarvi et al. proved that applications of ICA or PCA with wavelet transformation to six channels of acceleration signals from the waist level give better classification rate than the original data by using three multilayer perception neural networks [38]. Using six channels of acceleration signals is superfluous in human motion pattern classification. Even though

the best classification results for recognition were 83-90% for six channels, their method gives poor classification rate for three channels of acceleration signals. Moreover, application of neural networks needs a large number of training patterns to reduce the error. Since the low frequency component includes posture information and information about changes in motion, Sekine et al. studied the detection of walking pattern changes by using the low-frequency component of antero-posterior and vertical acceleration signals from the accelerometers at the waist level [39]. In the detection of pattern changes in ascending stairs from the antero-posterior acceleration signal, they manually set the individual's threshold level at the low frequency component of the signal and the times of walking pattern changes were obtained from the crossings of the threshold level and the low frequency component of the signal. In this method, manual thresholding is not practical for a large number of subjects. Again, Sekine et al. used wavelet-based fractal analysis method in human motion activity classification [40]. The fractal dimensions were computed from triaxial accelerometers located to the subject's back in the lumbosacral region of the vertebral column using an elastic waist belt. Even though the combination of the fractal dimensions from three dimensional acceleration signals were different (p<0.01) among the three walking types, this significant result was achieved for each individual subject and did not represent the whole population of subjects involved in the experiment. Finally, Coley et al. presented the detection of walking upstairs using miniature gyroscope attached to the shank of the subject [41]. High accuracy (sensitivity~98%) in identifying walking upstairs from other two walking types was obtained using only one sensor at the shank, but this method could not identify stairs descent. In pattern classification, the data length of the signal used in feature extraction

was fixed to two second duration in our method (Equation (4.8)). In compare to the equations that Sekine et al. applied with high classification rate (98%), we can reduce some processing steps at a slightly lower classification rate than their method [39].

4.3.3.5 Accuracy improvement using new features in human motion patterns classification

Some modifications were made for the accuracy improvement in human motion pattern classification (Figure 4.21). For the improvement, the power of extracted

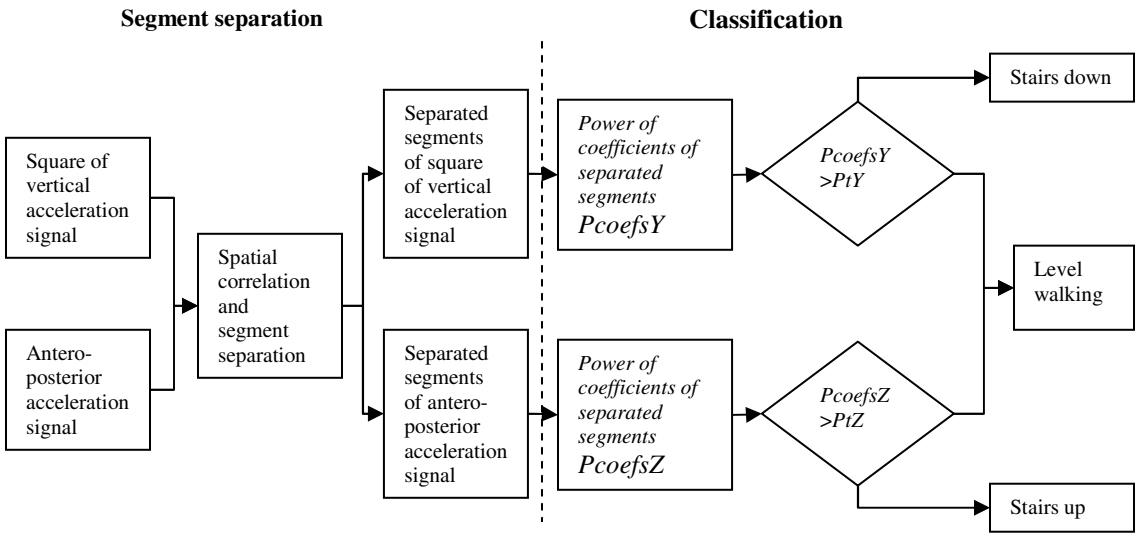

Figure 4.21. Human motion patterns classification flow chart (ii)

coefficients of separated segments from square of vertical acceleration signal (*PcoefsY*) and that of separated segments from antero-posterior acceleration signal (*PcoefsZ*) were used. *PcoefsY* and *PcoefsZ* were calculated as

$$PcoefsY = \frac{1}{N}\left\|d_y\right\|_2^2, \tag{4.9}$$

and

$$PcoefsZ = \frac{1}{N}\left\|d_z\right\|_2^2 \tag{4.10}$$

where N is the number of samples and d_v and d_z represent extracted coefficients of square of vertical and antero-posterior acceleration signal. After elimination process, there were no negative coefficients for descending stairs segment and no positive coefficients for ascending stairs segment and resulted in no misclassification between descending stairs and ascending stairs (Figure 4.19). Therefore, *PcoefsY* was used to classify between descending stairs and level walking and *PcoefsZ* was used to classify between ascending stairs and level walking. In classification, *PcoefsY* were calculated from coefficients of separated segments of square of vertical acceleration signal and *PcoefsZ* were calculated from coefficients of separated segments of antero-posterior acceleration signal. If *PcoefsY* was greater than the predetermined threshold value (*PtY* = 0.0018), predetermined threshold values are values determined from the experimental data used in the development stage of the algorithm, the segment was classified as descending stairs segment. If *PcoefsZ* was greater than the predetermined threshold value (*PtZ* =0.002), the segment was classified as ascending stairs segment. Finally, the rest portion of the acceleration signal was classified as level walking. This procedure is illustrated in Figure 4.21.

Table 4.5 Number of separated segments for level walking, ascending stairs and descending stairs

	Level walking	Ascending stairs	Descending stairs
Experiment using stairs	5 segments x 22 subjects=110 (5 segments are shown in Figure 4.19(h)	2 segments x 22 subjects=44 (2 segments are shown in Figure 4.19(h)	2 segments x 22 subjects=44 (2 segments are shown in Figure 4.19(h)
Level walking experiment	105 segments were separated from 16 subjects		
Total segments	215	44	44

4.3.3.6 Experimental results

The number of separated segments of human motion patterns by scale space filtering that were used in classification are shown in Table 4.5. This corresponds to 100% accuracy in segmentation of the signals for the experiment using stairs [106]. Sixteen out of twenty-two subjects were also conducted level walking for 15m distance in their self-selected speed. This experiment was conducted to assess the performance of the human motion segments separation algorithm and features (*PcoefsY* and *PcoefsZ*) with the acceleration signals of only level walking activity. Vertical and antero-posterior acceleration signals of level walking activity and their separated segments are shown in Figure 4.22. When the separation algorithm is applied to the acceleration signals of only level walking activity, the extracted coefficients are mostly from the square of vertical acceleration signal and those of antero-posterior acceleration signal are mostly zero after elimination process as discussed in section 4.3.3.2. For the level walking experiment, the number of separated segments was not constant for each individual subject. Altogether 105 segments were separated for all sixteen subjects.

Table 4.6 Number of segments with positive, negative and no extracted coefficients after applying the separation algorithm

	Number of segments with no extracted coefficients	Number of segments with positive extracted coefficients	Number of segments with negative extracted coefficients
Level walking	134	64	17
Ascending stairs	0	0	44
Descending stairs	0	44	0

Table 4.6 shows the number of segments with positive, negative and no extracted coefficients for each human motion activity conducted in the experiment after applying

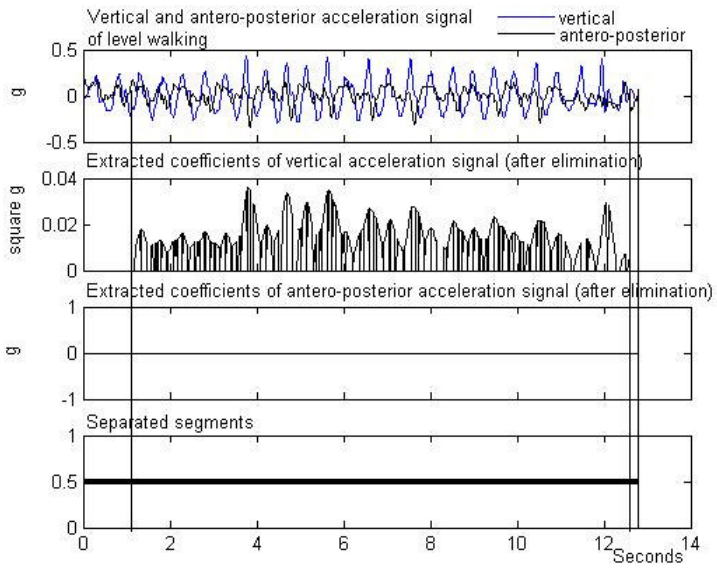

Figure 4.22. Level walking activity and its separated segments

the separation algorithm. *PcoefsY* and *PcoefsZ* for separated segments of level walking, ascending stairs and descending stairs activities are shown in Figure 4.23. In level walking, both *PcoefsY* and *PcoefsZ* were zero for 134 segments. Therefore, most (*PcoefsY, PcoefsZ*) points of level walking segments were accumulated near the origin of *PcoefsY PcoefsZ*-coordinate plane (Figure 4.23, and Figure 4.24). Figure 4.24 is the magnified plot showing the relationships between *PcoefsY* and *PcoefsZ* of level walking segments from Figure 4.23(a). The classification rate (segments that can be classified correctly/total number of segments for each walking type) of descending stairs, ascending stairs and level walking were 97.67%, 100%, and 100%, respectively.

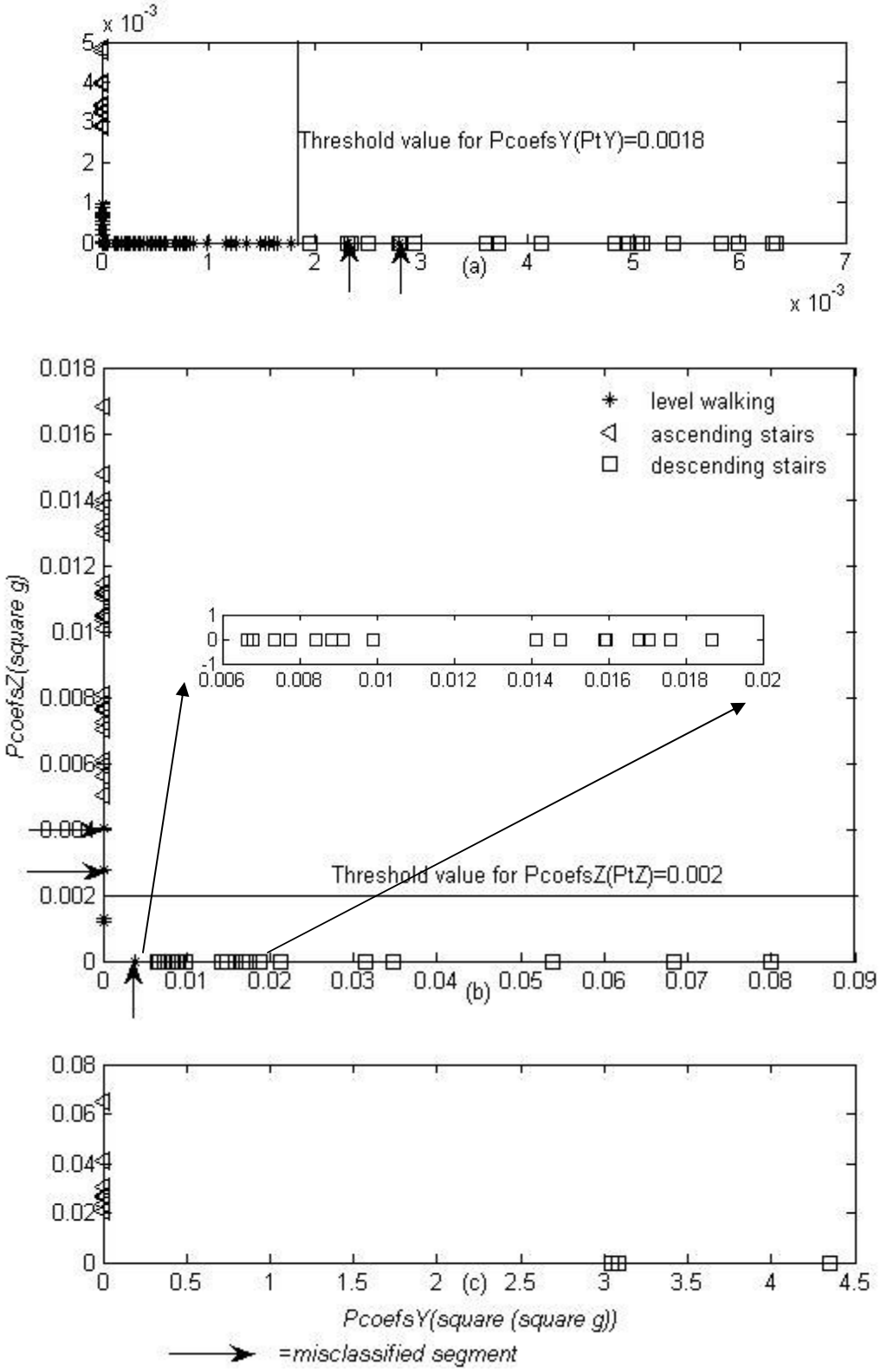

Figure 4.23. *PcoefsY* and *PcoefsZ* of level walking, ascending stairs and descending stairs activities.

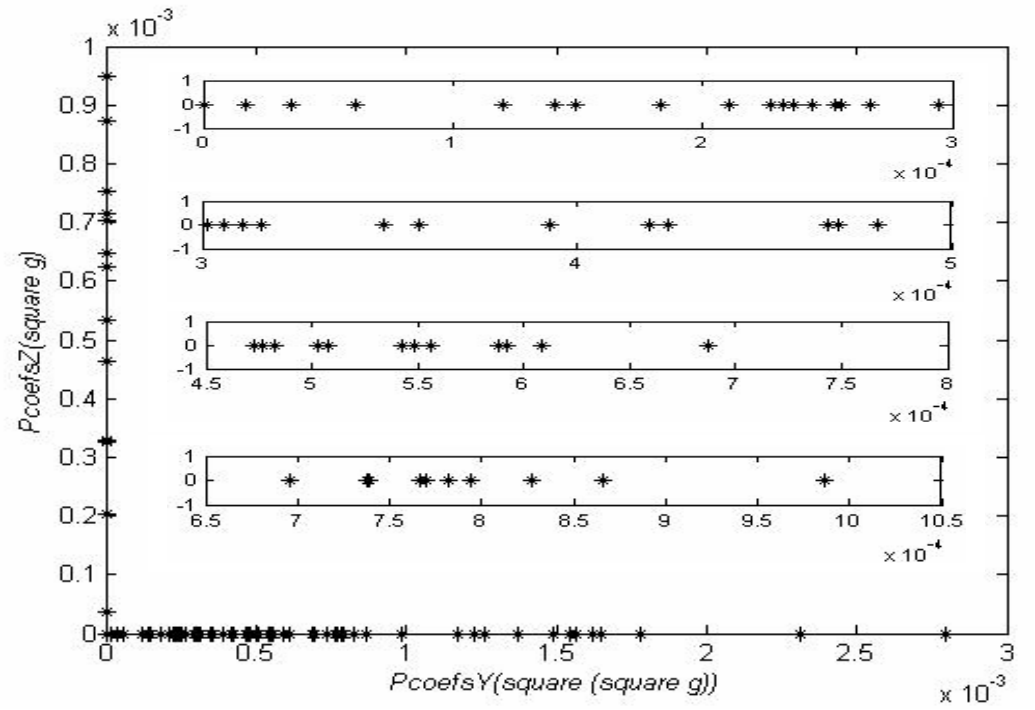

Figure 4.24. Magnified plot showing relationships between *PcoefsY* and *PcoefsZ* for level walking segments of Figure 4.22(a) (134 out of 215 points of (*PcoefsY* , *PcoefsZ*) are zero and subplots are magnified version for the interval 0-0.001 of *PcoefsY* axis).

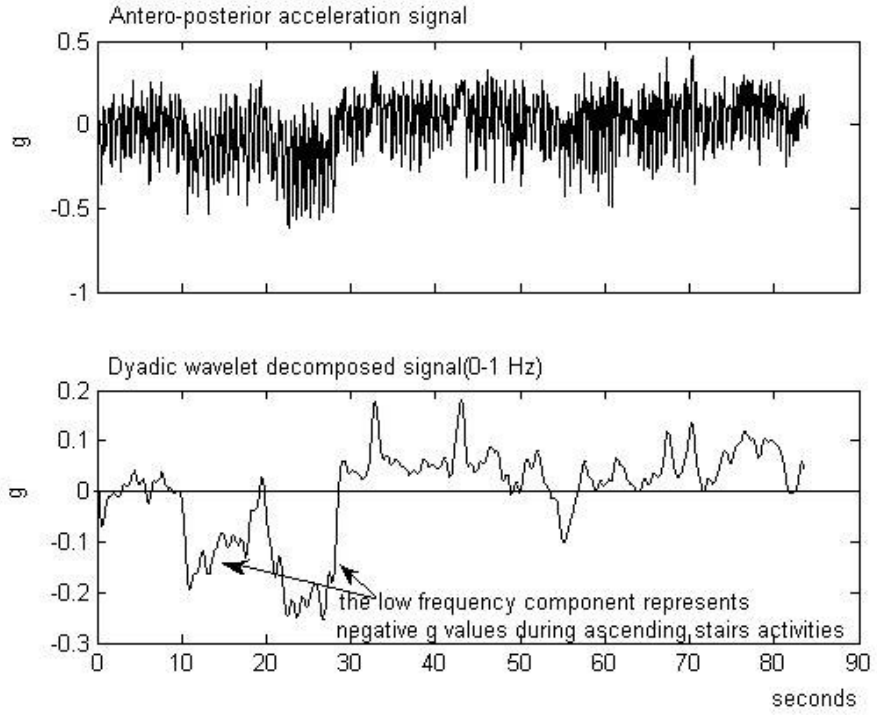

Figure 4.25. During ascending stairs, the body posture is forward tilting and prone position. Because of the changes in accelerometer response due to gravity, the low frequency component represents negative g values in ascending stairs portion of antero-posterior acceleration signal.

4.3.3.7 Discussion

In dyadic wavelet decomposition of the filtration algorithm, the low frequency component (0-1 Hz) of antero-posterior acceleration signal reveals the body posture changes of human motion patterns (Figure 4.25). During ascending stairs, the body posture is forward tilting caused by the changes in accelerometer response due to gravity [110]. Therefore, the low frequency component represents negative g values in ascending stairs portion of antero-posterior acceleration signal and results in negative extracted coefficients after filtration [106]. Consequently, this is the crucial feature of ascending stairs portion to be discriminated from descending stairs segment since the extracted coefficients for descending stairs are always positive because of the exploitation of square of vertical acceleration signal [106].

We compare the new classification method with our earlier classification approach. In our earlier approach [106], three types of walking patterns were segmented applying scale space filtering technique. Then a pair of features (P_a, P_v), P_a, P_v – power of wavelet coefficients from two-second time duration of antero-posterior and vertical acceleration signals, was computed for each separated segment from vertical and antero-posterior acceleration signals and two-step decision process for classification: first, separation of stairs down from stairs up and level walking using P_v and secondly, classification between stairs up and level walking using $P_{a,}$ was carried out. Since all three categories (stairs down, up and level walking) involve in the first step of classification, potential for misclassification among three types of walking patterns is higher than the new approach. In our new approach, power of coefficients of separated segments were used as features in classification and there was no negative coefficients for descending stairs segment

(Figure 4.19(d)) and no positive coefficients for ascending stairs segment (Figure 4.19(g)). Therefore, classification was between stairs down and level walking and between stairs up and level walking and resulted in no misclassification between stairs down and stairs up activities. This is the first point that can enhance the classification rate. Moreover, most of the extracted coefficients of level walking signals were zero and positive (Figure 4.19 and Figure 4.22) and it can reduce the misclassification between level walking activity and ascending stairs activity (Figure 4.20). This is the second factor in improving the classification rate. In addition, some signal processing steps used in our previous classification method such as wavelet decomposition for power of wavelet coefficients are reduced. Therefore, our new method brings superior effects such as higher classification rate and lesser processing steps compared to our earlier effort.

In conclusion, we have developed a new detection method by securing miniature accelerometers on a garment that allows non-intrusive monitoring of human motion activities. We have applied scale space filtering method in the classification of human motion patterns into level walking (97.67%), ascending stairs (100%) and descending stairs (100%) with high classification rate.

Chapter 5

Detection of falls: post impact and pre-impact

Wearable fall detection system was developed. The system can summon medical assistances via SMS (Short Messaging Services) when the wearer encounters fall incident. Fall notification can be sent to individuals and health care unit at the same time to get a shortened interval before the arrival of the assistance. The ability to detect a fall in an older person who is alone, with the resultant activation of a response/help system is of immense benefit as this will lead to a shortened interval before the arrival of assistance and reduce both the physical as well as the psychological trauma of the event. Moreover, pre-impact fall detection was investigated using gyroscope sensors. The advantage of the investigation is that a fall injury minimization system can be developed by incorporating with an inflatable hip protection device.

5.1 Fall detection and fall incident notification

5.1.1 Methodology

Figure 5.1 shows the diagram of fall detection (post impact detection) system. The vest facilitated with a Bluetooth™ transmitter sends acceleration signals to a Personal Computer (PC) for data processing. Single axis accelerometers are arranged in medio-lateral, vertical and antero-posterior directions on the shoulder part of the vest. Using Bluetooth™ transmitter/receiver, signals sampled at 256Hz sampling rate are transmitted to a PC and processed in the PC for fall-detections. Upon detection of falls,

SMSs (Short Messaging Services) are sent by GSM (Global System for Mobile Communication) network supported by a local telecommunication service provider and emails are sent through internet. The primary advantage of our detection system in compared to other researchers' systems is that fall notification can be sent to individuals and medical health care unit simultaneously to lead to a shortened interval of the arrival of assistance.

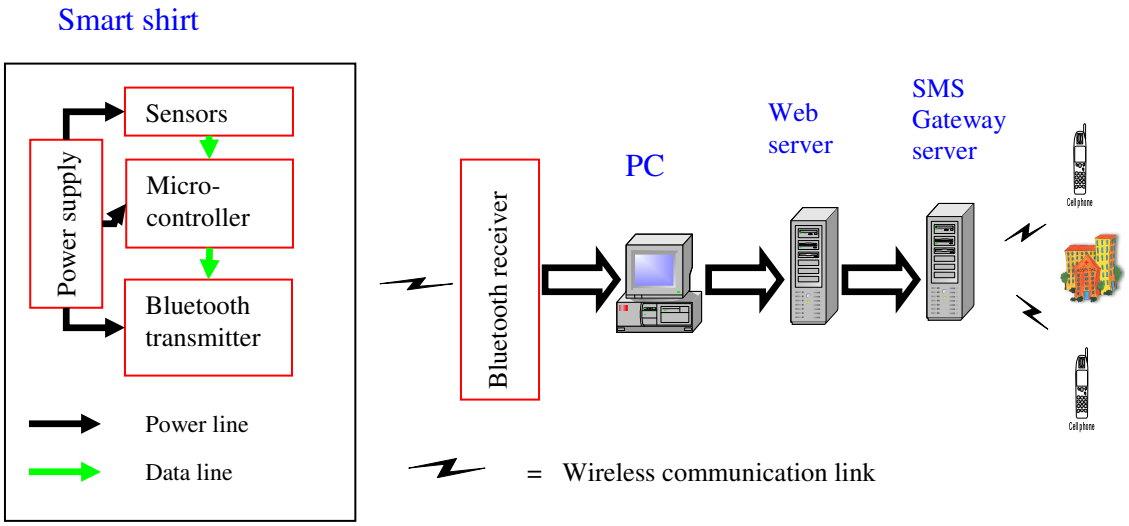

Figure 5.1. Fall detection system.

Fall detection (post impact detection)

In the PC, each dimension of three dimensional raw acceleration signals was segmented to 500 samples for one iteration of data processing. Data set was segmented to 500 samples for one iteration of data processing. Data set was normalized and absolute peak value from each dimension was calculated. Summation of absolute peak values greater than a threshold value (1.2 V, 4.8g) was determined as a fall event.

Table 5.1 Types of activities performed by each subject

Test number	Types of activities	Equipment used in the experiment
1	Sit-stand+ walk+ stand-sit	Chair without armrest (Seat height: 43cm)
2	Level walking, ascending stairs and descending stairs	40 feet long corridor for level walking. Half-turn stairs
3	Slippery falls (Forward and backward) Faint falls (Forward, left side and right side)	Piston-powered fall simulator for slippery falls (Figure 5.2) Soft mattress (6"x6'x4')
4	Sit-lie + lie-sit	Bed (Bed height:38cm)

Sending SMS and emails

When the fall event was detected, SMS and emails were sent as shown in Figure 5.1. Web Server is a centralized control between the clients and SMS server. The PHP code responsible for sending text messages and emails is located in the Web Server. SMS Gateway server is installed with SMS application to listen to a command for sending SMS and emails from the Web Server. This SMS server is connected to a GSM modem via the USB. SMSs are sent through GSM network supported by a local telecommunication service provider and emails are sent through internet.

5.1.2 Subjects and experimental procedure

To set a predefined threshold value in fall detection, the experiment was performed on 5 male and 5 female subjects (age ranged between 22 and 30 years, height between 1.694 and 1.92m, and weight between 47 and 75kg) in a research laboratory environment. All subjects gave consent for participation in the testing. Generally, the activities accepted as fundamental for daily routines include the following: sitting to

lying, lying to sitting, sit-stand, stand-sit, walking, ascending stairs and descending stairs. Therefore, measurement was performed according to test numbers (Table 5.1). To simulate the slippery falls, we used a piston-powered fall simulator (Figure 5.2). A movable platform translation is 30 cm and air pressure was set to 5 bars during the experiment. A soft mattress (6"x6'x4') was placed on the stationary platform. The subject, standing on the movable platform and facing to the stationary side, will fall down to his forward direction (slippery forward fall) when the simulator is activated. Slippery backward fall will occur when the person is facing to the other direction. Subjects performed only once for each test number.

5.1.3 Discussion

How threshold value was defined according to the experimental results

Figure 5.3(a) shows three dimensional acceleration signals for test number 1 to illustrate absolute peak value for each direction. The summation of absolute of peak

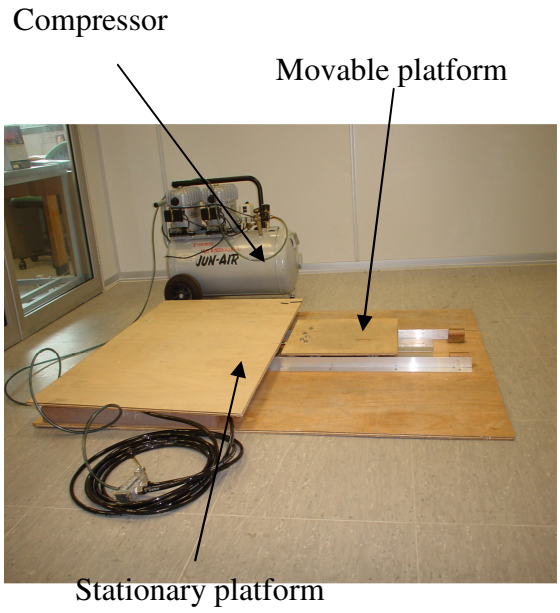

Figure 5.2. Fall simulator

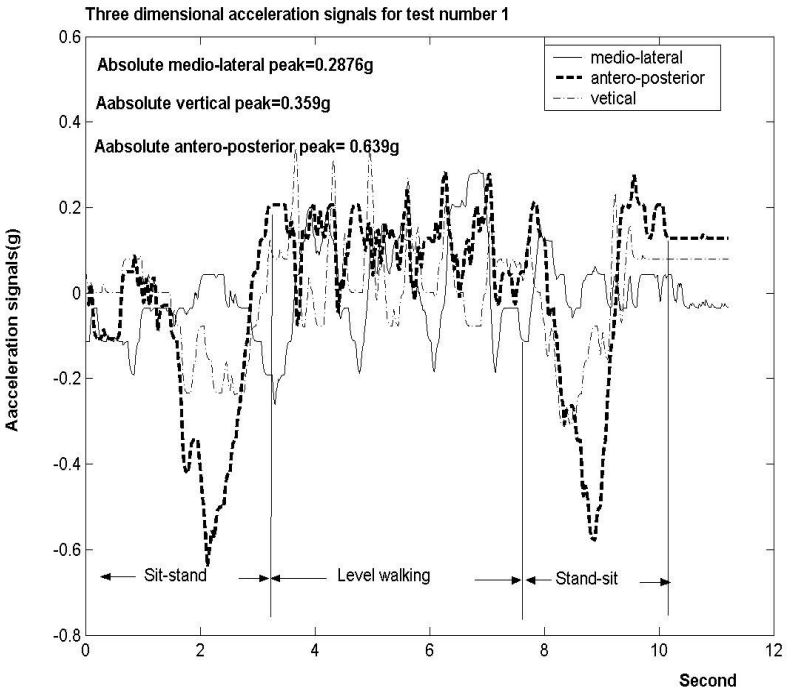
Three dimensional acceleration signals for test number 1
Absolute medio-lateral peak=0.2876g
Aabsolute vertical peak=0.359g
Aabsolute antero-posterior peak= 0.639g
medio-lateral
antero-posterior
vetical
Aacceleration signals(g)
Sit-stand
Level walking
Stand-sit
Second

(a)

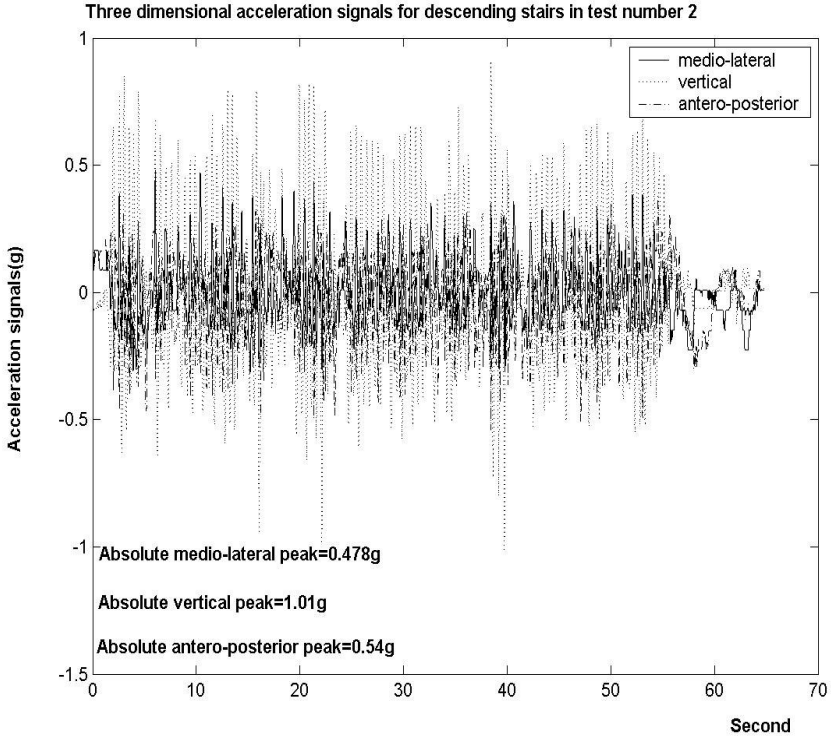
Three dimensional acceleration signals for descending stairs in test number 2
medio-lateral
vertical
antero-posterior
Acceleration signals(g)
Absolute medio-lateral peak=0.478g
Absolute vertical peak=1.01g
Absolute antero-posterior peak=0.54g
Second

(b)

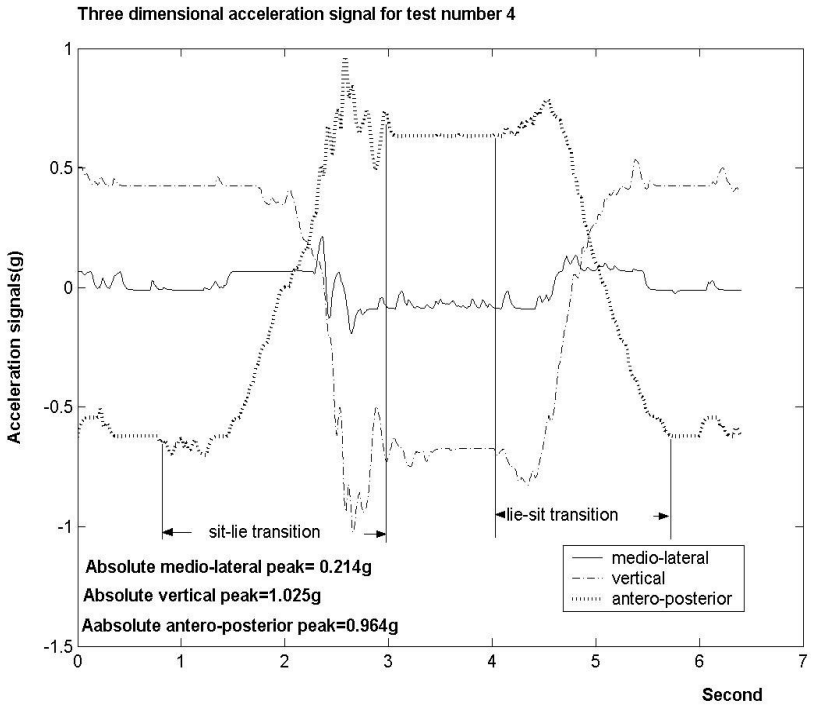

(c)

Figure 5.3. Three dimensional acceleration signals for (a) test number 1, (b) test number 2, and (c) test number 4, shown in Table 5.1.

values for test number 1 is 1.2856g. Figure 5.3(b) shows the acceleration signals of descending stairs for test number 2 and summation of peak values is 2.03g. Descending stairs has higher summation of absolute peak value than ascending stairs and level walking. Therefore, we included only descending stairs in our discussion. Figure 5.3(c) shows acceleration signals for test number 4 and summation value is 2.2032g. In sit to lie posture transition, the output voltage of the accelerometer measuring vertical acceleration changes from 2.75 V (vertically upward in sitting posture) to 2.5 V (horizontal in lying posture) (Appendix A). The difference 0.25 V can be converted to acceleration unit, g, as 0.25V *(1g/0.25V) = 1g for the sensor with 250mV/g sensitivity. Therefore, normalized vertical acceleration output changes from 0.5g to -0.5g, not exactly at ±0.5g as the sensor

is not exactly in vertical and horizontal orientation, in sit to lie transition and reverse transition occurs for the sensor measuring antero-posterior acceleration. However, lateral acceleration does not change much as the sensor is in the same orientation in both lying and sitting postures. Figure 5.4 shows the distribution of summation values of normal activities (test number 1, test number 2 and test number 4) and fall activities (test number 3) for 10 subjects. Complete separation of the two distributions shows perfect classification of normal activities and fall activities by using summation of peak values from acceleration signals. According to the experimental results, 1.2V or 4.8g was defined as a threshold value as shown in Figure 5.4.

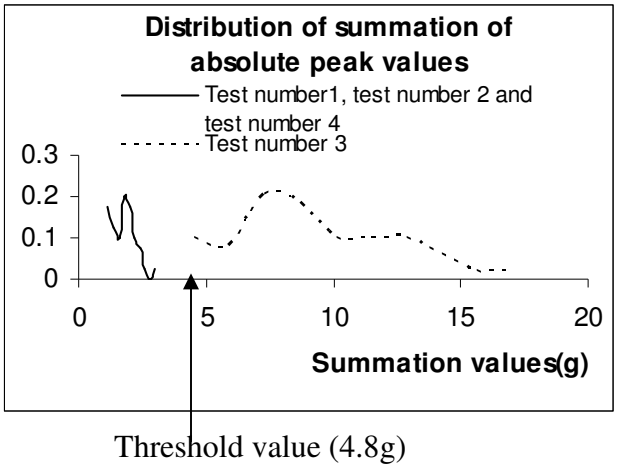

Figure 5.4. Distribution of summation of absolute peak values for normal activities and fall activities for 10subjects.

Reliability issue for the Bluetooth™ wireless data transmission

Bluetooth™ is a commonly used wireless communication technology, especially for short range, low bandwidth and, non-deterministic network infrastructure. There are some reliability issues in Bluetooth™ applications. These are Bluetooth™ link breaking

or being interrupted by walls, metallic objects, etc., and the delay incurred for re-establishing the link.

5.1.4 A smart device that can call for help after a fall

Because of the reliability issue in Bluetooth™ wireless data transmission, we did some modifications in detection system (Figure 5.5). The modified system consists of a wearable module, and a Series 60 Platform mobile phone. The wearable module consists of MSP430F1611 Mixed Signal Microcontroller (48KB+256B Flash Memory, 10KB RAM, 16 bit, and 8MHz), Bluetooth™ transmitter and 3-Axis accelerometer (MMA7260Q, ±1.5g-6g) (Figure 5.6). Acceleration signals are sampled at 100Hz sampling rate. The firmware on the wearable system, upon power up, initializes the Bluetooth™ transceiver and it establishes a data link with the Bluetooth™ receiver at the mobile phone. Having established the link, it starts to collect and analyze data from the 3-axis accelerometer to detect fall. When a fall is detected, it sends a pre-defined code to the mobile phone. Apart from the fall, the user can generate 'Emergency Help' event by pressing a button on the wearable node.

Upon receiving a 'fall code' or 'emergency help code' from the wearable module, the Python SMS script inside the phone sends SMSs to a predefined group of mobile numbers. For the script, the Python interpreter natively interacts with the Symbian operating system of the phone. The script is implemented as a background process with no interference in the normal application of the mobile phone.

The key advantage of the modified detection system is that the Bluetooth™ transmitter and receiver can always be kept within their data transmission range (10

meters). Therefore, there is no limitation in effective detection range in fall detection. This is the detection system as perfect in its kind as that which can raise alarm on its own to individuals and health care unit at the same time to get a shortened interval of the arrival of assistance.

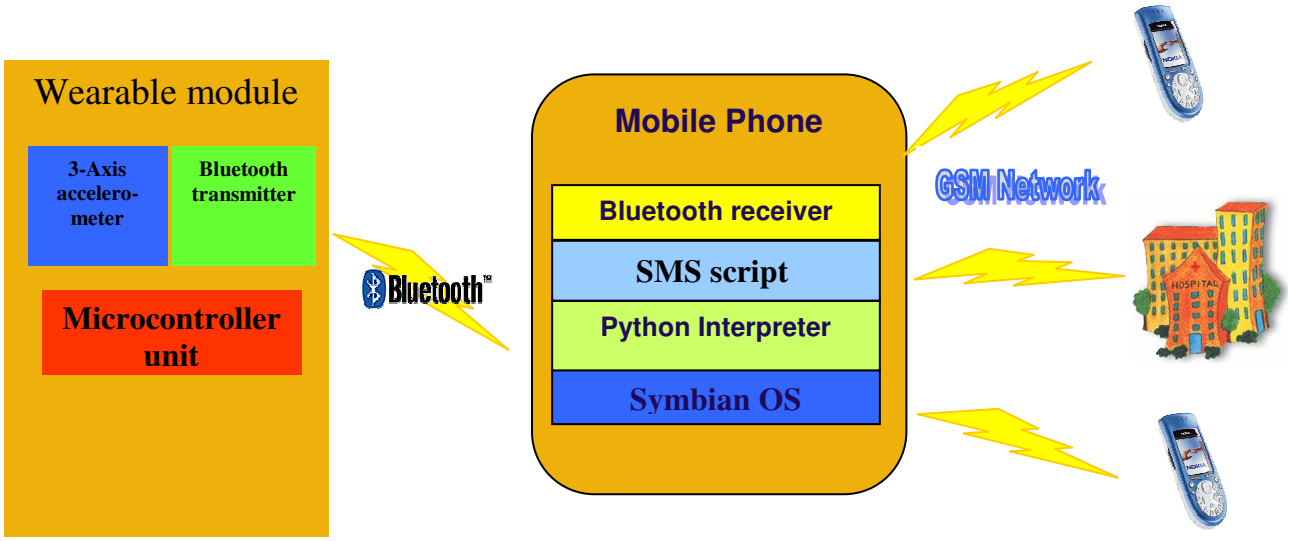

Figure 5.5. Modified fall detection system.

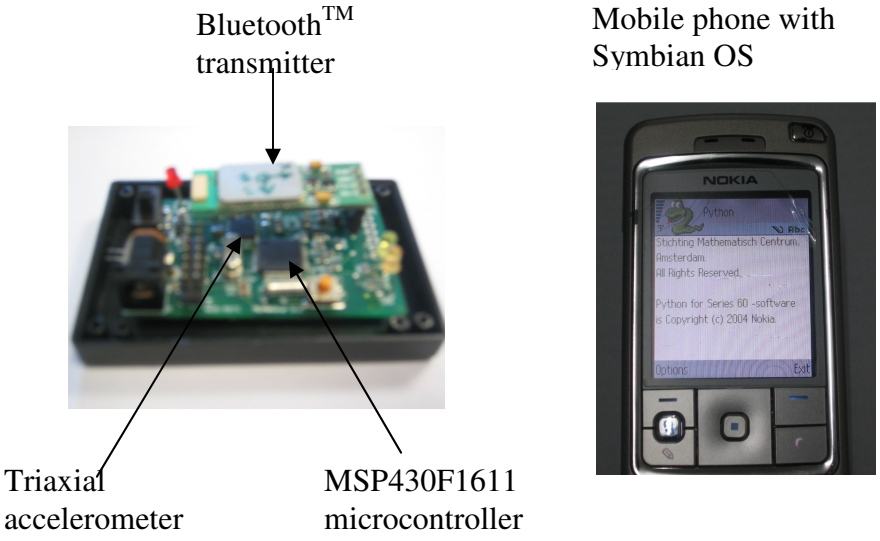

Figure 5.6. Real-time fall notification system

5.2 Pre-impact fall detection

5.2.1 Distinguishing fall activities from normal activities by angular rate characteristics and high speed camera characterization

Distinguishing sideways and backward falls from ADL using angular rate sensors (gyroscopes) was explored in this section. Gyroscopes were secured on MEMSWear at the positions of sternum (S), front of the waist (FW) and right underarm (RU) to measure angular rate in lateral and sagittal planes of the body during falls and normal activities. Moreover, the motions of the fall incidents were captured by a high-speed camera at a frame rate of 250 frames per second (fps) to study the body configuration during fall. The high-speed camera and the sensor data capture system were activated simultaneously by an observer by switching the systems on at the same time to synchronize the picture frame of high-speed camera and the sensor data. The threshold level for each sensor was set to distinguish fall activities from normal activities. Lead time of fall activities (time after threshold value is surpassed to the time when the hip hits the ground), and relative angle of body configuration (angle β between the vertical line and the line from the center point of the foot or the center point between the two legs to that of the waist (Figure 5.7)) at the threshold level were studied. This is the first study that investigates fall dynamics in detection of fall before the person hits the ground using angular rate sensors (gyroscopes). In this study we addressed the following parameters: (1) positive and negative peak values of angular rate of fall activities and normal activities to establish a threshold value between these two types of activities, (2) lead times of fall activities (time after threshold value is surpassed to the time when the hip hits the ground), and (3)

relative angle of body configuration at the threshold level via high speed visual inspection of fall incidents.

Figure 5.7. Angle of body configuration at the threshold level

5.2.2 Materials and methods

Volunteers were recruited via advertisements on notice boards on local university campus. They were selected according to age (between 20 to 30 years old), gender and scheduling availability. Ten volunteers participated, 5 males and 5 females. The average ages were 28 and 26.4 years old, respectively, with a range of 25 to 30 for males and 24 to 27 for females. The mean height and mass ± standard deviation of the males were 167.1 ± 5.2 cm and 67 ± 2.7 kg, respectively. For the female volunteers, the mean height ± standard deviation is 155.9 ± 4.3 cm, and for mass it is 49.6 ± 4.5kg. Informed consent was obtained from each of the subjects.

Before activation After activation

Figure 5.8. Experimental set-up of pneumatically-actuated fall simulator for back slip.

The experimental setup consisted of a pneumatically-actuated fall simulator (Figure 5.8). The subject stood on a movable platform (35cm by 35cm) actuated by compressed air of 5bar. When activated, the platform dashed away from the cushioning mattresses (two single-size foam mattresses 6in thick) at a speed of approximately 30cm/sec and caused the fall backward thereby simulating a slipping incident.

In the case of fainting incidents for sideways falls, the simulator was not used. The subjects were told to stand on the mattress and simply relaxed themselves and fall to the sides. The subjects did the fainting incidents on 6 inches thick soft foam mattresses. When doing the falls, the subjects were fitted with protective gear at the wrist, elbow and knee areas to prevent injury.

For this study, the vest was fitted with gyroscopes (ADXRS150, ±150°/sec, temperature drift=5mV(delta from 25°C)) at the sternum (S), front of the waist (FW) and right underarm (RU) positions to measure angular rate in lateral and sagittal planes during fall incidents and normal activities. Sensors at positions S and FW were used to measure the body movement in lateral plane (e.g., sideways fall) and sensor at position RU was used to measure in sagittal plane (e.g., backward fall). The two sensors measuring the body movement in the same plane were located at two positions (FW and

S) to investigate the effect of sensor location difference on the trunk. The amplifier gain of the gyroscopes was set to a sensitivity of 4.5mV/deg/sec. All gyroscope sensors were attached to the inner surface of the shirt.

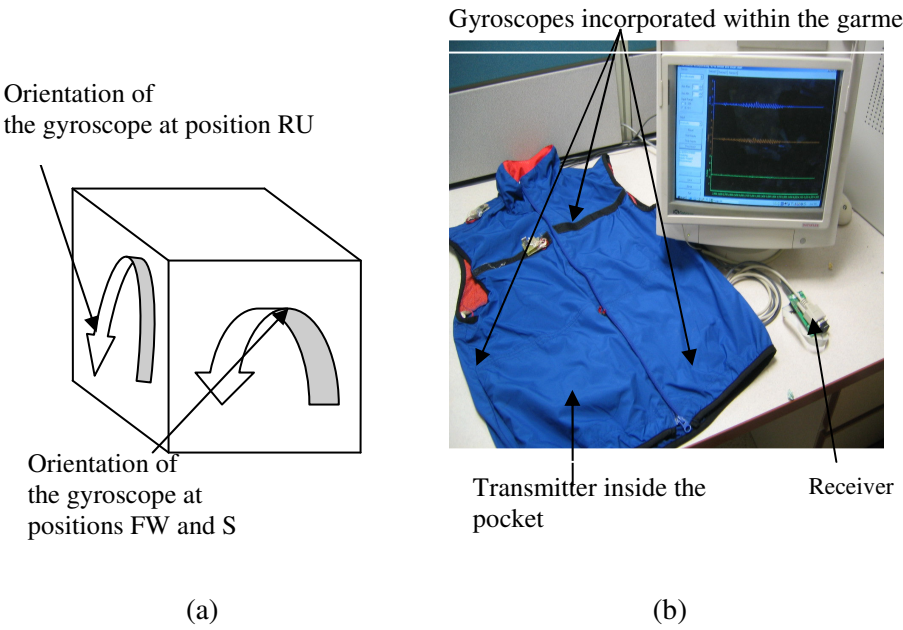

Figure 5.9. Orientation of the gyroscopes incorporated (a) and the vest with real-time data acquisition (b).

Figure 5.9(a) shows the orientation of the gyroscopes. Figure 5.9(b) shows the smart shirt, from which the data was gathered and transmitted to a base station (PC) via a Bluetooth™ wireless communication system. In this way, the sensor data was sampled at 230 Hz sampling rate and stored into the PC. Bluetooth chips with 10 meter effective data transmission range were used in the experiment. The transmitter was powered by a 9V DC power supply and was located inside the pocket of the smart shirt. The receiver was connected to the serial port of the PC and powered by the PC's USB port.

Each of the volunteers was first instructed to carry out a series of normal activities, which were chosen as representative of what an elderly individual might

encounter during activities of daily living. The order of activities were predetermined as: (1) standing up from a chair without arms (height, 46cm), (2) walking straight (5 sec), (3) bending down to pick up a pen on the floor, (4) walking straight (8 sec), (5) sitting down onto a bed (height : 27cm), (6) lying down on the bed, (7) posture transition from lying to sitting on the bed, (8) standing up, (9) walking straight (8 sec), and (10) sitting down onto the chair again (height , 46 cm) (Figure 5.10). After the volunteers had completed the normal activities, they were asked to carry out fall activities. For each activity, subjects were asked to repeat two times at a self-selected speed and strategy. The motion of the fall incidents was captured by a high-speed camera (Fastcam 10k) at a frame rate of 250fps. The high-speed camera and the sensor data capture system in PC were simultaneously activated by the observer by switching the two systems on at the same time. The purpose of this is to synchronize the picture frames from high-speed camera and the data from MEMSWear so that the signals from the sensors are in correspondence with the picture frames (e.g., 100^{th} sample of sensor data = $\left(100 \times \frac{250}{230}\right) = 109^{th}$ picture frame). To simulate slipping, the volunteer was asked to stand on the simulator platform and the simulator was activated upon command of the investigator. For fainting to sides, the volunteers were instructed to suddenly relax all muscles and fall flaccidly at the command of the investigator. The whole duration of each fall incident (~2.1s) was captured by the high-speed camera, which produced a total of 546 sequential pictures with a time interval of 4ms. Since we were particularly interested in hip injuries, we defined the end of a fall as the point when the volunteer's hip first comes in contact with the mattress. This point was determined in the picture frames of high speed camera. Segmentation of the sensor data related to normal activities was provided by the

investigator according to the preobserved data segment of normal activities and predetermined order of activities (Figure 5.10). Positive and negative peak values of normal activities were taken from each segment of the activities (Figure 5.10).

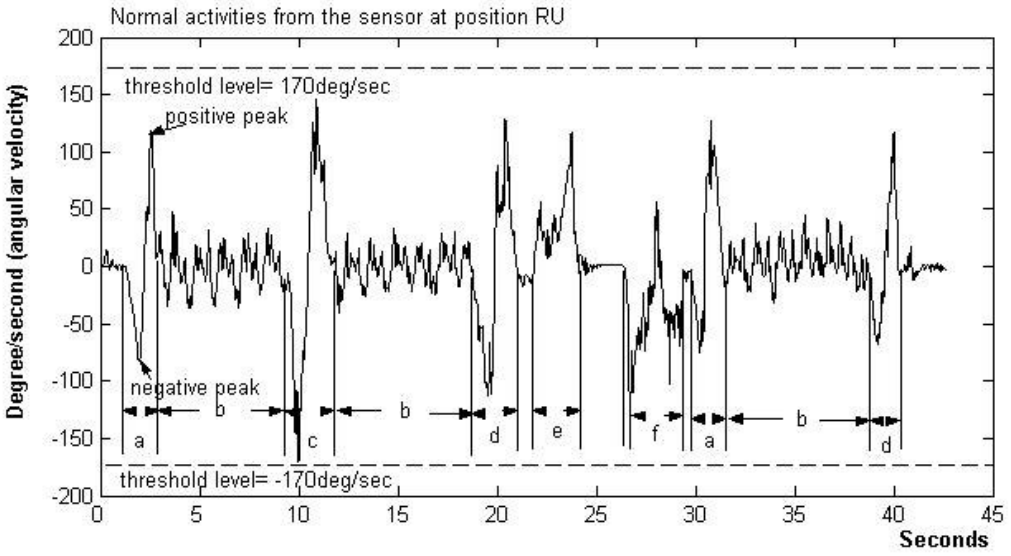

Figure 5.10.Normal activities from the sensor at position RU (a=standing up, b= walking straight, c= bending down to pick up a pen on the floor, d=sitting down onto a bed, e= lying down on the bed, and f= posture transition from lying to sitting on the bed).

To familiarize the volunteers with the experimental setup and protocol, they were permitted to fall freely onto the mattress before the experiments. The volunteers were told not to anticipate the command of the investigator but to concentrate on falling naturally with their muscles relaxed all the way to the mattress.

5.2.3 Results

Figure 5.11 shows the mean and one-sided standard deviation of fall activities and normal activities of positive peak and negative peak angular rates of gyroscope sensors at different positions (FW, S, and RU). ANOVA analysis indicated that positive and

negative peak angular rates of fall activities were significantly higher ($p<0.0001$) than those in the normal activities (Figure 5.11). For the sensor at position FW, peak values

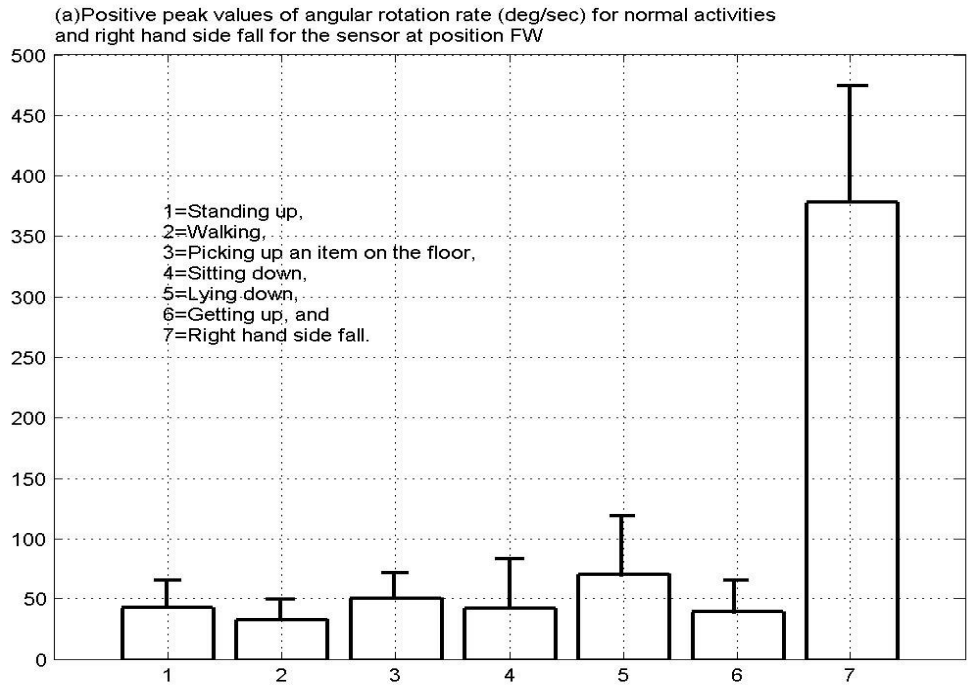

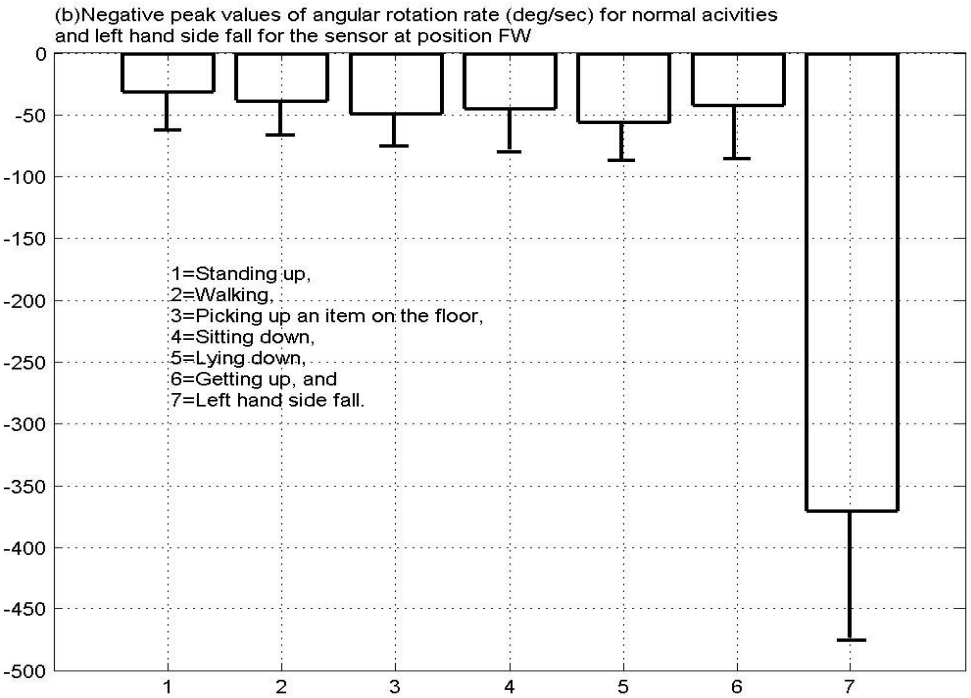

(c)Positive peak values of angular rotation rate (deg/sec) for normal activities and right hand side fall from the sensor at position S

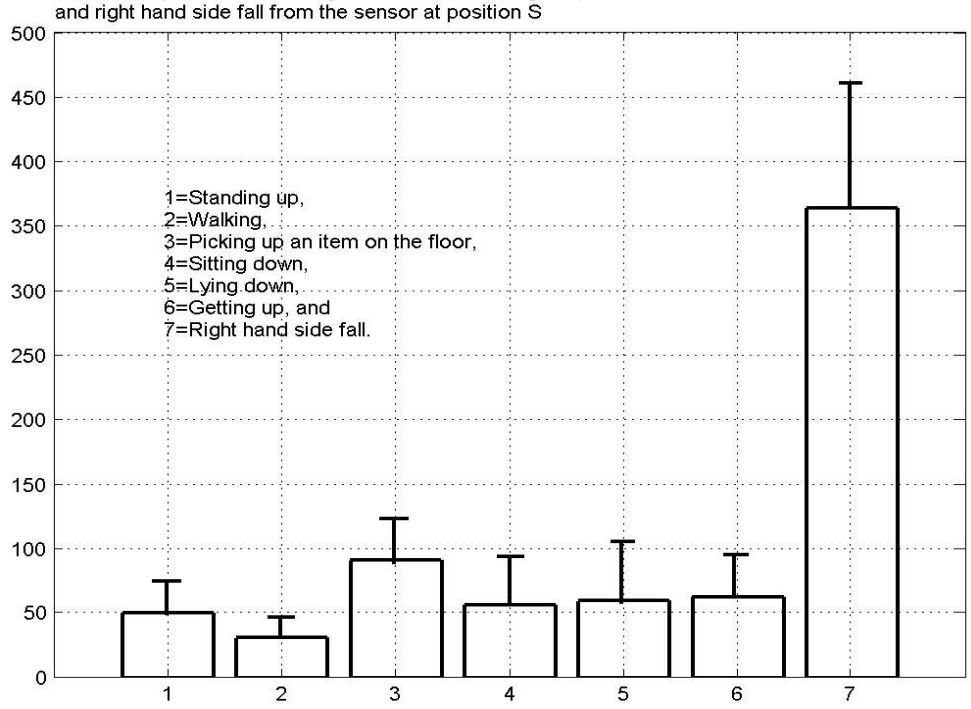

(d)Negative peak values of angular rotation rate (deg/sec) for normal activities and left hand side fall for the sensor at position S

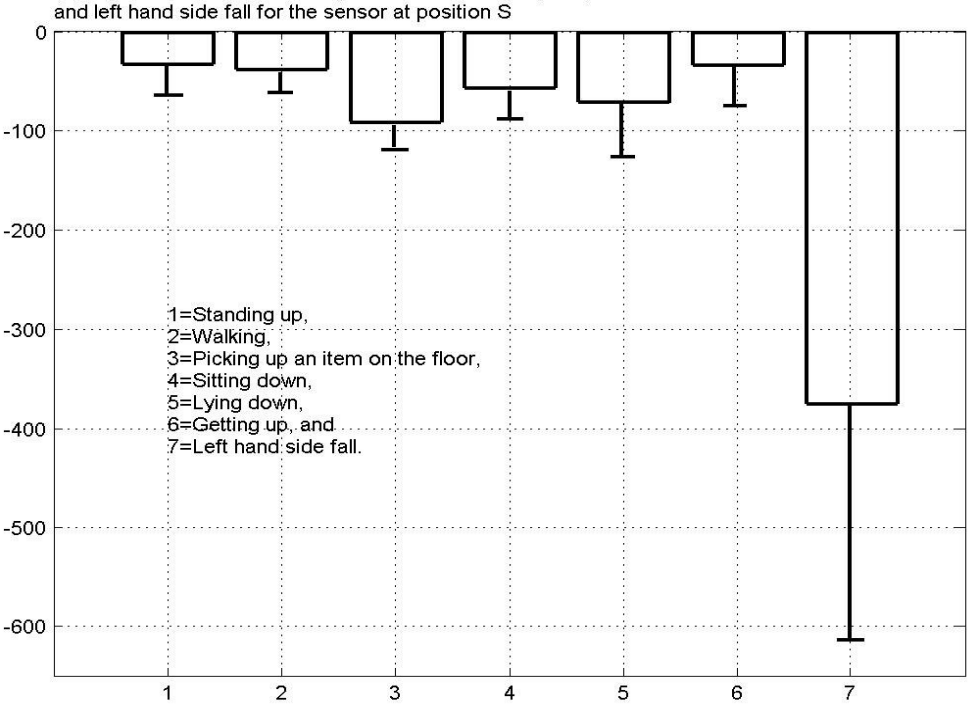

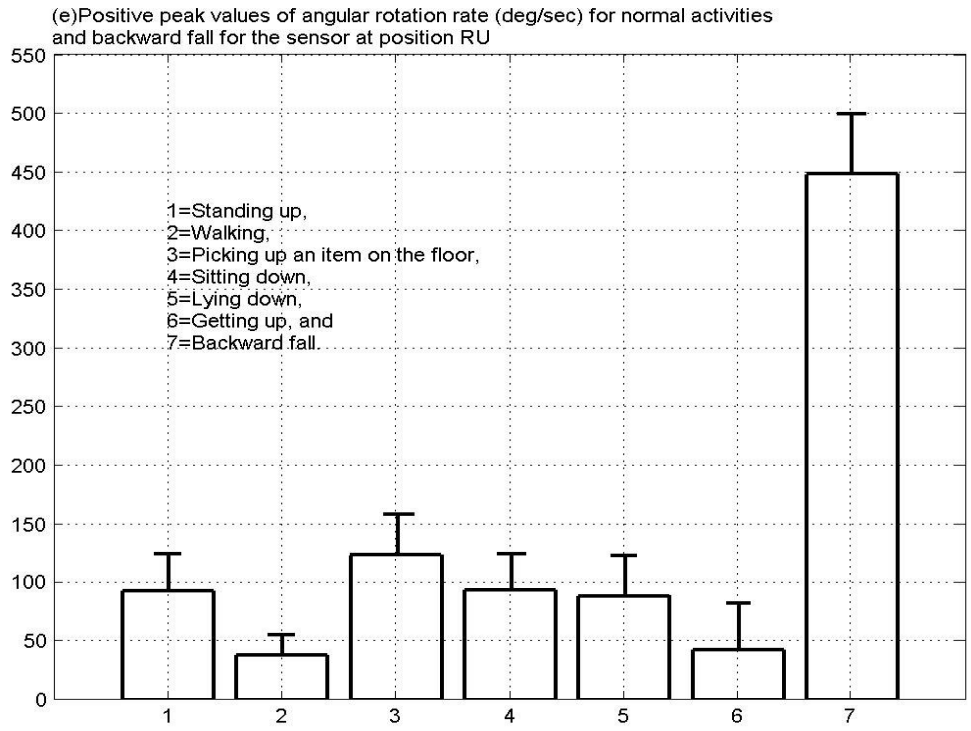

Figure 5.11. The mean and one side standard deviation of positive peak and negative peak angular rates of gyroscope sensors at position FW, S and RU. Both positive and negative peak angular rates of fall activities are significantly higher than those of the normal activities ($p < 0.0001$).

were limited within ±100 deg/sec (Figure 5.11(a) and 5.11(b)) and this value was set as the threshold level for that sensor in distinguishing fall activities (sideways falls) from normal activities. However, ±130 deg/sec was chosen as a threshold level for the sensor at position S and +170 deg/sec was chosen for the sensor at position RU. Positive and negative peak values of normal activities were limited within their respective ranges (Figure 5.11(c), 5.11(d), and 5.11(e)). Walking was perhaps one of the activities that had the least amount of angular rate for both positive and negative peaks of all three sensors. Lying down had the largest amount of angular rate for the sensor at position FW, while picking up a pen on the floor had the largest amount for sensors at positions S and RU. The angular rate of upper trunk was higher than that of the waist for activities especially

for bending over at waist to pick up a pen on the floor. Therefore, the threshold level of the sensor at position S was higher than that of the sensor at position FW. Moreover, the highest threshold level was set for the sensor at position RU because motion related to normal activities was faster in sagittal direction than in the lateral direction.

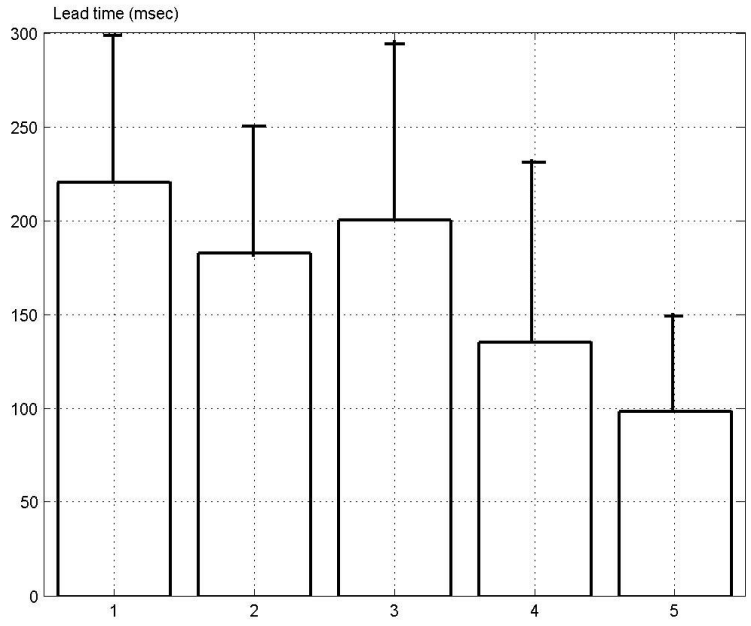

Figure 5.12. The mean and one side standard deviation of lead time for fall activities (20 trials for each fall activity) (1 = left hand side fall (FW), 2 = left hand side fall (S), 3 = right hand side fall (FW), 4 = right hand side fall (S), and 5 = backward fall (RU)).

Figure 5.12 shows the lead times of all fall activities. Definition of lead time, time after threshold value is surpassed to the time when the hip hits the ground, in fall activities is shown in Figure 5.13. For sideways falls, the lead time of the sensor at position FW (±100 deg/sec threshold levels) was about 200-220 msec and that of the sensor at position S (±130 deg/sec threshold levels) was about 135-182 msec. Simulated slippery backward fall had shorter lead time when compared to sideways falls and the lead time was about 98 msec for the sensor at position RU. The body configuration at threshold level for sideways fall and backward fall, expressed by β (between the vertical

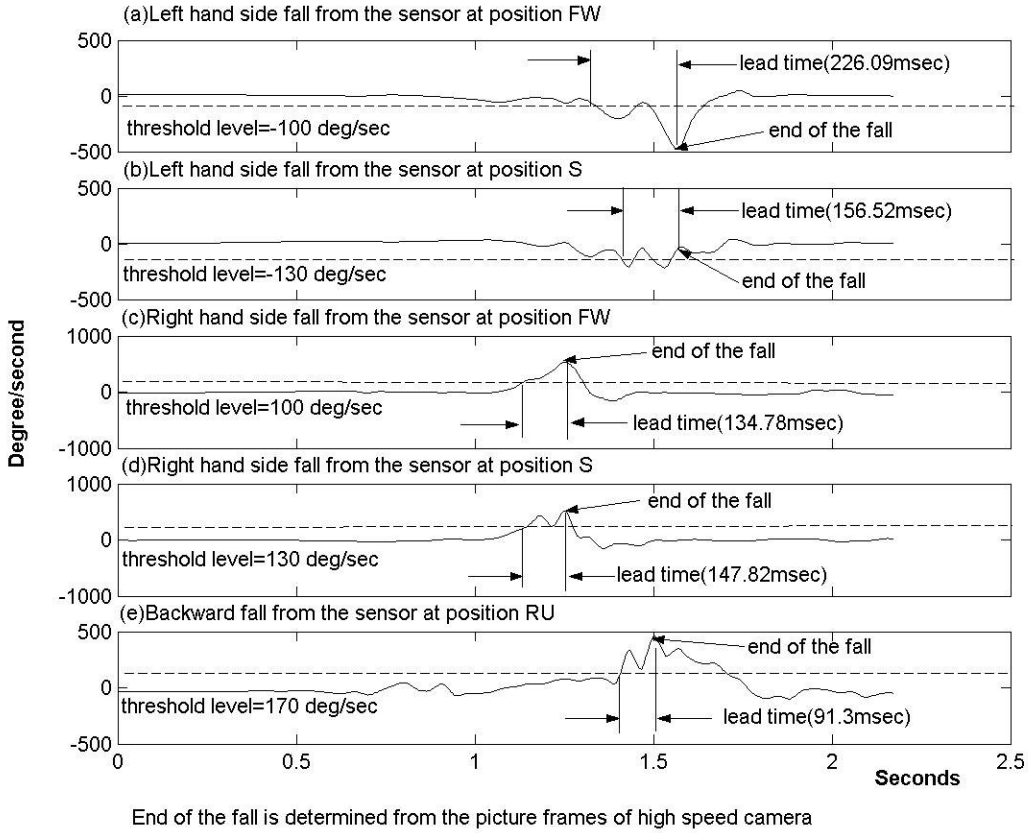

Figure 5.13. Sensor signals showing the lead times for sideways falls (left hand side and right hand side) and backward fall.

line and the line from the center point of the foot or the center point between the two legs to that of the waist, (Figure 5.14)), were about 40-43 deg for the sensor at position FW, about 43-52 deg for the sensor at position S and about 54 deg for the sensor at position RU, respectively (Figure 5.15). In the comparison of two sensors at positions FW and S, the sensor at position FW had longer lead time and lower β angle. In this study, all fall activities were correctly detected. To estimate the performance of fall detection using angular rate sensors, sensitivity, specificity, negative predictive value and positive predictive value were estimated as follow:

- Sensitivity = (true positives/(true positives + false negatives))*100%.
- Specificity= (true negatives/(true negatives + false positives))* 100%.

- Negative predictive value (NPV)= (true negatives/(true negatives + false negatives))* 100%.

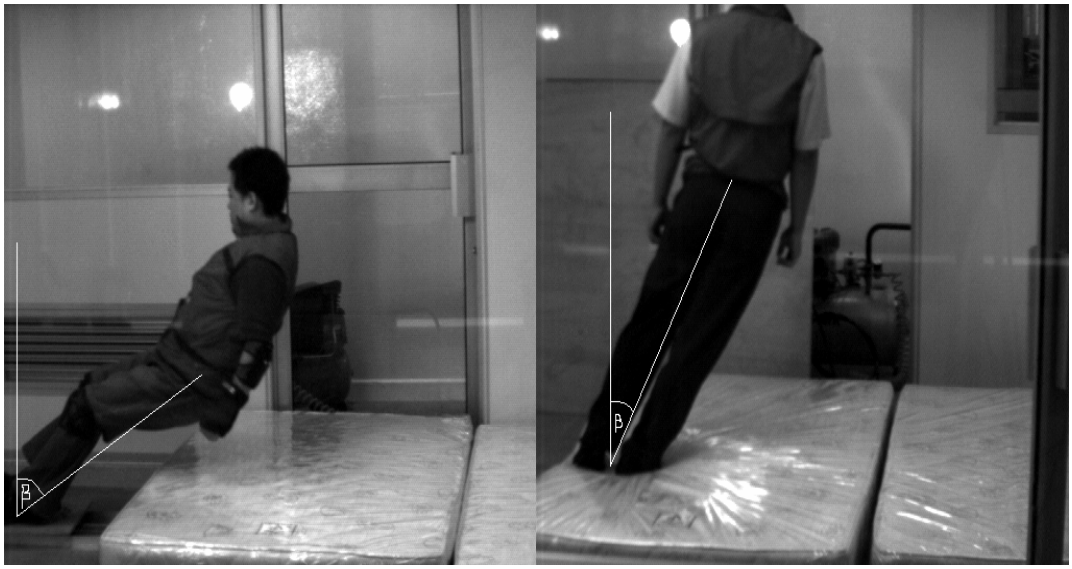

Figure 5.14. Typical body configuration at threshold level for backward fall and sideways fall.

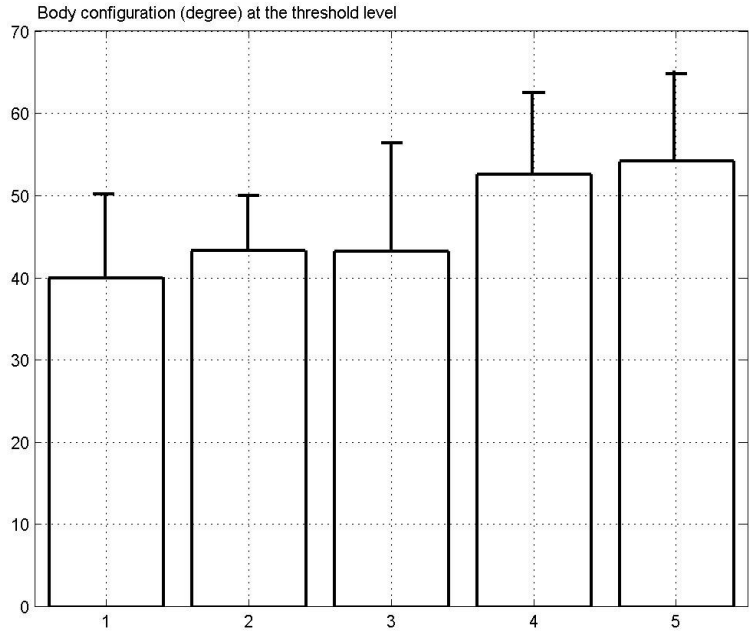

Figure 5.15. The mean and one-sided standard deviation of the body configuration at threshold level (20 trials for each fall activity) (1 = left hand side fall (FW), 2 = left hand side fall (S), 3 = right hand side fall (FW), 4 = right hand side fall (S), and 5 = backward fall (RU)).

- Positive predictive value (PPV)= (true positives/(true positives + false positives))* 100%.

In estimation, true positives were equal to the number of falls those were detected and false negatives were equal to the number of undetected falls. True negatives were equal to the number of daily activities those were not detected as falls and false positives were equal to the number of daily activities detected as falls. The estimations are presented in Table 5.2.

Table 5.2 Estimation the performance of fall detection using angular rate sensors

Sensors	Sensitivity	Specificity	NPV	PPV
FW	(60/(60+0))*100=100%	(185/(185+15))*100=92.5%	(185/(185+0))*100=100%	(60/(60+15))*100=80%
S	(60/(60+0))*100=100%	(188/(188+12))*100=94%	(188/(188+0))*100=100%	(60/(60+12))*100=83.3%
RU	(60/(60+0))*100=100%	(195/(195+5))*100=97.5%	(195/(195+0))*100=100%	(60/(60+5))*100=92.3%

Total number of normal activities=200 (Table 5.2).
Total number of falls= (number of left hand side falls+ number of right hand side falls+ backward falls)*number of subjects,
= (2+2+2)*10=60.

5.2.4 Discussion

The purpose of this study was to explore the automatic detection of fall, which can cause hip injuries, during its descending phase using body-worn devices. Since most of the fall-related injuries in the elderly occur after the body hits the ground [90,111], detection before the person's hip hits the ground offers some possibilities in reducing the severity of hip injuries [90]. To date, no work has been done on the characteristics of fall movement that diverge from normal activities using angular rate sensors. Compared to the camera-based system (eg. Vicon^{TM} system), the system based on body-worn devices (small and lightweight sensors) is more appropriate for free-living conditions as there is no limited effective space in surveillance.

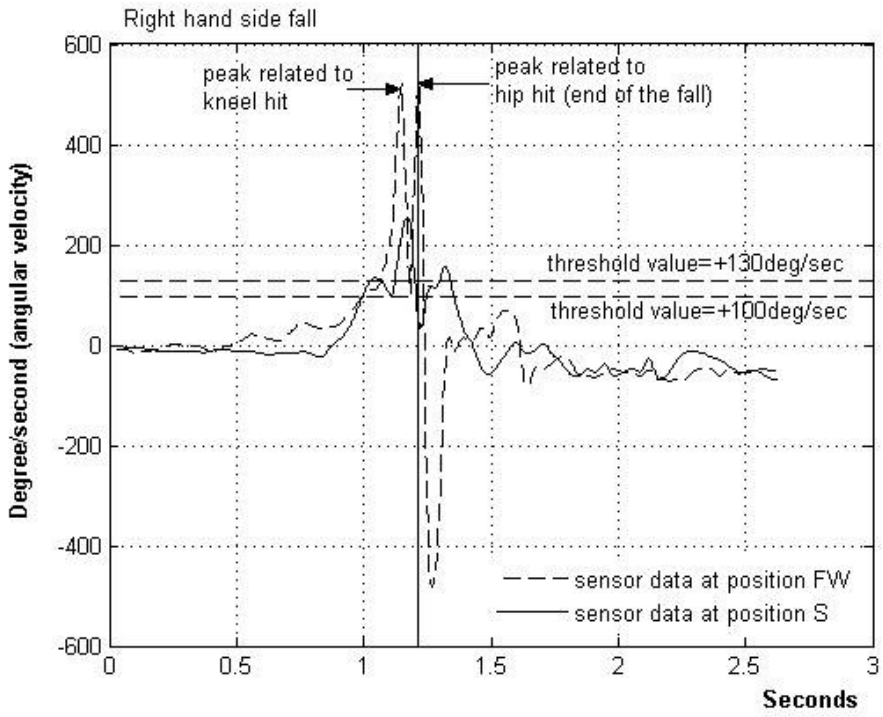

Figure 5.16. The angular rate of right hand side fall from the sensor at position FW and position S

The results in this study suggest that angular rate characteristics at various locations of the body are different for different types of activities. For the sensors measuring the lateral movements of the trunk, the amplitude of the sensor output from the upper trunk is larger than that of the sensor at the lower trunk for the activities like bending over at the waist. However, for fall activities, there are no significant differences between the sensor signals at these two positions, i.e., the amplitude of the sensor output from the upper trunk (position S) is not always larger than that of the sensor output from the lower trunk (position FW) (Figure 5.16). The consequence is that the sensor at upper trunk (position S) has higher threshold value, shorter lead time and larger β angle at the threshold value. According to the experimental results, the sensor at the waist level (position FW) gives around 200 msec lead time and about 40 deg β angle for sideways falls. However, for the sensor measuring in the sagittal direction, the experimental results

for slippery backward fall (about 98 msec lead time and about 54 deg β angle) are shorter in lead time and larger in β angle compared with those of the sensors in lateral direction detecting sideways falls. To reduce the severity of the hip fractures in sideways falls, we can activate the prevention system within this limited time duration. The prevention system could be employed in conjunction with existing injury prevention methods or any system to regain the consciousness of the faller.

Obviously, if the threshold value is increased, false alarms will be reduced. The consequence is that lead time will be decreased and angle β will be increased. For the threshold values set in the experiment, we can see the false alarm table for normal activities (Table 5.3). The sensor at position FW has more false alarms than the sensor at position S by setting lower threshold level ±100 deg/sec. The angular rate of upper trunk is higher than that of the waist for activities especially for bending over at waist to pick up a pen on the floor and hence, the sensors at upper trunk (position S and RU) have more false alarms for that activity than the sensor at position FW. In ADL, downward movements such as sitting down and lying down move faster (i.e., higher angular velocity) than upward movements such as standing up and lying to sitting posture transition. Therefore, majority of the false alarms happen in sitting down and lying down activities as shown in Table 5.3.

We considered increasing the frame rate of the camera up to 1000 fps. Pictures presenting the fall process were very redundant for 1000 fps. Moreover, the camera system did not allow saving all the pictures of the whole fall process for frame rate more than 250 fps. Therefore, we decided to choose 250 fps. In this study, the picture

corresponding to the subject's hip first comes in contact with the mattress was taken as the end of the fall process (Figure 5.17). Actually, most of the hip fractures in the elderly

Table 5.3 False alarm table for normal activities (Number of false alarms)

Sensor position	FW	FW	S	S	RU
Threshold level	+100 deg/sec	-100 deg/sec	+130 deg/sec	-130 deg/sec	+170 deg/sec
Standing up (10 subjects x 2 times x 2 segments=40 trials)	1	0	0	0	1
Walking (10 subjects x 2 times x 3 segments=60 trials)	0	0	0	0	0
Bending down (10 subjects x 2 times x 1 segment=20 trials)	0	0	2	3	4
Sitting down (10 subjects x 2 times x 2 segments=40 trials)	4	3	1	1	0
Lying down (10 subjects x 2 times x 1 segment=20 trials)	4	1	2	3	0
Posture transition from lying to sitting (10 subjects x 2 times x 1 segment=20 trials)	1	1	0	0	0

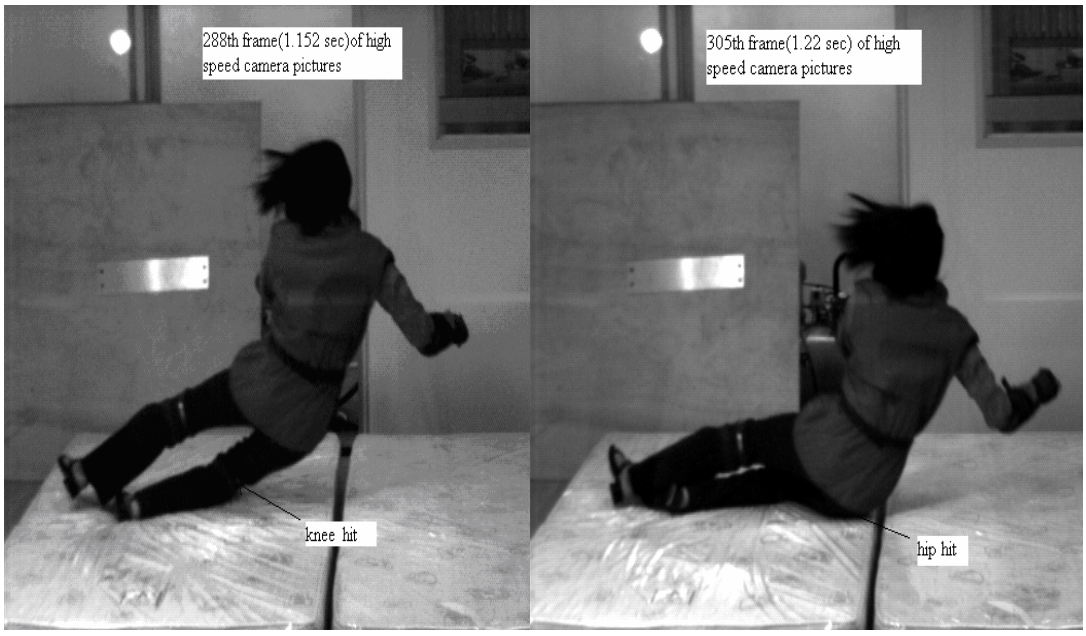

Figure 5.17. Picture frames related to knee hit and hip hit (end of the fall).

occur after their hips hit the ground [111]. Therefore, our lead time duration is well within the time duration necessary for hip fracture. In this study, we focused on sideways and backward falls since such a fall has the highest risk of hip fractures [70,71,112,113]. Our data on lead time and angle β at threshold level can be used in design consideration of hip fracture prevention mechanism. To our knowledge, this is the first study that investigates fall dynamics using human subjects wearing angular rate sensors (gyroscopes) in detection of fall before the person hits the ground. Even though there are some false alarms in this study, we can pave the way for protecting hip fracture for the elderly in a free living environment. It should be pointed out that all the activities tested in the experiment were performed by healthy individuals below the age of 30 years. The movement of this group of people will not be exactly the same as the movement of the elderly in fall activities. All the experimental results presented above are from simulated falls and there may be some discrepancy between the responses to the simulated falls and the responses to the real faintings and slippery backward falls. Moreover, we found that some subjects hit the mattress with their knees first followed by the hips (Figure 5.17). Although our subjects appeared to comply with the instruction of not attempting to recover before their hips hit the ground, we cannot guarantee that subtle attempts at recovery were not made. Since our concern is mainly on the lead time and body configuration at the threshold level, this knee hit does not result in any deviation in our experimental results. From this study we presented the characteristics of fall activities to distinguish fall activities from normal activities using gyroscope sensors. Lead times, about 200-220 msec and 135-182 msec, were observed by locating the sensors at

positions, FW and S, and about 98 msec lead time was achieved by locating the sensor at position RU (Figure 5.12). The angle β between the vertical line and the line from the center point of the foot or the center point between the two legs to that of the waist were about 40-43 deg for the sensor at position FW, about 43-52 deg for the sensor at position S and about 54 deg for the sensor at position RU, respectively (Figure 5.15). However, further exploration of how to reduce the false alarm and further tests on the older population in real-life situations are still needed. Moreover, suitable temperature compensation strategy needs to be considered in long term application because the temperature drift may affect the performance of the sensor in distinguishing fall activities from normal activities.

Chapter 6

Real-time detection of falls and ADL using wearable computing platform

Real-time detection of ADL and falls (post impact detection) using methods discussed in Chapter 4 and Chapter 5 based on a wearable data processing system is discussed in this chapter. The system consists of MCF5282 ColdFire® Microcontroller (32 bit, 80MHz, 512KB Internal Flash, 64KB Internal SRAM and 16MB external SDRAM), Bluetooth™ transmitter, SD (Secure Digital) card and 7.6V battery power supply (Figure 6.1). MMA7260Q (±1.5g - 6g Triaxial Low-g Micromachined Accelerometer, 300mV/g) accelerometer was used in the system. The accelerometer was located at the shoulder location of the garment. In real-time detection, the sampling rate is reduced from offline sampling rate, 256 samples/second (chapter 4), to 50 samples/second to save processing time. However, the new sampling rate is still in line with other researchers' applications and it is high enough to detect ADL and falls [19,42].

6.1 Methodology

Figure 6.2 shows the data collection and data processing of real-time fall and ADL detection algorithm. In the algorithm (Figure 6.3), fall detection, sit-stand/stand-sit transition detection, lie-sit/sit-lie transition detection, and level walking detection are done for all 350-sample segments. Three hundred and fifty sample data is segmented with 40% overlapping. If fall incident happens, daily activities are not detected for that

segment and next 350-sample segment is proceeded. In sit-stand/stand-sit detection, extracted sit-stand/stand-sit segments are confirmed using rest-state (variance of one-sec long data<0.002g in time duration [t_P-4sec,t_P+4sec], where t_P is time of posture transition point P (Figure 4.10) and data length (>0.7sec). Then, sit-stand/stand-sit and lie-sit/sit-lie

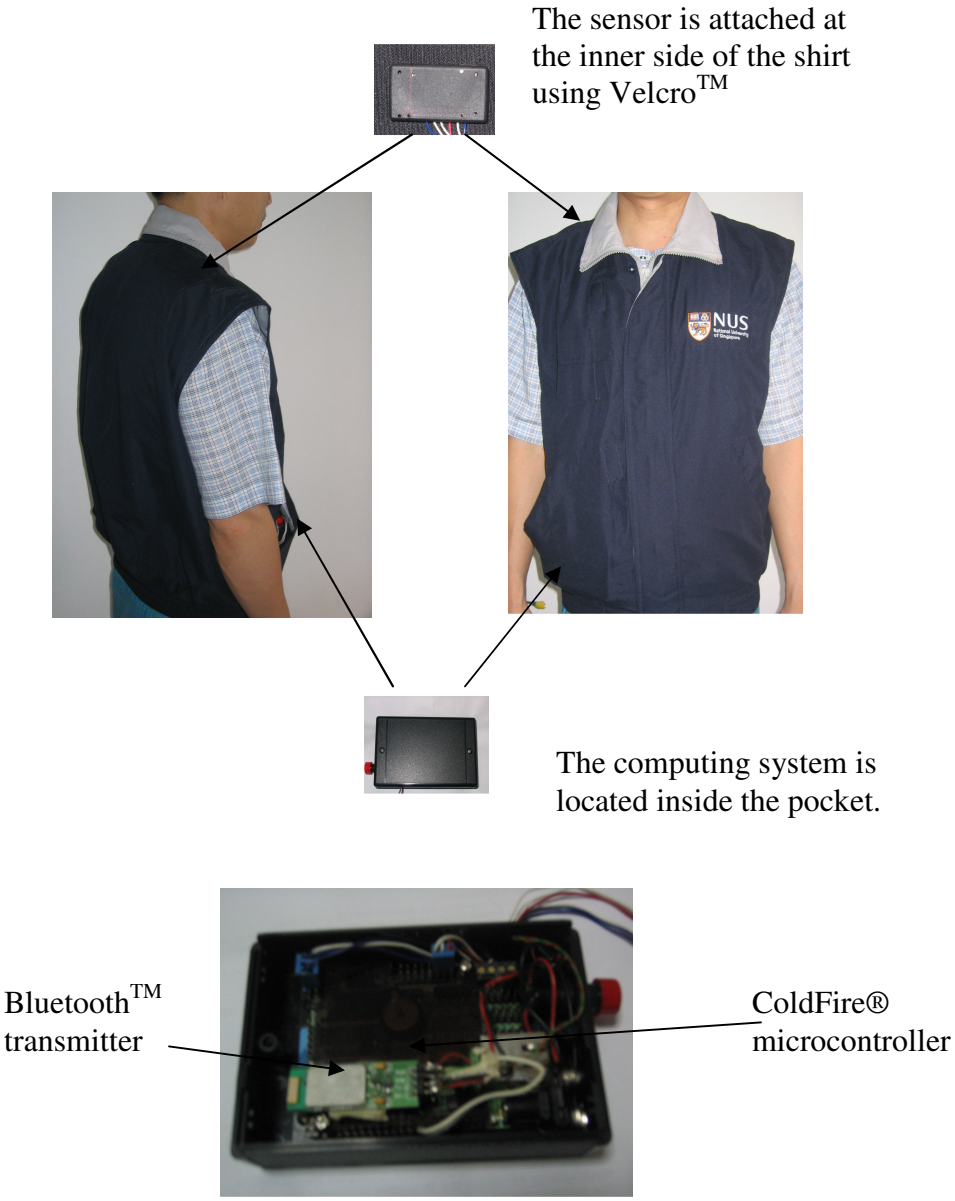

Figure 6.1. Wearable real-time falls and activities detection system

transition activities data in both 350-sample segment and 2660-sample segment of vertical and antero-posterior acceleration signals are replaced with zeros if they are detected. Level walking, ascending stairs and descending stairs were classified as discussed in section 4.3.3.

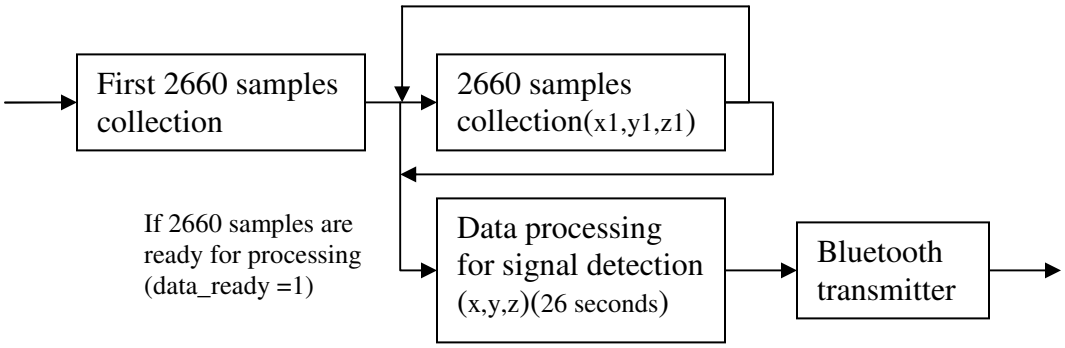

Figure 6.2. The process of data collection and data processing for falls and ADL detection

The time duration of the experimental data for the continuous activities, sit-stand + level walking + stand-sit, is about 7 sec (Figure 4.11). Therefore, 350 samples (50 samples/sec * 7 sec=350 samples) data length is chosen for sit-stand, stand-sit, sit-lie and lie-sit activities detection. The data length for level walking and walking on two flights of stairs (one flight with 15 steps) is about 70 sec long (Figure 4.16). Hence, 50 sec data length (2660 samples) is chosen for the detection of level walking and walking on two flights of stairs (one flight with 6 steps) for the experimental setting shown in Figure 6.4. Since data lengths of lie-sit/sit-lie and stand-sit/sit-stand activities are about 2 sec long (Figure 4.7 and Figure 4.12), forty percent (0.4*7 sec=2.8 sec) overlapping is chosen not to miss the activity in segmentation. Therefore, (350-(350*0.4))*11+350=2660 samples data length is used in the detection algorithm (Figure 6.2 and 6.3). Maximum decomposition levels *J* are different from previous discussions, section 4.3.1, 4.3.2 and

4.3.3, because of using different sampling rates between the real-time detection (50Hz) and offline detection (256Hz). The relations between the decomposition levels (scales) and frequency bandwidths were discussed in Table 3.1.

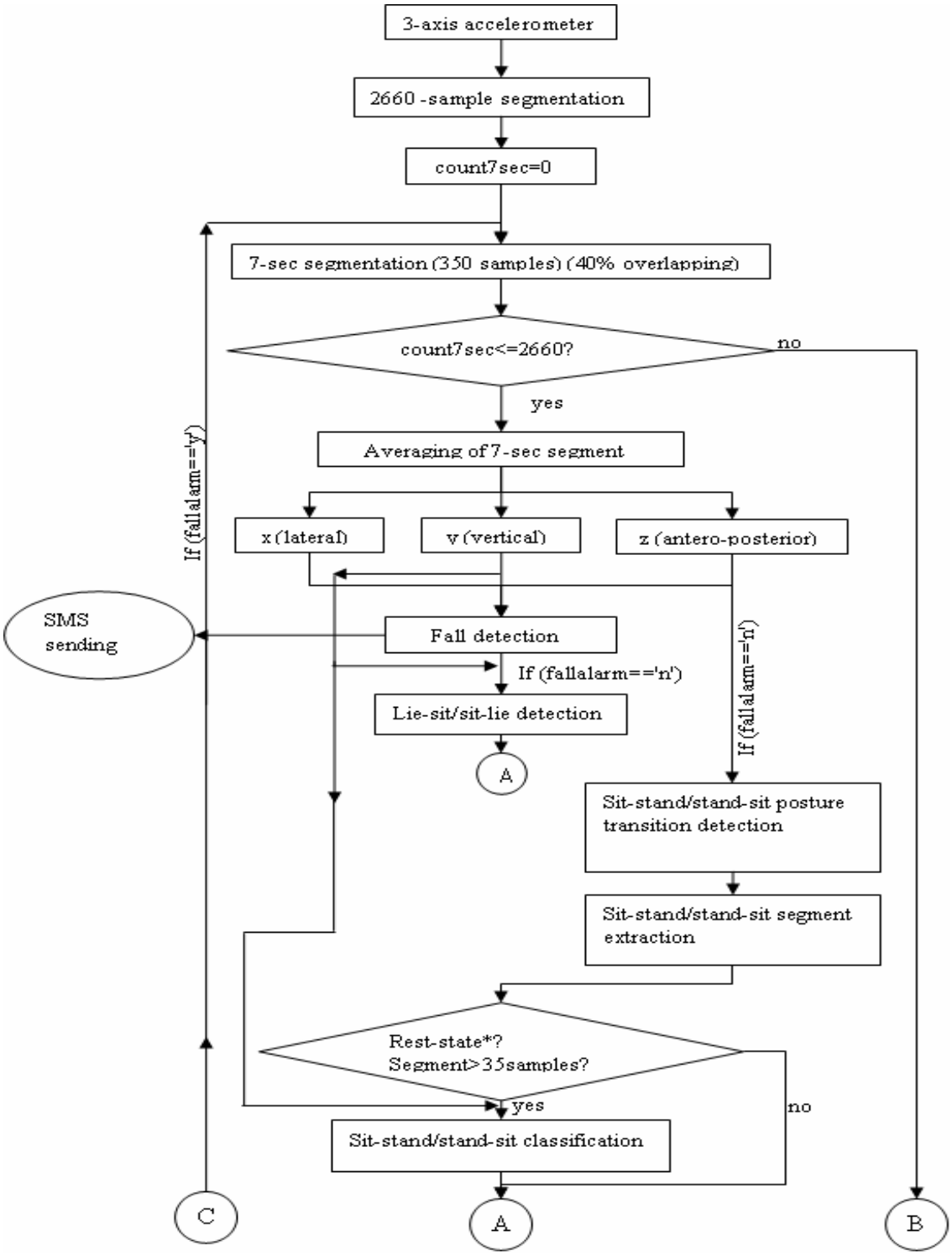

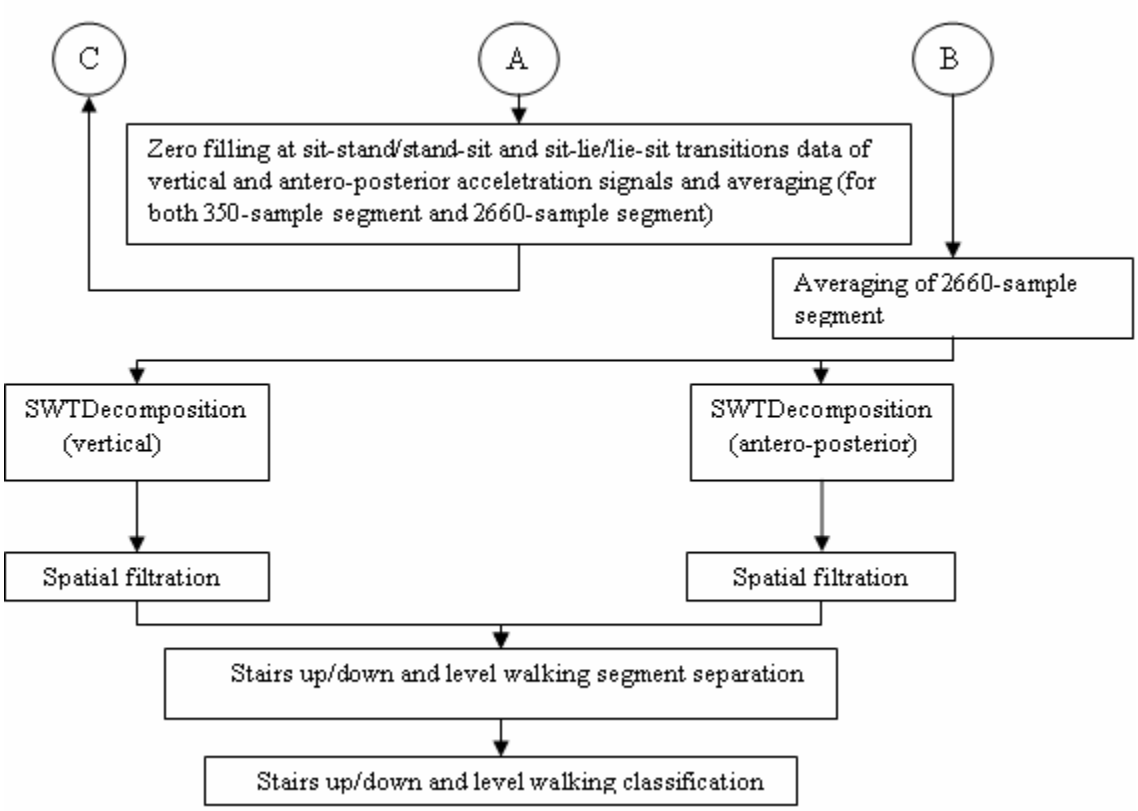

* - variance of one-sec long data<0.002g in time duration [t_P-4sec,t_P+4sec], where t_P is time of posture transition point
J=4 for lie-sit/sit-lie detection, sit-stand/stand-sit posture transition detection
J=1 for sit-stand/stand-sit classification
J=3 for SWTDecomposition (vertical)
J=4 for SWTDecomposition (antero-posterior)

Figure 6.3. ADL and falls detection algorithm flow chart.

6.2 Subjects and experimental procedure

The experiments were performed on 3 male and 3 female subjects (age between 30 and 49 years, height between 152.5cm and 172.7cm, and weight between 49kg and 75kg). Two different experimental settings (Figure 6.4) were used for two different groups, i.e., group1 at setting-a (Figure 6.4(a)) includes subject 1, subject 4, subject 5, and subject 6 and group 2 setting-b (Figure 6.4(b)) includes subject 2 and subject 3. Each

subject did approximately five-hour-long experiment. During the experiment, all subjects did the predefined ADL of sit-stand/stand-sit transition, lie-sit/sit-lie transition, level walking, stairs up, and stairs down. However, the sequence of the activities was not restricted. The activities done in the experiment are common ADL among the elderly [19,104,105]. All six subjects conducted altogether 1495 activities in that approximately five-hour-long experiment. All the activities detected by the system were sent to Notebook™ through Bluetooth™ transmitter/receiver together with the time information of the activity. An observer was together with the subject during the experiment and recorded when the error occurred. Informed consent was obtained from each of the subjects.

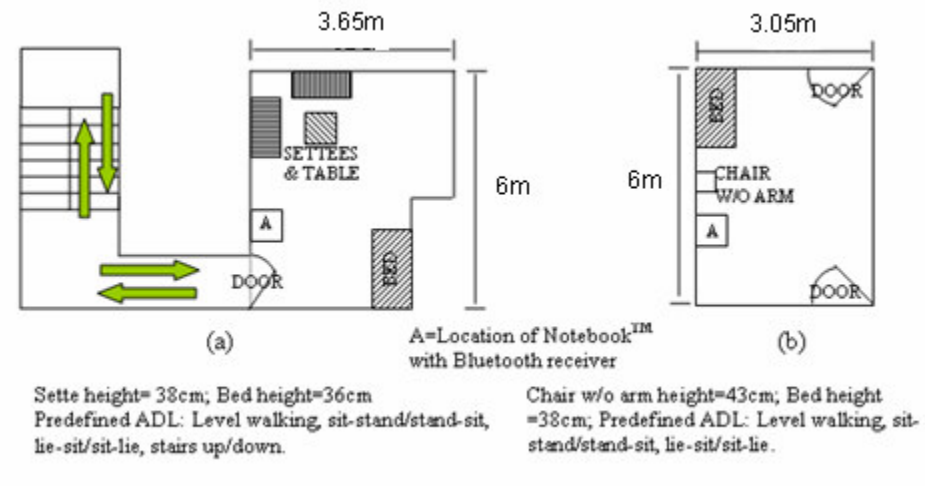

Figure 6.4. Two different experimental setups

Table 6.1 The sensitivity and specificity of activities in approximately five-hour long experiment

	1			**2**			**3**			**4**			**5**			**6**		
Age	32			49			45			30			29			30		
Sex	Male			Female			Female			Male			Female			Male		
Height	165.1			157cm			152.5cm			172.7cm			160cm			172.7cm		
Weight	65kg			50kg			49kg			51kg			50kg			75kg		
Duration of monitoring	300.4min			303.05min			302.18min			303.1min			286.7min			279.62min		
Total number of activities	131			84			204			586			263			227		
	N	Se %	Sp %	N	Se %	Sp %	N	Se %	Sp %	N	Se %	Sp %	N	Se %	Sp %	N	Se %	Sp %
Level walking	32	100	100	22	100	100	39	100	100	114	100	100	57	100	100	57	100	100
Sit-stand	42	92.9	100	28	92.9	98.2	76	93.4	100	215	95.3	99.4	95	92.63	98.8	76	93.4	98.7
Stand-sit	41	95.1	100	28	92.9	100	73	94.5	98.5	215	87.9	98.9	95	95.8	98.2	78	93.6	99.3
Lie-sit	6	100	100	3	100	100	8	100	100	19	100	100	7	100	100	5	100	100
Sit-lie	6	100	100	3	100	100	8	100	100	19	100	100	7	100	100	7	100	100
Stairs up	2	100	100							2	100	100	1	100	100	2	100	100
Stairs down	2	100	100							2	100	100	1	100	100	2	100	100
Overall sensitivity for 1495 activities								1420/1495=94.98%										
Overall specificity for 1495 activities								1437/(1437+17)=98.83%										

N=number of activities; Se=sensitivity; Sp=specificity

Overall sensitivity=Number of activities correctly detected by the system/total number of activities

Overall specificity**=**Total number of detected activities/(Total of detected activities+wrongly detected activities)

6.3 Results

The sensitivity and specificity of each subject is presented in Table 6.1. Sensitivities (defined as the ability of the system to correctly identify the true activities) and specificities (defined as the ability of the system not to generate false detection) were calculated as sensitivity = (true positives/(true positives+ false negatives)) and specificity = (true negatives/(true negatives+ false positives)). True positives, false negatives, true negatives and false positives of one type of activities, e.g., sit-stand transition, were estimated as follows:

- True positives were equal to the number of true sit-stand transitions, correctly detected by the system.

- False negatives were equal to the number of sit-stand transitions, not detected by the system.
- True negatives were equal to the number of other types of activities detected by the system, which were not true sit-stand transitions.
- False positives were equal to the number of other types of activities wrongly detected as sit-stand transitions.

6.4 Discussion

The results show that the system, based on only one triaxial accelerometer attached onto the shoulder part of the garment, performs well in detecting ADL. Even though the system can detect fall, according to the experimental results presented in section 5.1, it was not included in real-time detection experiment because the subjects were not willing to do during the experiment.

The real-time detection of ADL is useful in several applications such as detecting the attempts of elderly patients to get out of bed or to rise from a chair, another fall prevention scenario as these activities can lead to fall events, [114] or detection of the abnormal behaviors of the patients suffering dementia. Moreover, real-time fall incidence detection is one of the major health care issues in the elderly because an undetected fall in an older person, especially for the elderly in solitary lives, can result in a person lying conscious and uncomfortable for hours before being saved, and the resultant activation of a response/help system is of immense benefit leading to a shortened interval before the arrival of assistance.

Several falls and ADL detection algorithms have been proposed in the past [19,32-51]. Although much work has been done in fall and ADL detection, more studies need to be conducted in view of the need for comfort in assessment for long-term use. In our case, the sensors are fixed onto the garment unlike the other researchers who attached the sensors onto the body. Investigations using similar off-line detection approaches, i.e., locating the sensors on the trunk, were published by Najafi et al., [19] and Mathie et al., [42]. Najafi et al. detected ADL using a kinematic sensor attached to the chest. The kinematic sensor includes a biaxial accelerometer and a gyroscope. The gyroscope measures the sagittal plane information of the body movement. The sensor is protruding out of the chest and no detail description is provided on how the sensor is attached on the chest. The placement of the sensor may not be comfortable for the subject for long term application. The sensitivity (>90%) was achieved in time-frequency based activity detection. Mathie et al. detected falls and ADL using a framework structured around a binary tree in which movements were divided into classes and subclasses at different hierarchical levels. A triaxial accelerometer mounted at the waist level was used in his detection. Fixed threshold, pattern matching, and expert system methods were applied to detect falls and activities. Pattern matching is not the appropriate method in fall detection (sensitivity 80.5%) because the patterns of 3-axis accelerometer related to fall activities are very arbitrary. The overall sensitivity 97.7% and specificity 98.7% over a data set of 1309 movements were achieved. However, this high sensitivity and specificity were accomplished performing the predefined set of sequence of activities. Even though we put the sensor on the garment, our detection procedure can produce comparable results, sensitivity 94.98% and specificity 98.83% for altogether 1495 activities, to their

implementations in which sensors are directly attached onto the body using belt or other elastic materials.

The place of the attachment of sensors on the human body is an important issue. Waist level on the vest is not appropriate for the sensor to be located because normally the lower parts of the vest around waist level would fold during sitting posture and it is the most interfered location by hand movements on the vest such as touching the sensor very often in normal movements. Therefore, the locations that sensors can be attached at the vest are on the chest and on the shoulder. From the methodological point of view, all of the features used in the detection methods presented in chapter 4 are based on fundamental facts that every body follows in their ADL movements. The features that accelerometer outputs carry by locating the sensors on the shoulder will not be changed if the sensor location is moved to the chest. Therefore, from the methodological point of view, the system performance is not different because of the different locations between the chest and the shoulder. However if we consider other factors such as (1) the sensor to be least interfered by the subject's activities, (2) the sensor will cause minimal discomfort to the subject and (3) the sensor will not injure the wearer during the severe incidents such as falls, the shoulder location is the optimum choice for the wearable application. In activity detections, the sensors are mostly attached to the body directly using adhesive tape or elastic straps in avoiding the artifacts due to the movements of clothes (Bouten et al. [32]). According to our experimental results (Figure 4.7, Figure 4.8, Figure 4.10, Figure 4.11 and Figure 4.13), even the signals from human motion activities did not interfere with the detection of sit-stand/stand-sit and sit-lie/lie-sit transitions. Therefore, there is no significant effect of the vest on the acceleration data that can decline the

performance of the algorithm and the artifacts caused by the clothes are not a serious issue in our detection method.

There are some points to be mentioned in this study. Firstly we used limited number of subjects and these results should still be confirmed with larger population. Secondly these subjects were volunteers and not representative of people at different ages. However, 37 subjects altogether, including the subjects volunteered in the previous analysis (section 4.3.2 and section 4.3.3), where 9 subjects for experiment of sit-stand/stand-sit transition detection, 22 subjects for experiment of gait patterns classification and 6 subjects for approximately five-hour-long experiment, show reliable results using our detection method. Despite these limitations, we believe this system has the potential for extended clinical research applications. Particularly, our wearable system will be useful in long term in-home health care implementations.

Chapter 7

Conclusions and recommendations

In this thesis, a novel approach of fall and activities of daily living (ADL) detection based on a normal garment (vest) that can detect a broad range of ADL using relatively fewer sensors, in comparison to other researchers' systems, for the comfort of the user in long term application was developed. The system can detect falls and send fall notifications to individuals and the health care unit at the same time without user intervention. A triaxial accelerometer measuring lateral, antero-posterior and vertical directions is attached at the shoulder position of the garment. ADL detected in our studies are vital daily activities such as sit-stand/stand-sit transitions, sit-lie/lie-sit transitions, level walking, ascending stairs and descending stairs. Conclusions and contributions of the research work undertaken are summarized as follows.

ADL were detected in the time-frequency domain. In the detection of motion activities (level walking, and walking on stairs), segments related to different types of activities were separated using an algorithm based on the spatially selective filtration technique. The filter algorithm (Table 4.3) enhances and extracts the portion if wavelet coefficients are well correlated across the decomposed levels. In this way, ascending stairs/descending stairs segments with well correlated wavelet coefficients across decomposed levels were separated from level walking segments. After segment separation process, power of extracted coefficients of vertical acceleration signal, *PcoefsY*, was used to classify between level walking and descending stairs and that of

antero-posterior acceleration signal, *PcoefsZ*, was used to classify between level walking and descending stairs. There were no negative coefficients for descending stairs segment and no positive coefficients for ascending stairs segment and resulted in no misclassification between descending stairs and ascending stairs. Moreover, most of the extracted coefficients of level walking signals were zero and positive and it can reduce the misclassification between level walking activity and ascending stairs activity. Therefore, our gait activities detection algorithm is as perfect in its kind as it can detect all three types of activities in high accuracy (>97.67%), and the detection parameters (e.g., threshold levels used in detection) are not varied with individuals in compared to other detection methods [39, 40].

In the detection of sit-stand/stand-sit posture transition activities, wavelet reconstructed antero-posterior acceleration signal was used in transition segment extraction and wavelet coefficients of extracted vertical acceleration signal were used as features in classification. First fifty wavelet coefficients carried the important characteristics of transition segments such as a positive peak followed by a negative peak for sit-stand transition and a negative peak followed by a positive peak for stand-sit transition. Applying wavelet coefficients from vertical acceleration signal offers the reduction of the complexity of detection procedures using minimum number of features in classification. The classification rates 93.65% and 95.24% for sit-stand and stand-sit activities are better than other similar detection methods in which 93.5% for sit-stand/stand-sit activities (Mathie et al.) and 93% for sit-stand activities and 90.2% for stand-sit activities (Najafi et al.) were achieved [19,42].

Lie-sit/sit-lie posture transition is detected by considering the orientation of the accelerometer with respect to the gravitational axis. In detection, the reconstructed vertical acceleration signal (<1Hz) was applied to cancel additional peaks with different frequency components. Then, we have developed a real-time fall and ADL detection system using a garment as a wearable platform. We did five-hour long experiment using six male and female subjects. Overall sensitivity of 94.98% is achieved for detection of altogether 1495 different activities.

In contribution, we have developed new wavelet based ADL detection methods that can provide high accuracy in ADL detection. Using these methods, we have proved that a broad range of ADL can be detected using single triaxial accelerometer located on the garment (vest) for the comfort of the wearer in long term application. In previous activity detection research, accelerometers are located at different body segments such as foot, thigh, waist, and sternum using belt, elastic belt, double-sided tape or Velcro™. Using considerable number of sensors, located at different parts of the body, may not be suitable for long-term use. Moreover, tightness of fixing materials in long term use is also a necessary consideration in applying elastic belt, belt, double-sided tape or Velcro™ in securing the sensors on the body. In comparison to other researchers' works (Table 2.1), we could detect a broad range of ADL using single triaxial accelerometer located at only one location, shoulder, with high classification rate. Bouten et al. [32] also used only one sensor set of three uniaxial accelerometers in broad range of ADL assessment application. The sensor set is located at the low back of the subjects at the level of the second lumbar vertebra by using an elastic belt. The application is more specific to the study of relations between ADL and energy expenditure due to ADL and their developed

method cannot classify activities. Our implementation of real-time detection of ADL is useful in several applications such as the system can help detect and send alarm for the patient's abnormal behavior such as patient is attempting to get out of the bed at night time, another fall prevention scenario as this attempt can lead to fall incident, or wandering of a patient suffering from dementia.

Our new detection approach interferes minimally with the activities of the subject. The sensor, placed in a casing (20mmx30mmx10mm), is light weight and attached to the vest using Velcro™ at the inner side of it. The casing (50mmx80mmx25mm) for the processing unit (a processor, rechargeable flat Lithium-ion battery, and Bluetooth™ transmitter) is inside the pocket of the vest. The cable connecting the sensor and the processing unit is between the two layers of cloths, near the zipper, of the vest. Then, the two layers are fastened using Velcro™. For washing the shirt, the cable, sensor casing, and processing unit casing, can be easily dismantled from the shirt. Moreover, the weight of the detection system (sensor casing and processing unit casing), nearly 150 g, will not bother the wearer in applying the system. Therefore, monitoring falls and ADL in free living environment with minimal interference and maximum comfort of the wearer is possible using the system we developed.

In fall detection, the system can summon medical assistances via SMS. This is the best detection system in its kinds as that which can raise fall alarm (fall SMS) on its own to individuals to get a shortened interval of the arrival of assistance with no detection range limitation. Moreover, we have studied pre-impact fall detection using angular rate sensors (gyroscopes). This is the first study to investigate the automatic detection of fall, which can cause hip injuries, during its descending phase using body-worn devices. The

advantage is that a fall injury minimization system can be developed by incorporating with an inflatable hip protection device.

Based upon the ADL and fall detection capabilities of this research, development of the smart wear by incorporating detection of abnormal vital physiological signs, such as blood pressure, heart rate, body temperature, and SpO2 (arterial oxygen situation) is recommended. The smart wear facilitated with wireless Body Area Network will be more practical for the comfort of the wearer. The system applying wireless communication and networking infrastructures can help caregivers with in time information of vital sign changes together with the wearer's abnormal behaviors, e.g., excessive walking, the subject is in lying posture for a long time, etc., so that necessary actions can be taken before serious incidents happen to the wearer. Moreover, another useful application of the smart ware is the fall prediction, especially for faint fall, by detecting abnormal vital physiological signs before faint and the onset of faint fall using motion sensors. These predictive measurements may further complement the injury minimization system such as an inflatable hip protection device which would be activated upon imminent fall. These systems have the potential to allow elderly with some cognitive and/or physical deficits to remain in their home for a longer time, i.e., the system can help the elderly postpone or prevent institutionalization. Moreover, it can help increase autonomy or independence of the elderly.

References

[1] Health Facts Singapore 2001, Ministry of Health, Singapore.

[2] Najafi, B., Aminian, K., Loew, F., Blanc, Y., Robert, P.A., 2002. Measurement of stand-sit and sit-stand transitions using a miniature gyroscope and its application in fall risk evaluation in the elderly. IEEE Trans Biomed Eng., 49(8), pp 843-851.

[3] Tinetti, M.E., Speechley, M., Ginter, S.F., 1988. Risk factors for falls among elderly persons living in the community. N Engl J Med, 319, pp 1701-1707.

[4] Tinetti, M.E., Williams, C.S., 1997. Falls, injuries due to falls and the risk of admission to a nursing home. N Engl J Med, 337(18), pp1279-1284.

[5] Langlois, J., Kegler, S., Butler, J., Gotsch, K., Johnson, R., Reichard, A., Webb, K., Coronado, V., Selassie, A., Thurman, D., 2003. Traumatic brain injury related hospital discharges: results from a 14-state surveillance system. MMWR, 52, pp 1-18.

[6] Jager, T., Weiss, H., Coben, J., Pepe, P., 2000. Traumantic brain injuries evaluated in U. S. emergency departments, 1992-1994. Academic Emergency Medicine, 7, pp 134-140.

[7] http://www.alexhosp.com.sg/patients_library/fall.asp.

[8] Adekoya, N., Thurman, D., 2002. Surveillance for traumatic brain injury deaths-United States, 1989-1998. MMWR 51 (SS10), pp 1-16.

[9] Kannus, P., Palvanen, M., Niemi, S., Parkkari, J., Natri, A., Vuori, I., Jarvinen, M., 1999. Increasing number and incidence of fall-induced severe head injuries in older adults: nationwide statistics in Finland in 1970-1995 and prediction for the future. Am J Epidemiol, 149, pp 143-50.

[10] Stevens, J., Hasbrouck, L., Durant, T., Dellinger, A., Batabyal, P., Crosby, A., Valluru, B., Kresnow, M., Guerrero, J., 1999. Surveillance for injuries and violence among older adults. MMWR, 48, pp 27-50.

[11] Luukinen, H., Koski, K., Honkanen, R., Kivela, S.L., 1995. Incidence of injury-causing falls among older adults by place of residence: A population-based study. J Am Geriatr Soc, 43, pp 871-876.

[12] Myers, A.H., Young, Y., Langlois, J.A., 1996. Prevention of falls in the elderly. Bone, 18(1), Supplement 1, pp 87-101.

[13] Campbell, A.J., Borrie, M.J., Spears, G. F., 1989. Risk factors for falls in a community-based prospective study of people 70 years and older. J Gerontol, 44, pp 112-117.

[14] Cumming, R.G., Klineberg, R. J., 1994. Fall frequency and characteristics and the risk of hip fractures. J Am Geriatr Soc, 42, pp 774-777.

[15] Nevitt, M.C., Cummings, S. R., Kidd, S., Black, D., 1989. Risk factors for recurrent nonsyncopal falls. JAMA, 261, pp 2663-2668.

[16] Tinetti, M.E., 1987. Factors associated with serious injury during falls by ambulatory nursing home residents. J Am Geriatr Soc, 36, pp 644-648.

[17] Turner, C.H., 2005. The biomechanics of hip fracture. The Lancet, 366(9480), pp 98-99.

[18] Nabhani, F., Bamford, J.S., 2004. Impact properties of floor coverings and their role during simulated hip fractures. Journal of Materials Processing Technology, 153(54), pp 139-144.

[19] Najafi, B., Aminian, K., Paraschiv-Ionescu, A., Loew, F., Bula, C.J., Robert, P., 2003. Ambulatory system for human motion analysis using a kinematic sensor: monitoring of daily physical activity in the elderly. IEEE Trans Biomed Eng, 50(6), pp 711-723.

[20] Yamaguchi, A., Ogawa, M., Tamura, T., Togawa, T., 1998. Monitoring behavior in the home using positioning sensors. Engineering in Medicine and Biology Society, Proceedings of the 20th Annual International Conference of the IEEE, 4, pp 1977-1979.

[21] Noury, N., Herve, T., Rialle, V., Virone, G., Mercier, E., Morey, G., Moro, A., Porcheron, T., 2000. Monitoring behavior in home using a smart fall sensor and position sensors. Microtechnologies in Medicine and Biology, 1st Annual International Conference, pp 607-610.

[22] Ogawa, M., Ochiai, S., Shoji, K., Nishihara, M., Togawa, T., 2000. An attempt of monitoring daily activities at home. Engineering in Medicine and Biology Society, Proceedings of the 22nd Annual International Conference of the IEEE, 1, pp 786-788.

[23] Caspersen, C.J., Powell, K.E., Christenson, G.M., 1985. Physical activity, exercise and physical fitness: Definitions and distinctions for health related research. Public Health Rep., 110, pp 126-131.

[24] Laporte, R.E., Montoye, H.J., Caspersen, C.J., 1985. Assessment of physical activity in epidemiological research: Problems and prospects. Public Health Rep., 200, pp 131-146.

[25] Kemper, H.G.C., Verschuur, R., 1977. Validity and reliability of pedometers in habitual activity research. Eur. J. Appl. Physiol., 37, pp 71-82.

[26] Avons, P., Garthwaite, P., Davies, H.L., Myrgatroyd, P.R., James W.P.T., 1988. Approaches to estimating physical activity in the community: Calorimetric validation of actometers and heart rate monitoring. Eur. J. Clin. Nutr., 42, pp 185-196.

[27] Meijer, G.A.L., Westerterp, K.R., Verhoeven, F.M.H., Koper, H.B.M., ten Hoor, F., 1991. Methods to assess physical activity with special reference to motion sensors and accelerometers. IEEE Biomed. Eng., 38, pp 221-229.

[28] Montoye, H., Washburn, R., Servais, S., Ertl, A., Webster, J.G., Nagle, F.J., 1983. Estimation of energy expenditure by a portable accelerometer. Med. Sci. Sports Exerc., 15, pp 403-407.

[29] Wong, T.C., Webster, H.J., Montoye, H., Washburn, R., 1981. Portable accelerometer device for measuring human energy expenditure. IEEE Trans. Biomed. Eng., 28, pp 467-471.

[30] Currie, G., Rafferty, D., Duncan, G., Bell, F., Evans, A.L., 1992. Measurement of gait by accelerometer and walkway: A comparison study. Med. Biol. Eng. Comput., 30, pp 669-670.

[31] Morris, J.R.W., 1973. Accelerometry—A technique for the measurement of human body movements. J. Biomech., 6, pp 729-736.

[32] Bouten, C.V.C.; Koekkoek, K.T.M.; Verduin, M.; Kodde, R.; Janssen, J.D., 1997. A triaxial accelerometer and portable data processing unit for the assessment of daily physical activity. IEEE Trans. Biomed. Eng., 44(3), pp 136-147.

[33] Veltink, P.H., Bussmann, H.B.J., de Vries, W., Martens, WimL.J.; Van Lummel, R.C., 1996. Detection of static and dynamic activities using uniaxial accelerometers. IEEE Trans. Rehab. Eng., 4(4), pp 375-385.

[34] Foerster, F., Smeja, M., Fahrenberg J., 1999. Detection of posture and motion by accelerometry: a validation study in ambulatory monitoring. Computers in Human Behavior, 15(5), pp 571-583.

[35] Frost, J.D., 1978. Triaxial vector accelerometry: A new method for quantifying tremor and ataxia. IEEE Trans. Biomed. Eng., 25, pp 17-27.

[36] Salzer, M., 1972. Three-dimensional tremor measurements of the hand. J. Biomech., 5, pp 217-221.

[37] Aminian, K., Robert, P., Jequier, E., Schutz, Y., 1995. Estimation of speed and incline of walking using neural network. IEEE Trans.Inst.Meas., 44(3), pp 743-746.

[38] Mantyjarvi, J., Himberg, J., Seppanen, T., 2001. Recognizing human motion with multiple acceleration sensors. Systems, Man, and Cybernetics, 2001 IEEE International Conference on, 2, pp 747-752.

[39] Sekine, M., Tamura, T., Togawa, T., Fukui, Y., 2000. Classification of waist-acceleration signals in a continuous walking record. Medical Engineering & Physics, 22(4), pp 285-291.

[40] Sekine, M., Tamura, T., Akay, M., Fujimoto, T., Togawa, T., Fukui, Y., 2002. Discrimination of walking patterns using wavelet-based fractal analysis. IEEE Trans. Neural. Syst. Rehabil. Eng., 10(3), pp 188-196.

[41] Coley, B., Najafi, B., Paraschiv-Ionescu, A., Aminian, K., 2005. Stair climbing detection during daily physical activity using a miniature gyroscope. Gait & Posture, 22(4), pp 287-294.

[42] Mathie, M.J., Celler, B.G., Lovell, N.H., Coster, A.C.F., 2004. Classification of basic daily movements using a triaxial accelerometer. Medical & biological engineering & computing, 42(5), pp 679-687.

[43] Lyons, G.M., Culhane, K.M., Hilton, D., Grace, P.A., Lyons, D., 2005. A description of an accelerometer-based mobility monitoring technique. Medical Engineering & Physics, 27(6), pp 497-504.

[44] Sorock, G.S., 1998. Falls among the elderly: epidemiology and prevention. Am J Prev Med, 4, pp 282-288.

[45] Tinetti, M., Speechly, M., 1989. Prevention of falls among the elderly. New Engl J med, 320(16), pp 1055-1059.

[46] Greenhouse, A.H., 1994. Falls among the elderly. Clinical Neurology of Aging, second ed. New York, Oxford University Press, pp 611-625.

[47] Berg, W.P., Alessio, H.M., Mills, E.M., Tong, C., 1997. Circumstances and consequences of falls in independent community-dwelling older adults. Age and Ageing 26, pp 261-268.

[48] Blake, A.J., Morgan, K., Bendall, M.J., Dallosso, H., Ebrahim, S.B., Arie, T.H., Fentem, P.H., Bassey, E.J., 1988. Falls by elderly people at home: prevalence and associated factors. Age and Ageing, 17, pp 365-372.

[49] Prudham, D., Evans, J.G., 1981. Factors associated with falls in the elderly: a community study. Age and Ageing, 10, pp 141-146.

[50] Tinetti, M.E., Doucette, J., Claus, E., Marottoli, R., 1995. Risk factors for serious injury during falls by older persons in the community. J Am Geriatr Soc, 43, pp 1214-1221.

[51] Cummings, S.R., Nevitt, M., Kidd, S., 1988. Forgetting falls: the limited accuracy of recall of falls in the elderly. J Am Geriatr Soc, 36, pp 613-616.

[52] Rivara, F.P., Grossman, D.C., Cummings, P., 1997. Injury prevention. Second of two parts. New England Journal of Medicine, 337, pp 613- 618.

[53] Sjogren, H., Bjornstig, U., 1989. Unintentional injuries among elderly people: incidence, causes, severity and costs. Accident, Analysis and Prevention, 21, pp 233–242.

[54] Sterling, D.A., O'Connor, J.A., Bonadies, J., 2001. Geriatric falls: injury severity is high and disproportionate to mechanism. Journal of Trauma, 50, pp 116-119.

[55] Brummel-Smith, K., 1989. Falls in the aged. Prim Care, 16, pp 377-393.

[56] Englander, F., Hodson, T.J., Terregrossa, R.A., 1996. Economic dimensions of slip and fall injuries. Journal of Forensic Sciences, 41, pp 733-764.

[57] Courtney, T.K., Sorock, G.S., Manning, D.P., Collins, J.W., Holbein- Jenny, M.A., 2001. Occupational slip, trip, and fall related injuries—can the contribution of slipperiness be isolated? Ergonomics, 44, pp 1118-1137.

[58] Leamon, T.B., Murphy, P.L., 1995. Occupational slips and falls: more than a trivial problem. Ergonomics, 38, pp 487-498.

[59] Rice, D., MacKenzie, E., 1989. Cost of injury in the United States: A report to Congress. Baltimore, MD, Injury Prevention Center, The John Hopkins University. Institute for Health & Aging, University of California, San Francisco, CA.

[60] Bakken, G.M., Cohen, H.H., Abele, J.R., Hyde, A.S., LaRue, C.A., 2007. Slips Trips, Missteps and Their Consequences, second ed. Lawyers and Judges Publishing, Inc., Arizona.

[61] Li, F.Z., Fisher, K.J., Harmer, P., McAuley, E., Wilson, N.L., 2003. Fear of falling in elderly persons: Association with falls, functional ability, and quality of life. Journals of Gerontology Series B-Psychological Sciences and Social Sciences, 58(5), pp 283-290.

[62] DeGoede, K.M., Ashton-Miller, J.A., Schultz, A.B., 2003. Fall-related upper body injuries in the older adult: a review of the biomechanical issues. J. Biomech., 36, pp 1043-1053.

[63] Cooper, C., 1997. The crippling consequences of fractures and their impact on quality of life. Am. J. Med., 103 (Part A), pp12S-19S.

[64] Reginster, J.Y., Gillet, P., Gosset, C., 2001. Secular increase in the incidence of hip fractures in Belgium between 1984 and 1996: need for a concerted public health strategy. Bull. World Health Org., 79, pp 942-946.

[65] Sanders, K.M., Nicholson, G.C., Ugoni, A.M., Pasco, J.A., Seeman, E., Kotowicz, M.A., 1999. Health burden of hip and other fractures in Australia beyond 2000. Projections based on the Geelong Osteoporosis Study. Med. J. Aust., 170, pp 459-460.

[66] Marks, R., Allegrante, J.P., MacKenzie, C.R., Lane, J.M., 2003. Hip fractures among the elderly: causes, consequences and control. Ageing Research Reviews, 2(1), pp 57-93.

[67] Smeesters, C., Hayes, W.C., McMahon, T.A., 2001. Disturbance type and gait speed affect fall direction and impact location. J. Biomech., 34(3), pp 309-317.

[68] Nyberg, L., Gustafson, Y., Berggren, D., Brannstrom, B., Bucht, G., 1996. Falls leading to femoral neck fractures in lucid older people. J Am Geriatr Soc, 44, pp 156-160.

[69] Palvanen, M., Kannus, P., Parkkari, J., Pitkajarvi, T., Pasanen, M., Vuori, I., Jarvinen, M., 2000. The injury mechanisms of osteoporotic upper extremityfractures

among older adults: a controlled study of 287 consecutive patients and their 108 controls. Osteoporosis International, 11, pp 822-831.

[70] Hayes, W.C., Myers, E.R., Morris, J.N., Gerhart, T.N., Yett, H.S., Lipsitz, L.A., 1993. Impact near the hip dominates fracture risk in elderly nursing home residents who fall. Calcified Tissue International, 52(3), pp 192-198.

[71] Nevitt, M.C., Cummings, S.R., 1993. Type of fall and risk of hip and wrist fractures: the study of osteoporotic fractures. J Am Geriatr Soc, 41(11), pp 1226-1234.

[72] Vu, M.Q., Weintraub, N., Laurence Z. Rubenstein, L.Z., 2006. Falls in the Nursing Home: Are They Preventable? Journal of the American Medical Directors Association, 7(3), pp 53-58.

[73] Jester, R., Wade, S., Henderson, K., 2005. A pilot investigation of the efficacy of falls risk assessment tools and prevention strategies in an elderly hip fracture population. Journal of Orthopaedic Nursing, 9(1), pp 27-34.

[74] Anacker, S. L., Di Fabio, R. P., 1992. Influence of sensory inputs on standing balance in community-dwelling elders with a recent history of falling. Phys Ther, 72, pp 575-584.

[75] Clark, R.D., Lord, S.R., Webster, I. W., 1993. Clinical parameters associated with falls in an elderly population. Gerontology, 39, pp 117-123.

[76] Cwikel, J., 1992. Falls among elderly people living at home: Medical and social factors in a national sample. Isr J Med Sci, 28, pp 446-453.

[77] Feltner, M.E., MacRae, P.G., McNitt-Gray, J.L., 1994. Quantitative gait assessment as a predictor of prospective and retrospective falls in community dwelling older women. Arch Phys Med Rehabil, 75, pp 447-453.

[78] Gabell, A., Simons, M.A., Nayak, U.S.L., 1985. Falls in the healthy elderly: Predisposing causes. Ergonomics, 28, pp 965-975.

[79] Grisso, J.A., Kelsey, J.L., Strom, B.L., Chiu, G.Y., Maislin, G., O'Brien, L.A., Hoffman, S., Kaplan, F. The Northeast Hip Fracture Study Group. Risk factors for falls as a cause of hip fracture in women. N Eng J Med, 324, pp 1326-1331.

[80] Mahoney, J., Sager, M., Dunham, N.C., Johnson, J., 1994. Risk of falls after hospital discharge. J Am Geriatr Soc, 42, pp 269-274.

[81] O'Loughlin, J. L., Robitaille, Y., Boivin, J. F., Suisssa, S., 1993. Incidence of and risk of factors for falls and injurious falls among the community-dwelling elderly. Am J Epidemiol, 137, pp 342-354.

[82] Prudham, D., Evans, J.G., 1981. Factors associated with falls in the elderly: A community study. Age Ageing, 10, pp 141-146.

[83] Robbins, A.S., Rubenstein, L.Z., Josephson, K.R., Schulman, B.L., Osterweil, D., Fine, G., 1989. Predictors of falls among elderly people: Results of two population-based studies. Arch Intern Med, 149, pp 1628-1633.

[84] Stewart, R.B., Moore, M.T., May, F.E., Marks, R.G., Hale, W.E.N, 1992. A risk for falls in the elderly. J Am Geriatr Soc, 40, pp 1217-1220.

[85] Teno, J., Kiel, D.P., Mor, V. Multiple stumbles: A risk factor for falls in community-dwelling elderly. J Am Geriatr Soc, 38, pp 1321-1325.

[86] Nait-Charif, H., McKenna, S.J., 2004. Activity summarisation and fall detection in a supportive home environment. Pattern Recognition, 17th International Conference, 4, pp 323-326.

[87] Sixsmith, A., Johnson, N., 2004. A smart sensor to detect the falls of the elderly. IEEE Pervasive Computing, 3(2), pp 42-47.

[88] Hwang, J.Y., Kang, J.M., Jang, Y.W., Kim, H.C., 2004. Development of novel algorithm and real-time monitoring ambulatory system using Bluetooth module for fall detection in the elderly. Engineering in Medicine and Biology Society (EMBC), 26th Annual International Conference, 1, pp 2204 - 2207.

[89] Williams, G., Doughty, K., Cameron, K., Bradley, D.A., 1998. A smart fall and activity monitor for telecare application. Int. Proc. IEEE-EMBS, Hong Kong, pp 1151-1154.

[90] Wu, G., 2000. Distinguishing fall activities from normal activities by velocity characteristics. J. Biomech., 33(11), pp 1497-1500.

[91] Kroonenberg, A.J. van den, Hayes, W.C., McMahon, T.A., 1996. Hip impact velocities and body configurations for voluntary falls from standing height. J. Biomech., 29(6), pp 807-811.

[92] Rioul, O., Vetterli, M., 1991. Wavelets and signal processing. IEEE Signal Processing Mag., 8(4), pp 14-38.

[93] Mallat, S.G., 1989. A theory for multi-resolution signal decomposition (The wavelet representation). IEEE Trans. Pattern Anal. Machine Intell., 11, pp 674-693.

[94] Mallat, S., Hwang, W.L., 1992. Singularity detection and processing with wavelets. Information Theory, IEEE Trans. Inf. Theory., 38(2), Part 2, pp 617-643.

[95] Mallat, S., Zhong, S., 1992. Characterization of signals from multiscale edges. IEEE Trans Pattern Anal Machine Intell, 14(7), pp 710-732.

[96] Meyer, Y., 1992. Wavelets and Operators. Cambridge, New York: Cambridge University Press.

[97] Daubechies, I., 1992. Ten Lectures on Wavelets. no. 61 in CBMS-NSF Series in Applied Mathematics, Philadelphia: SIAM.

[98] Daubechies, I., 1988. Orthonormal bases of compactly supported wavelets. Commun. on Pure and Appl. Math., 41(7), pp 909-996.

[99] Mallat, S.G., 1989. Multiresolution approximations and Wavelet Orthonormal Bases of $L2(R)$. Trans. Amer. Math. Soc., 315(1), pp 69-87.

[100] Kierat, W., Sztaba, U., 2003. Distributions, integral transforms, and applications. New York: Taylor & Francis.

[101] Percival, D., Walden, A., 2000. Wavelet methods for timeseries analysis. Cambridge University Press.

[102] Yansun, X., Weaver, J.B., Healy, D.M., Jian, L., 1994. Wavelet transform domain filters: a spatially selective noise filtration technique. IEEE Trans Image Process, 3(6), pp 747-758.

[103] Witkin, A., 1983. Scale space filtering. Proceedings of Seventh Joint, Conference on Artificial Intelligence, Germany, pp 1019-1022.

[104] Mathie, M.J., Coster, A.C.F., Lovell, N.H., Celler, B.G., 2003. Detection of daily physical activities using a triaxial accelerometer. Medical & Biological Engineering & Computing, 41, pp 296-301.

[105] Najafi, B., Aminian, K., Loew, F., Blanc, Y., Robert, P.A., 2002. Measurement of stand-sit and sit-stand transitions using a miniature gyroscope and its application in fall risk evaluation in the elderly. IEEE Trans Biomed Eng., 49(8), pp 843-851.

[106] Nyan, M. N., Tay, E. H. F., Seah, K. H. W., Sitoh, Y. Y., 2005. Classification of gait patterns in the time–frequency domain. J. Biomech., 39, pp 2647-2656.

[107] Tay, E. H. F., Nyan, M. N., Koh, T. H. Z., Seah, K. H. W., Sitoh, Y. Y., 2005. Smart Shirt That Can Call for Help after a Fall. International Journal of Software Engineering and Knowledge Engineering, 15(2), pp 183-188.

[108] Nyan, M. N., Tay, E. H. F., Manimaran M., Seah K. H. W., 2006. Garment-based detection of falls and activities of daily living using 3-axis MEMS accelerometer. Journal of physics, 34 (International MEMS Conference), pp 177-185.

[109] Sita, G., Ramakrishnan A.G., 2000. Wavelet domain nonlinear filtering for evoked potential signal enhancement. Computers and Biomedical Research, 33(6), pp 431-446.

[110] http://www.analog.com/UploadedFiles/Data_Sheets/411410542ADXL105_a.pdf.

McGill, S.M., Callaghan, J.P., 1999. Impact forces following the unexpected removal of a chair while sitting. Accident Analysis and Prevention 31 (1-2), pp 85-89.

[111] Oliver, D., Hopper, A., Seed, P., 2000. Do hospital fall prevention programs work? A systematic review. J Am Geriatr Soc; 48, pp 1679-1689.

[112] Greenspan, S.L., Myers, E.R., Maitland, L.A., Resnick, N.M., Hayes, W.C., 1994. Fall severity and bone mineral density as risk factors for hip fracture in ambulatory elderly. The Journal of the American Medical Association, 271(2), pp 128-133.

[113] Greenspan, S.L., Myers, E.R., Kiel, D.P., Parker, R.A., Hayes, W.C., Resnick, N.M., 1998. Fall direction, bone mineral density, and function: risk factors for hip fracture in frail nursing home elderly. The American Journal of Medicine, 104(6), pp 539-545.

[114] Oliver, D., Hopper, A., Seed, P., 2000. Do hospital fall prevention programs work? A systematic review. J Am Geriatr Soc, 48, pp 1679-1689.

[115] Analog Devices ADXL105 Specification Sheet.

Publication list

Published papers

Conference:

[1] Nyan Myo Naing, Francis E.H. Tay, K. H. W. Seah. Dynamic Pattern Recognition for Signal Identification using Eigenvectors. Proceedings of the 22nd Southern Biomedical Engineering Conference, 26-28 Sep 2003, pp 77.

[2] Nyan Myo Naing, Francis E.H. Tay, K. H. W. Seah. Signal identification based on an eigenvector approach. System Theory, 2004. Proceedings of the Thirty-Sixth Southeastern Symposium on 2004, pp 137-140.

[3] Myo Naing Nyan, Francis Eng Hock Tay, Teck Hong Koh, Yih Yiow Sitoh, Kwong Luck Tan. Location and sensitivity comparison of MEMS accelerometers in signal identification for ambulatory monitoring. Electronic Components and Technology, 2004. ECTC '04. Proceedings, Volume 1, 1-4 June 2004, pp 956-960.

[4] Nyan Myo Naing, Francis E.H. Tay, K. H. W. Seah. Segment extraction using wavelet multiresolution analysis for human activities and fall incidents monitoring system. Proceedings of the 2nd international Conference on Smart homes and Health telematics 2004, pp 177-185.

[5] M. N. Nyan, F. E. H. Tay, M. Manimaran, K. H. W. Seah, 2006. Garment-based detection of falls and activities of daily living using 3-axis MEMS accelerometer. Journal of Physics: Conference Series, 34 (International MEMS Conference) (2006), pp 1059-1067.

Journal:

[1] F. E. H. Tay, M. N. Nyan, T. H. Koh, K. H. W. Seah and Y. Y. Sitoh, 2005. Smart Shirt That Can Call for Help after a Fall. **International Journal of Software Engineering and Knowledge Engineering**, 15 (2), pp 183-188.

[2] F. E. H. Tay, M. N. Nyan, K. H. W. Seah, 2005. MEMSWear: Biomonitoring devices that you can wear!. Accepted for publication in **Biomedical Micro devices Journal**.

[3] M. N. Nyan, F. E. H. Tay, A.W.Y. Tan, K. H. W. Seah; Y. Y. SITOH, 2005. Classification of Gait Patterns in the time-frequency domain. **Journal of Biomechanics**, 39, pp 2647-2656.

[4] M. N. Nyan, F. E. H. Tay, A. W. Y. Tan, K. H. W. Seah, 2005. Distinguishing fall activities from normal activities by angular rate characteristics and high speed camera characterization. **Medical Engineering and Physics**, 28, pp 842-849.

[5] M. N. NYAN; Francis E. H. TAY; K. H. W. Seah; N. H. Ismail, 2006. Detection of daily physical activities in the time-frequency domain. **Journal of Mechanics in Medicine and Biology**, 6(4), pp 429-446.

Appendix A: Theory of Operation of the Accelerometer

The accelerometer is a complete acceleration measurement system on a single monolithic IC. It is a surface micromachined polysilicon structure built on top of the silicon wafer. Polysilicon springs suspend the structure over the surface of the wafer and provide a resistance against acceleration induced forces. Deflection of the structure is measured with a differential capacitor structure that consists of 2 independent fixed plates and a central plate attached to the moving mass. A 180° out of phase square wave drives the fixed plates. An acceleration causing the beam to deflect will unbalance the differential capacitor and thus results in an output square wave whose amplitude is proportional to acceleration. Phase sensitive demodulation techniques are then used to rectify the signal and determine the direction of the acceleration. The accelerometer is capable of measuring both positive and negative acceleration to a certain level of $\pm$g. The signals from the accelerometers consist of DC and AC components. The DC component (static acceleration) allows the assessment of the change in position in relation to the gravitational axis and thus the accelerometer can be used as a tilt sensor. The variation of DC component due to the difference in sensor orientation is shown in Fig A.1. The AC component represents the acceleration along the sensitive axis of the accelerometer.

An uncommitted amplifier is supplied for setting the output scale factor, filtering and other analog signal processing. A ratiometric voltage output temperature sensor measures the exact die temperature and can be used for proportional calibration of the accelerometer over temperature [115].

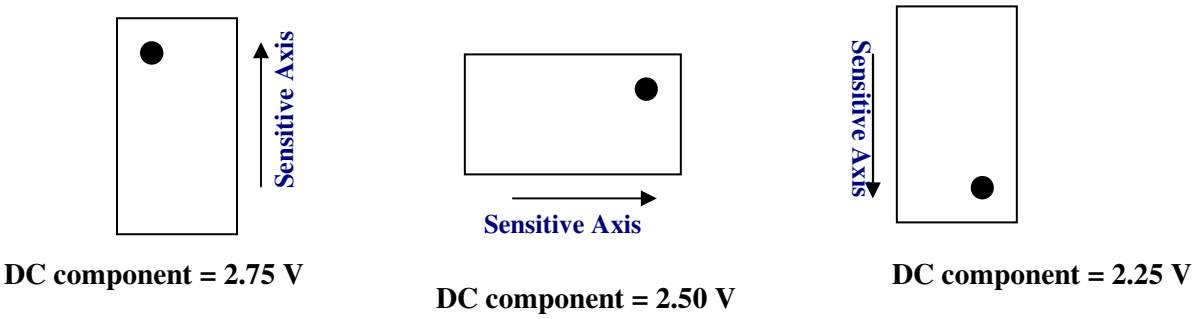

Fig.A.1. The Schematic Layout of the Accelerometer at Different Orientations with the corresponding DC component values